Synaptic computations in the olfactory bulb glomerular microcircuit

By

Christopher Edward Vaaga

A DISSERTATION

Presented to the Neuroscience Graduate Program,

Vollum Institute,

Oregon Health and Science University,

And School of Medicine

In partial fulfillment of

the requirements for the degree of

Doctor of Philosophy

April 2017

School of Medicine

Oregon Health & Science University

CERTIFICATE OF APPROVAL

This is to certify that the Ph.D. dissertation of

CHRISTOPHER VAAGA

has been approved on April 25, 2017

Advisor, Gary Westbrook, MD

Member and Chair, Tianyi Mao, PhD

Member, Craig Jahr, PhD

Member, John Williams, PhD

Member, Vivek Unni, MD, PhD

Member, Henrique von Gersdorff, PhD

Table of Contents

Acknowledgements

The work that has culminated in this dissertation has been supported by a variety of mentors, coworkers, family, and friends, all of whom deserve my deepest gratitude. First, this work would not be possible without the mentorship and guidance of Dr. Gary Westbrook. Under Gary's mentorship, I have become a better scientist, experimentalist, and communicator. He has consistently pushed me to critically evaluate my own work, and encouraged me to pursue scientific questions with rigor and excitement. I would also like to thank my dissertation advisory committee: Drs. Tianyi Mao, Craig Jahr, John Williams, Vivek Unni and Henrique von Gersdorff, who have provided invaluable input to this project throughout its many stages of development.

This work wouldn't be possible without the funding agencies that have directly supported this work and my personal scientific development: the National Science Foundation Graduate Research Fellowship, the LaCroute Neurobiology of Disease Fellowship, the Tartar Trust Fellowship and the ARCS Scholarship.

I would also like to thank all the members of the Westbrook and Schnell labs, with whom I have had the fortune of working. In addition to the much appreciated scientific input and training, they have been a constant source of enthusiasm, support, and perhaps most importantly they have created a truly enjoyable work environment. In particular, I would like to thank Dr. Ken Tovar and Dr. Maria Borisovska who trained me in the basics of electrophysiology and

olfactory bulb research, respectively. I also thank Dr. Jordan Yorgason, who taught me cyclic voltammetry, and whose work contributed to the data presented in chapter 1, Figure 1.

Finally, I would also like to thank all the members of my family, without whom none of this would be possible. In particular, my parents, Per and Cindy Vaaga, fostered my scientific interests from an early age and encouraged me to pursue a path in the sciences. Finally, to my wife Tricia and daughter Lucy, you have encouraged and supported me through each day of this long journey. Quite simply, without your continued love and support, I wouldn't be where I am today.

Abstract:

The ability to respond to cues in the environment is one of the most well conserved features of the nervous system. Sensory systems can be divided into sensory transduction pathways, necessary for converting physical stimuli in the environment into electrical signals, and the downstream sensory processing necessary to encode salient features of the sensory stimulus. In the olfactory system, initial processing of sensory input occurs in the glomerular microcircuit of the olfactory bulb. The glomerular microcircuit can be further subdivided into axodendritic inputs, resulting from direct synapses with primary sensory neurons, and dendrodendritic synapses, mediated by recurrent dendritic glutamate release and electrical coupling. Although multiple principal neuron subtypes, including mitral cells and external tufted cells, are thought to serve as parallel input pathways, the afferent connectivity, presynaptic properties, and subsequent synaptic processing across cell types remains controversial and poorly understood. To address these questions, I used whole-cell voltage clamp and current clamp recordings in acute mouse olfactory bulb slices. I first demonstrate that a population of juxtaglomerular interneurons, which release both dopamine and GABA, can effectively inhibit transmitter release from primary afferent neurons, thereby potently controlling the strength of afferent input. Using single glomerular afferent stimulation, I further demonstrate that the afferent olfactory receptor nerve terminal has an extraordinarily high release probability, which is mediated by a single pool of slowly recycling vesicles. Furthermore, although

mitral cells and external tufted cells receive homogenous afferent input with respect to quantal amplitudes and release probabilities, the postsynaptic processing of brief afferent input differs widely between cell types. Compared to external tufted cells, mitral cells showed robust dendrodendritic amplification of afferent input, significantly prolonging the EPSC and increasing the total synaptic charge. This amplification allowed mitral cells to respond to high frequency afferent stimulation with sustained spiking responses, despite robust synaptic depression of axodendritic input. External tufted cells, on the other hand, despite larger monosynaptic EPSCs, responded to high frequency stimulation with transient responses. This work provides important insight into the divergent synaptic processing of common olfactory input, and defines the synaptic mechanisms underlying parallel processing of afferent input.

Introduction and Background:

The ability to interact with the external world is one of the most basic and well-conserved features of the nervous system across all organisms. In fact, even single cell organisms respond to cues in the environment, including chemicals and light (Adler, 1969; Sineshchekov *et al.*, 2002; Nagel *et al.*, 2003). Sensory systems have expanded in higher organisms with dedicated nervous systems. For example, in the mammalian central nervous system, multiple sensory streams converge to inform a wide range of motivated behaviors as diverse as predator avoidance, mating, and foraging (Kaas, 1989). Such behaviors are predicated on accurate representations of the external world (for example, identifying prey versus predator), and at the neurophysiological level require the coordination of multiple complex circuits: including sensory, decision-making, and motor circuits (Kaas, 1989). Sensory systems, therefore, serve a critically important role within the central nervous system by providing an interface with the external world.

One of the fundamental questions, therefore, is how the external world is encoded in the brain. Sensory systems have two basic components: transduction and processing. Sensory transduction pathways are necessary to convert physical stimuli in the environment into an electrical impulse, and vary widely across sensory modalities depending on the nature of the physical stimulus. However, many core features of downstream processing are conserved across sensory modalities. For example, computations such as lateral inhibition to

sharpen signal to noise ratios, labeled lines to encode different properties of the sensory input, and gain control mechanisms to encode stimuli over a large dynamic range, are found across sensory modalities (Hudspeth and Logothetis, 2000; Gardner and Johnson, 2013).

Although, in humans, the chemical senses may seem less important than other more dominant senses such as vision, 68% of patients with olfactory impairments report a reduced quality of life (Doty, 2012*a*). Olfaction is also critical to survival, mediating behaviors such as mating and prey avoidance. Furthermore, the olfactory system is capable of discriminating between a large number of odorants with exquisite sensitivity, requiring complex synaptic processing of afferent sensory input.

The olfactory bulb, the first central brain region devoted to processing olfactory input, is particularly amenable to electrophysiological studies in part because of the modular organization of the circuitry. The work presented in this dissertation aims to better define the properties of synaptic transmission between primary sensory neurons and two populations of principal neurons in the olfactory bulb, with a particular focus on understanding how each principal neuron differentially encodes common input to provide multiple, complementary streams of information to higher olfactory cortex.

Olfactory transduction encodes odorant identity and concentration

One of the fundamental computational challenges of sensory transduction is encoding the relevant features of the stimulus, as initial stimulus encoding fundamentally limits the possible downstream processing. In the olfactory system, at least two stimulus features are encoded by primary sensory neurons: odorant identity and concentration. Although the exact number of discernible odorants is controversial (Bushdid *et al.*, 2014; Meister, 2014), conservatively, humans are capable of detecting thousands of unique odorants. This large repertoire of perceivable odorants is combined with exquisite sensitivity, in some cases reaching 1 part per 10^{15} molecules (Julius and Katz, 2004).

Molecular mechanisms of olfactory transduction: Olfactory transduction is initiated in the nasal epithelium through interactions with primary sensory neurons referred to as olfactory receptor neurons (ORNs). Odorants passing through the nasal cavity bind to G-protein coupled odorant receptors expressed on the dendritic cilia of ORNs. Each ORN expresses a single 7-transmembrane G-protein coupled odorant receptor from a large multigene family (Buck and Axel, 1991; Chess *et al.*, 1994; Malnic *et al.*, 1999; Serizawa *et al.*, 2000, 2004), which, in mice, contains over 1000 members (Zozulya *et al.*, 2001; Zhang and Firestein, 2002; Malnic *et al.*, 2004).

The transduction cascade following odorant binding has been well characterized (Figure 1; Kleene, 2008), and shares many similarities to the rhodopsin-signaling cascade in photoreceptors of the retina (Kleene, 2008;

Molday and Moritz, 2015). Upon binding an odorant, the olfactory receptor activates a unique G-protein, G_{olf} (Jones and Reed, 1989), which stimulates adenylyl cyclase III, producing cAMP (Bakalyar and Reed, 1990; Takeuchi and Kurahashi, 2005). cAMP in turn gates a cyclic nucleotide gated cation channel, resulting in Na^+, K^+, and Ca^{2+} influx and depolarization (Nakamura and Gold, 1987; Dhallan *et al.*, 1990). Ca^{2+} activated Cl^- channels further amplify the receptor potential, which owing to high intracellular chloride (Kaneko *et al.*, 2004), results in chloride efflux and further depolarization (Kurahashi and Yau, 1993; Lowe and Gold, 1993). The amplification resulting from both cAMP and Ca^{2+} gated Cl^- channels, along with the high input resistance of ORNs, may allow individual odorant binding events to trigger an action potential in some ORNs (Lynch and Barry, 1989), although the exact number of binding events necessary to trigger an action potential remains controversial (Kleene, 2008).

The ensemble of olfactory receptor neurons encodes odorant identity: Most odorants are composed of complex mixtures of multiple molecular structures, called odotopes, each of which binds to a unique odorant receptor. Therefore, encoding odorant identity in the periphery requires a combinatorial, labeled line system. To this end, each olfactory receptor neuron expresses a single olfactory receptor through monoallelic expression and cross-repression of odorant receptor genes (Mombaerts, 1999; Malnic *et al.*, 1999; Antunes and Simoes de Souza, 2016; Nagai *et al.*, 2016). Structurally, olfactory receptors contain a hypervariable amino acid sequence along transmembrane 3, 4 and 5, which likely forms the ligand-binding pocket (Pilpel and Lancet, 1999). Residues

within the ligand-binding pocket are predicted to form relatively weak hydrophobic and van der Waals interactions with ligands (Katada *et al.*, 2005). Such weak ligand interactions allows each olfactory receptor to bind multiple odotopes, albeit with a wide range in affinities (Malnic *et al.*, 1999). The broad molecular tuning of olfactory receptors indicates that most odorants are encoded by the complex ensemble activity of multiple olfactory receptor neurons subtypes. Such combinatorial activity allows the olfactory system to encode a wide range of odorants, which far exceeds the repertoire of odorant receptors.

Odorant evoked activity in olfactory receptor neurons: In voltage clamp recordings of olfactory receptor neurons, odorant binding elicits an inward receptor current, depolarizing the ORN, as described above. The concentration of the odorant is encoded in the amplitude of the receptor potential, which is steeply dependent on both ligand concentration and identity (Firestein *et al.*, 1993; Picco *et al.*, 1998). The biochemical amplification of odorant binding by the signaling cascade introduces a delay in the generation of the receptor potential, which is further lengthened by odorant diffusion through mucous layers (Kleene, 2008).

Initial recordings of odorant-evoked electrical currents in intact preparations measured the electrical potential across the olfactory epithelium, the so-called electroolfactogram (Ottoson, 1971), which represents the summed electrical activity of olfactory receptor neurons (Kleene, 2008). Strong, prolonged odorant presentation elicits a response that slowly adapts, reflecting both adaptation and desensitization of receptors in individual ORNs (Kurahashi and

Shibuya, 1990; Firestein *et al.*, 1990; Kurahashi and Menini, 1997; Duchamp-Viret *et al.*, 1999; Kleene, 2008). In single unit recordings from olfactory receptor neurons, the firing rate increases monotonically with odorant concentration (Sicard, 1986; Duchamp-Viret *et al.*, 1999; Tan *et al.*, 2010), and can reach a peak frequency of approximately 100 Hz. As expected, the firing rate of individual ORNs also decreases with prolonged odorant presentation (Sicard, 1986; Duchamp-Viret *et al.*, 1999; Tan *et al.*, 2010). It is also worth noting here that the lifetime of ORNs is quite short in mammals, as ORNs are fully replaced approximately every 30 days (Graziadei and Graziadei, 1979). Together, these results suggest that ORNs encode odorant concentration with increases in the receptor potential amplitude and resulting increases in ORN firing rate.

Connectivity and structure of olfactory bulb glomeruli

Olfactory receptor neurons project to the olfactory bulb, by first passing their axons through the cribriform plate. Within the olfactory bulb, ORN axons terminate in the synaptic rich neuropil of the glomerulus, which serves as the locus of initial olfactory processing (Figure 2). Each glomerulus represents an anatomically and functionally discrete cortical module, resulting from unimodal afferent input from ORNs expressing the same odorant receptor (Vassar *et al.*, 1994; Ressler *et al.*, 1994; Mombaerts *et al.*, 1996). Thus, the combinatorial activation of odorant receptors in the epithelium is faithfully transmitted to the olfactory bulb, wherein different odorants produce distinct maps of activated

glomeruli, which encodes odorant identity (Rubin and Katz, 1999; Xu *et al.*, 2000; Wachowiak and Cohen, 2001). In mice, there are approximately 2000 glomeruli in the main olfactory bulb (Royet *et al.*, 1988), consistent with each ORN subtype projecting to ca. two glomeruli, one lateral and one medial (Mombaerts *et al.*, 1996). Afferent input to the olfactory bulb is massively convergent, with 5,000-10,000 ORN axons innervating each glomerulus (Allison, 1953; Chen and Shepherd, 2005). Although such redundancy is unusual in the brain (Rieke, 1999), it likely serves a critical function in amplifying olfactory input (Chen and Shepherd, 2005).

The glomerulus is composed of distinct synaptic compartments: Afferent nerve terminals are restricted to a circumscribed outer layer of the glomerulus, collectively referred to as the glomerular shell (Chao *et al.*, 1997; Kasowski *et al.*, 1999; Kim and Greer, 2000; Kosaka and Kosaka, 2005). At the ultrastructural level, ORN axons make axodendritic synapses with principal cells and interneurons (Pinching and Powell, 1971; Kasowski *et al.*, 1999). The synaptic interactions of the glomerular microcircuit are complicated, however, because the majority of neurons within the olfactory bulb release neurotransmitter from dendrites (Reese and Brightman, 1970; Pinching and Powell, 1971; Jahr and Nicoll, 1980; Schoppa and Urban, 2003). Somatodendritic transmitter release does occur in other circuits, for example in dopamine neurons in the ventral tegmental area (Rice and Patel, 2015), however, the role of somatodendritic release in the ventral tegmental area is primarily to modulate the firing pattern of dopamine neurons, via interactions with D_2 autoreceptors (Ford,

2014). Conversely, in the olfactory bulb, dendritic transmitter release from multiple cell types acts on both autoreceptors and across synaptic partners, and mediates a critical component of glomerular processing (Figure 3; Nicoll and Jahr, 1982; Isaacson, 1999; Urban and Sakmann, 2002; Schoppa and Westbrook, 2002; Christie and Westbrook, 2006). Dendrodendritic synapses are found within a distinct glomerular subcompartment, referred to as the glomerular core (Chao *et al.*, 1997; Kasowski *et al.*, 1999). The majority of dendrodendritic synapses within the glomerulus are between principal cell dendrites and inhibitory interneurons (Figure 3; Pinching and Powell, 1971; Bourne and Schoppa, 2017). These dendrodendritic synapses are generally viewed to be reciprocal in nature, that is the presynaptic dendritic release site is also the direct postsynaptic target (Schoppa and Urban, 2003). Anatomically, the presence of *bona fide* dendrodendritic synapses between principal cell dendrites is exceedingly rare; in fact, identifying presynaptic release sites is also difficult in principal cell dendrites, as small clear vesicles are dispersed throughout the dendrite (Pinching and Powell, 1971; Bourne and Schoppa, 2017). The unique synaptic architecture of the glomerulus defines the cortical module necessary for initial afferent processing.

Principal neurons: Within the glomerulus, there are two primary principal projection neurons: mitral cells and tufted cells. Although originally believed to encode similar information, it has become clear that mitral cells and tufted cells represent parallel input pathways of sensory input, either resulting from differential input, inhibition or intrinsic properties (Nagayama *et al.*, 2004; Najac

et al., 2011; Gire *et al.*, 2012; Igarashi *et al.*, 2012; Kikuta *et al.*, 2013; Burton and Urban, 2014; Geramita and Urban, 2017). Mitral cells are defined by their soma position in a single cell layer deep to the external plexiform layer. Mitral cells have a single apical dendrite that transverses the external plexiform layer and terminates in a specific glomerulus, preserving the one odorant receptor-one glomerulus rule (Nagayama *et al.*, 2014). Mitral cells also contain extensive lateral dendrites, which extend up to 1 mm in either direction within the external plexiform layer (Nagayama *et al.*, 2014), and mediate dendrodendritic reciprocal inhibition with granule cells (Egger and Urban, 2006).

Tufted cells can be broadly grouped into internal, middle and external tufted cells, depending on their relative position within the external plexiform layer. Internal and middle tufted cells are morphologically similar to mitral cells, in that their apical dendrites ramify in a single glomerulus and contain lateral dendrites (Nagayama *et al.*, 2014). External tufted cells, however, are located immediately adjacent to the glomerular layer and unlike other principal neurons, lack lateral dendrites (Hayar *et al.*, 2004*b*, 2004*a*). External tufted cells also have distinct synaptic and intrinsic properties, suggesting they represent a functionally discrete cell population (Hayar *et al.*, 2004*a*; De Saint Jan *et al.*, 2009; Najac *et al.*, 2011).

Diversity of Juxtaglomerular interneurons: Each glomerulus is surrounded by a variety of intrinsic interneurons, referred to collectively as juxtaglomerular neurons. Juxtaglomerular interneurons are heterogeneous with respect to morphology, transmitter phenotype, and function (Kiyokage *et al.*, 2010), and can

be broadly grouped into periglomerular neurons and short axon cells. GABAergic periglomerular neurons ramify within a single glomerulus (Kiyokage *et al.*, 2010). Approximately 70% of periglomerular neurons are driven exclusively by feedforward excitation from external tufted cells, whereas the remaining 30% receive input directly from ORNs (Shao *et al.*, 2009). Unlike periglomerular neurons, short axon cells ramify in upwards of 5-10 glomeruli (Kiyokage *et al.*, 2010), and are defined by the co-expression of dopamine and GABA synthesis enzymes (Gall *et al.*, 1987; Maher and Westbrook, 2008). Like periglomerular neurons, short axon cells can be driven by both direct ORN input or feedforward excitation (Kiyokage *et al.*, 2010).

Synaptic properties of the glomerular microcircuit

In order to understand circuit function one must understand how afferent input is transformed within the circuit, as a result of synaptic inhibition as well as intrinsic and synaptic properties. Because the identity of the odorant is encoded in the combinatorial activation of glomeruli throughout the olfactory bulb, the primary function of glomerular microcircuitry is to provide amplification of afferent input while maintaining odorant sensitivity. However the exact synaptic transformations that occur in the glomerulus are not fully understood.

Early experiments demonstrated that stimulation of the olfactory nerve generates a biphasic response in mitral cells that is composed of a rapid depolarization and a prolonged depolarization (Ennis *et al.*, 1996; Chen and

Shepherd, 1997; Aroniadou-Anderjaska *et al.*, 1997). The initial, fast depolarization is mediated by AMPA/kainate receptors, whereas the slow depolarization requires NMDA receptor activation (Ennis *et al.*, 1996; Aroniadou-Anderjaska *et al.*, 1997). However, the kinetics of the slow depolarization (upwards of 500 ms) far outlasts typical NMDA receptor responses (Aroniadou-Anderjaska *et al.*, 1997; De Saint Jan and Westbrook, 2007) suggesting that other mechanisms contribute to the slow current.

Properties of afferent olfactory input: Olfactory receptor neurons respond to increasing concentrations of odorants with monotonic increases in firing rate, producing a sigmoidal response curve across concentrations (Sicard, 1986; Duchamp-Viret *et al.*, 1999; Kleene, 2008; Tan *et al.*, 2010). The presynaptic properties of olfactory receptor neurons are not fully understood, but early experiments suggest some interesting features. The release probability of the ORN, as measured by progressive MK-801 block and mean-variance analysis, suggests that ORN synapses have among the highest release probabilities in the brain (ca. 0.9; Silver *et al.*, 2003; Murphy *et al.*, 2004). Furthermore, although most synapses show a 4th power relationship between extracellular calcium and transmitter release, it has been suggested that at the afferent ORN synapse, this relationship is significantly more shallow (Murphy *et al.*, 2004), suggesting that vesicle release dynamics may be different in ORNs.

Synapses that operate at high release probability are prone to vesicle depletion upon repeated stimulation, which results in synaptic depression in the postsynaptic cell (Regehr, 2012). Thus the high firing rates and release

probability of ORNs suggests that the postsynaptic responses of principal cells are dominated by synaptic depression. However, the synaptic dynamics of high frequency afferent stimulation have not been explored in olfactory bulb brain slices. In chapter 3, I examine the properties of transmitter release in response to high frequency stimulation.

The functional connectivity of the presynaptic ORN and principal neurons of the olfactory bulb has been controversial. Despite anatomical and early physiological evidence for monosynaptic afferent input to mitral cells (see for example Figure 2 A; Reese and Brightman, 1970; Pinching and Powell, 1971; Ennis *et al.*, 1996; Chen and Shepherd, 1997; Aroniadou-Anderjaska *et al.*, 1997; Najac *et al.*, 2011; Bourne and Schoppa, 2017), recent studies have suggested that mitral cells are primarily, if not exclusively, driven by feedforward excitation via external tufted cells (Gire and Schoppa, 2009; Gire *et al.*, 2012). In this view, the afferent input to mitral cells is relatively weak, and as a result is shunted across gap junctions between mitral cells (Gire *et al.*, 2012). Although ORN stimulation in some studies was capable of driving short latency responses in mitral cells (De Saint Jan *et al.*, 2009; Najac *et al.*, 2011), the interpretation that this is mediated by ORN glutamate release could be confounded by dendritic glutamate release within the glomerulus.

Furthermore, external tufted cells have distinct synaptic properties that could support a role in feedforward excitation of mitral cells. For example, external tufted cells are spontaneously active in the absence of synaptic input (Hayar *et al.*, 2004*b*) and stimulation of single external tufted cells can generate

slow synaptic responses in mitral cells, which closely resembles the slow, afferent evoked EPSC in mitral cells (Carlson *et al.*, 2000; Schoppa and Westbrook, 2001; Hayar *et al.*, 2004*a*; De Saint Jan *et al.*, 2009). Furthermore, in paired recordings, stimulation of external tufted cells produces short latency, unidirectional synaptic responses in mitral cells (De Saint Jan *et al.*, 2009; Najac *et al.*, 2011). External tufted cells also respond to afferent stimulation at lower stimulus intensities than mitral cells, and receive strong OSN input (Hayar *et al.*, 2004*a*; Murphy *et al.*, 2005; De Saint Jan *et al.*, 2009).

In vivo mitral cell spiking lags that of tufted cells in response to weak odorants; however, this lag shortens in response to higher odorant concentrations (Fukunaga *et al.*, 2012). Although in theory the delayed mitral cell response may result from feedforward activation, mitral cells also receive stronger glomerular layer inhibitory input, which delays mitral cell activity (Fukunaga *et al.*, 2012; Kikuta *et al.*, 2013; Geramita *et al.*, 2016; Geramita and Urban, 2017). Resolving the functional afferent connectivity of mitral cells has important implications for circuit function, as mitral cells are the primary output neuron of the olfactory bulb (Igarashi *et al.*, 2012). The afferent evoked synapses of mitral cells and external tufted cells are explored in chapters 2 and 3.

Recurrent dendrodendritic excitation amplifies afferent input: One of the primary functions of the glomerular microcircuit is the amplification of afferent input (Chen and Shepherd, 2005). The synaptic mechanisms underlying such amplification are varied and complex, and critically depend on dendritic glutamate release and electrical coupling of mitral cell dendrites (Figure 3b). The

initial amplification of afferent input results from dendritic glutamate release, which activates AMPA and NMDA autoreceptors and may contribute to lateral excitation of neighboring dendrites (Nicoll and Jahr, 1982; Urban and Sakmann, 2002; Christie and Westbrook, 2006; Pimentel and Margrie, 2008; De Saint Jan *et al.*, 2009; Najac *et al.*, 2011), despite the lack of ultrastructural evidence for direct synaptic connections (Reese and Brightman, 1970; Pinching and Powell, 1971; Najac *et al.*, 2011). The lateral excitation of principal cell dendrites may result from spillover of dendritic glutamate release (Isaacson, 1999; Christie and Westbrook, 2006), which, in other circuits, can activate postsynaptic receptors on neighboring cells and generate biphasic EPSCs (Carter and Regehr, 2000; Coddington *et al.*, 2014).

Evidence for dendrodendritic glutamate release comes, in part, from astrocyte recordings, in which two kinetically distinct glutamate transporter currents can be recorded, representing axodendritic glutamate release and secondary dendrodendritic glutamate release (De Saint Jan and Westbrook, 2005). Although the lifetime of neurotransmitter within the synaptic cleft is generally brief (Clements, 1996), unique anatomical arrangements, such as between climbing fibers and Purkinje cells in the cerebellum, can prolong the transmitter lifetime. Despite anatomical specializations within the glomerulus, the synaptic response to brief afferent stimulation lasts many hundreds of milliseconds, suggesting that recurrent dendrodendritic glutamate release is the primary means of generating the slow EPSC. Furthermore, unlike traditional synaptic responses, the mitral cell slow current is generated in an all-or-none

fashion (Carlson *et al.*, 2000; De Saint Jan *et al.*, 2009; Gire and Schoppa, 2009).

Generation of the afferent evoked slow current requires activation of NMDA and mGluR1 receptors (De Saint Jan and Westbrook, 2007; Johnston and Delaney, 2010). The activation of mGluR receptors in this circuit is atypical, because generally metabotropic glutamate receptors are expressed perisynaptically and are only activated following high frequency stimulation (Carter and Regehr, 2000). Activation of metabotropic glutamate receptors may be necessary to produce a hyperpolarizing shift in the activation voltage of T-type calcium channels, which are thought to provide the calcium necessary for dendritic glutamate release (Castro and Urban, 2009; Johnston and Delaney, 2010; Fekete *et al.*, 2014). Interestingly, even at rest, T-type calcium channels have a window current in mitral cells, resulting from overlapping activation and deactivation voltages (Johnston and Delaney, 2010), which may support subthreshold glutamate release (Castro and Urban, 2009). Furthermore, in mitral cells, metabotropic glutamate receptor activation requires disynaptic input, suggesting that some dendritic glutamate is released prior to mGluR1 activation (De Saint Jan and Westbrook, 2007). This initial dendritic release may be mediated by direct Ca^{2+} influx through NMDA receptors, as ORN stimulation elicits calcium hotspots, which are blocked by NMDA receptor antagonists (Yuan and Knöpfel, 2006). Similar roles for calcium influx through NMDA receptors in triggering dendritic transmitter release have been reported in granule cells of the olfactory bulb (Schoppa *et al.*, 1998; Christie *et al.*, 2001).

Electrical coupling of mitral cell dendrites: Yet another means of activating neighboring cells in the absence of direct, chemical synaptic connections is via electrical coupling by gap junction proteins (Connors, 2017). Gap junction coupling is prominent in mitral cells; however, the geometry of these electrical synapses is unusual. In most circuits, gap junctions are formed near the cell bodies of the coupled cells. In mitral cells, however, connexin 36 (Cx36) gap junctions are formed between the distal tufts of primary dendrites (Christie and Westbrook, 2006; Bourne and Schoppa, 2017). Such unique geometry ensures that all mitral cells associated with a given glomerulus are electrically coupled, and may be an especially effective arrangement for the transmission of slow electrical responses. Consistent with this view, all mitral cell dendrites targeting the same glomerulus are coupled by gap junctions, and synchronize the activity of principal neurons (Schoppa and Westbrook, 2002). The dendritic gap junctions also allows for the lateral transmission of slow dendritic events, such as the auto-excitation resulting from dendritic glutamate release (Nicoll and Jahr, 1982; Schoppa and Westbrook, 2002; Christie *et al.*, 2005; Christie and Westbrook, 2006).

In fact, in connexin 36 knockout mice, lateral transmission between mitral cells is completely lost suggesting that electrical coupling may be the primary form of lateral transmission between mitral cells (Christie *et al.*, 2005; Christie and Westbrook, 2006). Glutamate receptor dependent currents can be generated in mitral cells of Cx36 knockout animals, however, it requires high frequency bursts of action potentials in mitral cells, suggesting glutamate spillover (Christie

and Westbrook, 2006). Taken together, these data suggests that electrical coupling, dendritic glutamate release, and spillover all participate to generate the slow EPSC recorded in mitral cells. The slow current produced by dendrodendritic circuitry provides postsynaptic amplification of brief afferent input. However, the relative strength and dynamics of dendrodendritic circuitry has not been fully examined across principal cell subtypes. In chapters 2 and 3, I examine the differences in postsynaptic responses between mitral cells and external tufted cells following single stimuli and trains of stimuli, and demonstrate that differences in the strength of dendrodendritic circuitry dramatically alters the response properties of these two cell populations.

Mitral and tufted cells as parallel input paths

In many sensory systems, different cell types encode unique aspects of the sensory stimulus. This is perhaps the most evident in the retina, in which there are multiple functionally separable classes of ganglion cells, each of which encode unique features of the visual scene (Sanes and Masland, 2015). Similar coding strategies are likely used in the olfactory bulb, as emerging evidence suggests that mitral cells and tufted cells differentially respond to afferent input.

Mitral cells and external tufted cells encode distinct stimulus features: Mitral and tufted cells have unique responses to odorant stimulation, and as a result of different levels of feedforward inhibition, each cell type is differentially tuned to structurally similar odorants (Nagayama *et al.*, 2004). Mitral cells

receive comparatively larger feedforward inhibition (Geramita *et al.*, 2016; Geramita and Urban, 2017), which results in relatively narrow odorant tuning (Kikuta *et al.*, 2013). In brain slices, tufted cells receive stronger ORN input following electrical stimulation and are intrinsically more excitable than mitral cells (Burton and Urban, 2014). As a result, tufted cells respond to odorants at lower concentrations and have more consistent firing rates across varying odorant concentrations *in vivo* (Nagayama *et al.*, 2004; Igarashi *et al.*, 2012; Fukunaga *et al.*, 2012; Kikuta *et al.*, 2013). Conversely, mitral cells show a prominent delay at low odorant concentrations, which decreases at higher concentrations, (Fukunaga *et al.*, 2012), which may allow mitral cells to encode odorant concentration. Despite these results, the synaptic mechanisms that generate these distinct responses are not well understood. The distinct responses of mitral cells and external tufted cells, and how they may contribute to parallel processing of common afferent input are explored in chapters 2 and 3.

Mitral cells and external tufted cells have distinct axonal projections:

Axonal tracing also suggests that mitral cells and tufted cells compromise distinct parallel pathways, as they project to non-overlapping regions of olfactory cortex (Nagayama *et al.*, 2004; Igarashi *et al.*, 2012). Tufted cells project to a relatively circumscribed region of olfactory cortex, including the anterior olfactory nucleus, anterior piriform cortex and olfactory tubercle. Conversely, mitral cells innervate a much larger portion of olfactory cortex, including the anterior olfactory nucleus, anterior and posterior piriform cortex, olfactory tubercle and lateral entorhinal cortex (Igarashi *et al.*, 2012). Whether external tufted cells project to olfactory

cortex remains controversial. Although anatomical tracing studies (Nagayama *et al.*, 2004; Igarashi *et al.*, 2012) suggest that external tufted cells project to higher areas of cortex, the spectrum of tufted cells within the external plexiform layer and glomerular layer can be ambiguous at the anatomical level. If external tufted cells do in fact project to olfactory cortex, it is unclear what role they play in higher olfactory processing.

Juxtaglomerular cells shape principal cell and afferent activity

As in most circuits, the interplay of excitation and inhibition shapes the response properties of neurons, resulting in unique synaptic computations. In the olfactory bulb, intrinsic inhibitory interneurons are located in the glomerular layer, external plexiform layer, and granule cell layer (Nagayama *et al.*, 2014), and play a critical role in lateral inhibition and afferent gain control (Egger and Urban, 2006; Shao *et al.*, 2009; Banerjee *et al.*, 2015). Although granule cells play an important role in mediating glomerulus-independent lateral inhibition and recurrent inhibition (Egger and Urban, 2006), their function is outside of the scope of this dissertation.

Juxtaglomerular interneurons control the gain of afferent input: Juxtaglomerular interneurons form a heterogeneous population of interneurons surrounding each glomerulus. There are two primary juxtaglomerular neurons, with complementary, yet distinct function. Periglomerular neurons are exclusively GABAergic and ramify in a single glomerulus (Shao *et al.*, 2009;

Kiyokage *et al.*, 2010). Functionally, periglomerular neurons provide feedforward inhibition to principal neurons (Murphy *et al.*, 2005; Shao *et al.*, 2009), and can also inhibit presynaptic release, via activation of presynaptic $GABA_B$ receptors (Nickell *et al.*, 1994; Bonino *et al.*, 1999; Wachowiak *et al.*, 2005; McGann *et al.*, 2005). Periglomerular neurons provide both tonic and phasic inhibition of the presynaptic terminal (Aroniadou-Anderjaska *et al.*, 2000; Pirez and Wachowiak, 2008; Shao *et al.*, 2009), suggesting that the GABAergic tone provided by periglomerular neurons may function to reduce the high release probability of ORN nerve terminals at rest.

Unlike periglomerular neurons, short axon cells connect multiple glomeruli and release both dopamine and GABA (Maher and Westbrook, 2008; Kiyokage *et al.*, 2010; Borisovska *et al.*, 2013), suggesting they play a unique role in olfactory processing. Interestingly, dopamine and GABA may be released on different timescales, providing further flexibility in modulating the glomerular microcircuit (Borisovska *et al.*, 2013). Functionally, short axon cells inhibit external tufted cells, however, this is followed by rebound excitation mediated by D_1 receptors and a depolarizing shift in I_h currents (Whitesell *et al.*, 2013; Liu *et al.*, 2013, 2016). However, the GABAergic inhibition of external tufted cells has been proposed to reduce the feedforward excitatory drive onto mitral cells, thereby reducing the gain of afferent input (Banerjee *et al.*, 2015).

Emerging evidence suggests that short axon cells may globally control the gain of afferent input across prolonged timescales, as the density of short axon cells is dynamically modulated in response to global changes in olfactory activity

(Baker *et al.*, 1983, 1993). In fact, in Parkinson's disease, despite the loss of dopamine neurons in the midbrain, the density of dopaminergic short axon cells in the olfactory bulb nearly doubles (Huisman *et al.*, 2004; Mundiñano *et al.*, 2011; Doty, 2012*a*). This increased cell density is associated with a reduced sense of smell (Doty, 2012*a*), consistent with a role in the global modulation of afferent input strength.

The function of short axon cells, however, may not be entirely mediated by interactions with principal neurons, as olfactory receptor nerve terminals also express D_2 receptors, activation of which inhibits presynaptic release, via reductions in release probability (Hsia *et al.*, 1999; Ennis *et al.*, 2001; Maher and Westbrook, 2008). Presynaptic inhibition by endogenous activation of short axon cells has not been explored, and may provide a unique means of modulating the strength of afferent input over distinct timescales. I examine the issue of presynaptic inhibition by short axon cells in data chapter 1.

Summary of Work:

In Chapter 1, I examined presynaptic inhibition mediated by short axon cells, which release dopamine and GABA (Maher and Westbrook, 2008; Borisovska *et al.*, 2013). The implications of co-release of multiple neurotransmitters in the olfactory bulb and other circuits are examined in a recent review (Vaaga et al., 2014). I demonstrate that in addition to inhibiting a subset of olfactory bulb principal neurons (Liu *et al.*, 2013; Whitesell *et al.,* 2013), short axon cells also

inhibit the olfactory nerve terminal, suggesting that short axon cells regulate the strength of afferent input. In Chapter 2, I address the question of connectivity between ORNs and principal neurons by single glomerulus stimulation that allows for direct, focal stimulation of ORN afferents. I demonstrate that both mitral cells and external tufted cells receive direct ORN input, however, the postsynaptic processing of afferent input was dramatically different in each cell type. Finally in Chapter 3, I examined the responses of mitral cells and external tufted cells to high frequency ORN stimulation. Surprisingly, mitral cells and external tufted cells responded to common high frequency afferent input with distinct temporal filters, determined by the relative strength of recurrent dendrodendritic excitation in each cell.

Figure 1 Olfactory transduction pathway within olfactory receptor neurons. Olfactory transduction is initiated as an odorant binds a specialized 7-transmembrane domain G-protein coupled odorant receptor. The G_{α} subunit activates adenylyl cyclase III, resulting in increased cAMP levels. cAMP, in turn, gates a cyclic-nucleotide gated cation channel, resulting in Na^{+}, K^{+}, and Ca^{2+} influx. Intracellular Ca^{2+} can further activate a Ca^{2+}-activated Cl^{-} channel, resulting in Cl^{-} extrusion and further depolarization.

Figure 2 Basic components of the olfactory bulb glomerular microcircuit ORNs expressing a specific olfactory receptor (denoted here by soma color) project to a single anatomically and functionally defined cortical module (glomerulus). Two principal cell subtypes (mitral cells and external tufted cells) receive afferent input and project to higher areas of olfactory cortex. A population of heterogeneous juxtaglomerular interneurons can also modulate information transfer within the glomerulus, xincluding short axon cells (SAC). Abbr. MC: mitral cell; ETC: external tufted cell; ORN: olfactory receptor neuron.

Figure 3: Dendrodendritic synapses within the glomerular microcircuit. (A) Modified electron micrograph from Pinching and Powell (1976) illustrating axodendritic inputs (presynaptic ORN terminal pseudo-colored red; mitral cell dendrite pseudo-colored blue) and reciprocal dendrodendritic synapses with juxtaglomerular interneurons (pseudo-colored green). (**B**) Schematic

demonstrating mechanism responsible for generating dendrodendritic amplification via activation of autoreceptors (AMPA/NMDA). Further activation of mGluR1 receptors hyperpolarizes the activation voltage of T-type calcium channels, resulting in further vesicle release. Dendrites associated with the same glomerulus are coupled by gap junctions, which spread the autoreceptor current.

Figure 1

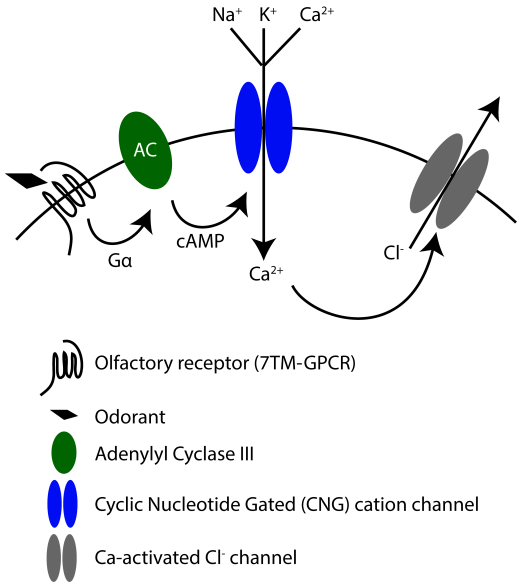
Na+ K+ Ca2+
AC
Gα
cAMP
Ca2+
Cl-
Olfactory receptor (7TM-GPCR)
Odorant
Adenylyl Cyclase III
Cyclic Nucleotide Gated (CNG) cation channel
Ca-activated Cl- channel

Figure 2

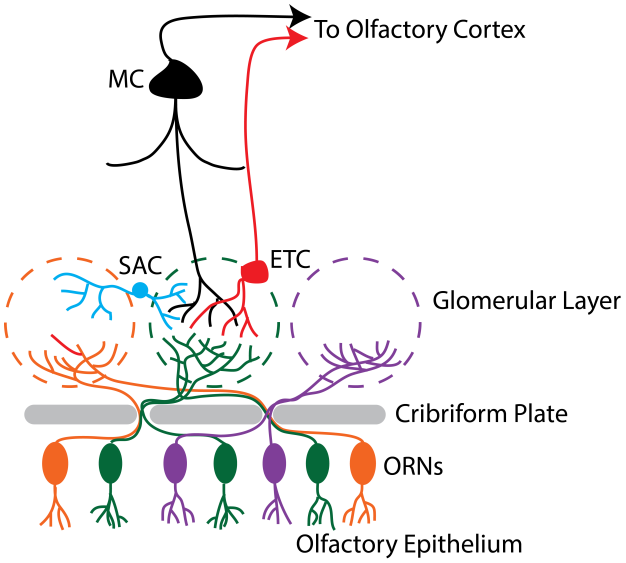
To Olfactory Cortex
MC
SAC
ETC
Glomerular Layer
Cribriform Plate
ORNs
Olfactory Epithelium

Figure 3

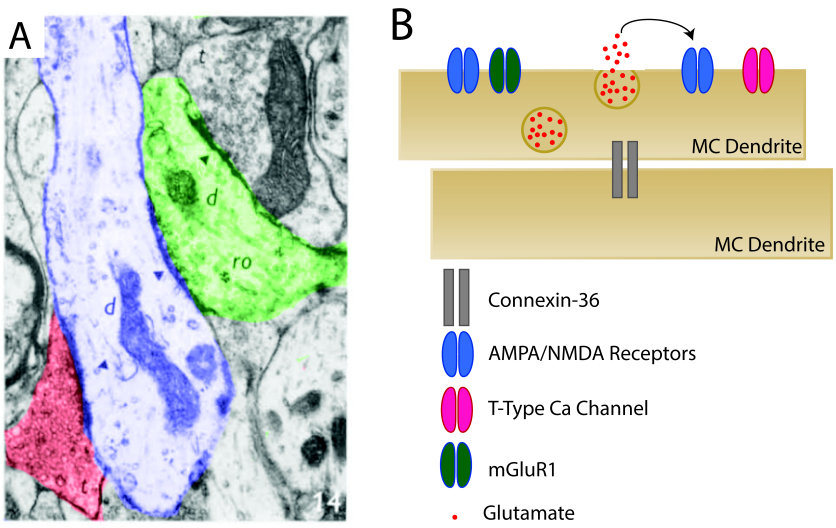
A
t
d
ro
d
t
B
MC Dendrite
MC Dendrite
Connexin-36
AMPA/NMDA Receptors
T-Type Ca Channel
mGluR1
Glutamate

Chapter 1

Presynaptic gain control by endogenous cotransmission of dopamine and GABA in the olfactory bulb

Christopher E. Vaaga[1,2], Jordan T. Yorgason[1], John T. Williams[1], Gary L. Westbrook[1]

[1]Vollum Institute, Oregon Health and Science University, Portland OR, USA, 97239

[2] Neuroscience Graduate Program, Oregon Health and Science University, Portland OR, USA, 97239

Published in Journal of Neurophysiology, March 2017

(DOI: 10.1152/jn.00694.2016)

Abstract:

In the olfactory bulb, lateral inhibition mediated by local juxtaglomerular interneurons has been proposed as a gain control mechanism, important for de-correlating odorant responses. Among juxtaglomerular interneurons, short axon cells are unique as dual-transmitter neurons that release dopamine and GABA. To examine their intraglomerular function, we expressed channelrhodopsin under control of the DAT-cre promoter, and activated olfactory afferents within individual glomeruli. Optical stimulation of labeled cells triggered endogenous dopamine release as measured by cyclic voltammetry, and GABA release as measured by whole-cell $GABA_A$ receptor currents. Activation of short axon cells reduced the afferent presynaptic release probability via D_2 and $GABA_B$ receptor activation, resulting in reduced spiking in both mitral and external tufted cells. Our results suggest that short axon cells influence glomerular activity not only by direct inhibition of external tufted cells, but also by inhibition of afferent inputs to external tufted and mitral cells.

New and Noteworthy:

Sensory systems, including the olfactory system, encode information across a large dynamic range, making synaptic mechanisms of gain control critical to proper function. Here we demonstrate that a dual-transmitter interneuron in the olfactory bulb controls the gain of intraglomerular afferent input via two distinct mechanisms: presynaptic inhibition as well as inhibition of a

principal neuron subtype, and thereby potently controls the synaptic gain of afferent inputs.

Introduction:

In the olfactory bulb, odorant identity is largely encoded in the spatial map of activated glomeruli (Rubin and Katz, 1999; Wachowiak and Cohen, 2001). One of the computational challenges of encoding odorant identity is the need to discriminate patterns of activated glomeruli, especially at high odor concentrations, where the spatial map is confounded by weak activation of many glomeruli (Cleland, 2010). Lateral inhibition between glomeruli may serve this function by filtering out weakly activated glomeruli (Cleland, 2010; Banerjee *et al.*, 2015), thereby increasing the signal to noise ratio. Short axon cells release both dopamine and GABA and broadly connect multiple glomeruli, and thus are well positioned to mediate lateral inhibition across glomerular microcircuits (Maher and Westbrook, 2008; Kiyokage *et al.*, 2010; Whitesell *et al.*, 2013; Borisovska *et al.*, 2013; Liu *et al.*, 2013; Banerjee *et al.*, 2015). Although many recent studies have examined the postsynaptic contribution of short axon cells to olfactory processing (Whitesell *et al.*, 2013; Liu *et al.*, 2013, 2016; Banerjee *et al.*, 2015), none have addressed the role of short axon cells in modulating the presynaptic terminal, which expresses D_2 and $GABA_B$ receptors (Maher and Westbrook, 2008). We examined the effects of endogenously released dopamine and GABA on afferent input to the olfactory bulb circuit using optogenetic targeting in acute mouse brain slices. Endogenous dopamine and GABA reduced

the olfactory receptor neuron (ORN)-evoked EPSC in mitral cells and external tufted cells, by a $GABA_B$ and D_2 mediated decrease in presynaptic release probability. Our results suggest that short axon cells have two distinct and computationally unique mechanisms to modulate the flow of information into the circuit: inhibition of external tufted cells and inhibition of presynaptic release.

Methods:

Animals: We used male and female mice (C57Bl/6J; p24-42). To express channelrhodopsin (ChR2) in dopaminergic short axon cells, a $DAT^{IREScre}$ transgenic mouse line was crossed to the Ai32 ChR2-YFP reporter line. Because of a moderate loss of dopamine transporter (DAT) expression in homozygous mice (Bäckman *et al.*, 2006), only heterozygous $DAT^{IREScre}$ mice were used. The Oregon Health and Science University Institutional Animal Care and Use Committee (IACUC) approved all animal procedures.

Slice preparation and electrophysiology: Acute brain slices were prepared as in Vaaga and Westbrook (2016). Whole-cell voltage- and current-clamp recordings were made from mitral cells and external tufted cells; cell-attached recordings were made from $ChR2^+$ short axon cells. Mitral cells and external tufted cells were distinguished morphologically as described previously (Hayar *et al.*, 2005). ORN-evoked EPSCs were elicited with a theta electrode as in Vaaga and Westbrook (2016), with an inter-stimulus interval of 10 seconds. To optically stimulate $ChR2^+$ short axon cells, LED illumination (2 ms, 470 nm; 16 mW/mm^2) was provided through a 40x objective, such that the maximal area of illumination

was approximately 450 μm in diameter. Given that a single glomerulus is approximately 100 μm in diameter (McCormick and Shepherd, 2004), this field illumination is predicted to activate SACs associated with the intraglomerular (target) glomerulus ±2 glomeruli in either direction. Therefore, this illumination pattern is predicted to strongly activate intraglomerular inhibition from SACs associated with the target glomerulus. Trials optically activate short axon cells included 5 LED flashes (2 ms each) at 10 Hz, 300 ms prior to ORN stimulation, unless otherwise noted. ORN-evoked responses were recorded with a potassium-based internal solution that contained (in mM): 130 K-gluconate, 20 KCl, 10 HEPES, 0.1 EGTA, 4 MgATP, 0.3 NaGTP, 0.07-0.1 Alexa-594 hydrazide (osmolality adjusted to 295, pH adjusted to 7.2 with KOH). GABAergic currents were recorded with a cesium-based internal solution, which contained (in mM): 125 CsCl, 10 HEPES, 10 EGTA, 2 MgATP and 0.3 NaGTP, 10 phosphocreatine 0.07-0.1 Alexa-594 hydrazide (osmolality adjusted to 290, pH adjusted to 7.2 with CsOH). We made no correction for the liquid junction potential (-7 mV). The intracellular sodium channel blocker QX-314-Cl was included (5 mM) in voltage clamp experiments. Cell-attached recordings were made using the K-gluconate internal and holding the pipette at -70 mV after achieving a gigaohm seal. All recordings were done at room temperature. Unless otherwise noted, cells were voltage clamped at -70 mV. Data was acquired using a Multiclamp 700B amplifier and AxographX acquisition software. Data was digitized at 10 kHz with a 4 kHz low-pass Bessel filter. Series resistance was continually monitored with a hyperpolarizing voltage step, and cells with >30% change were excluded from

analysis. For current clamp recordings, a hyperpolarizing bias current (-130 pA to -200 pA) was injected to maintain the membrane voltage at -60±5 mV. All drugs were bath applied by a recirculating pump. The drugs (Abcam Biosciences, Tocris Biochemicals) included: SR95531 (10 μM), CGP55845 (200 nM), sulpiride (500 nM), NBQX (10 μM), CPP (10 μM), SKF97541, quinpirole, and SCH23390 1 μM). All drugs were prepared as stock solutions according to manufacturer specifications.

Fast Scanning Cyclic Voltammetry: Olfactory bulb slices were prepared as above; dorsolateral striatum slices were prepared as in described previously (Ford *et al.*, 2010). Voltammetry recordings were collected and analyzed using Demon Voltammetry and Analysis (Yorgason *et al.*, 2011) and IgorPro (Wavemetrics, Lake Oswego OR). Using DIC optics, carbon fibers electrodes (7 μm x 150 μm) were placed either in a glomerulus or into the dorsolateral striatum. The voltage across the carbon fiber electrode was linearly ramped in a triangular waveform (-0.4 V to 1.2 V) at a scan rate of 400 V/s. Cyclic voltammograms were recorded at 10 Hz and used to generate current traces by plotting the oxidation peak current (current at 0.6 V) as a function of time. Dopamine release was stimulated every 2-3 minutes optogenetically with a 20 pulse, 10 Hz, 2 ms LED protocol. Voltammetry current traces and cyclic voltammograms represent the average of at least 3 sweeps.

Immunofluorescence: $DAT^{IREScre/WT}$;$Rosa26^{LSL\text{-}ChR2\text{-}YFP/WT}$ mice were anesthetized with an intraperitoneal injection of 2% 2,2,2-tribromoethanol then transcardially perfused with saline followed by 4% paraformaldehyde (10-12 mL).

Following standard IHC procedures (Chatzi *et al.*, 2015), sections (100 μm) were incubated in a mouse anti-tyrosine hydroxylase (TH) antibody (Sigma; monoclonal; 1:20,000) overnight at 4°C, then incubated in secondary antibodies (LifeTechologies; goat anti-mouse, 555, 1:200) and a GFP antibody (LifeTechnologies; rabbit anti-GFP, 488, 1:500) for 2 hours at room temperature. Sections were imaged on a Zeiss 780 confocal laser-scanning microscope.

Data Analysis: Electrophysiological data was analyzed in AxographX and Igor Pro (Vers. 6.22A, WaveMetrics, Inc., Lake Oswego, OR, USA). Current clamp recordings were imported and analyzed using the Igor Neuromatic plugin (Jason Rothman, http://www.neuromatic.thinkrandom.com). All voltage clamp traces represent the average of at least 10 sweeps after baseline subtraction. The peak EPSC amplitude was calculated using a built-in routine in AxographX. Action potentials were detected using a threshold criterion in Igor. At least 10 sweeps from a single cell in control condition were averaged and used to normalize subsequent, within-cell manipulations. The onset latency (10% of peak amplitude) for GABAergic currents was calculated with a built in Axograph routine from the time the LED stimulus terminated. Confocal data was analyzed and prepared in ImageJ (imagej.nih.gov). For colocalization cell counts, random glomeruli were imaged and $ChR2^{+}/TH^{+}$ cell counts were performed on all imaged glomeruli from a single confocal section.

Statistics: All data are reported as mean ± SE unless otherwise noted. Statistical analyses were performed in Prism6 (GraphPad Software Inc., La Jolla, CA, USA). Distributions were tested for normality using the Shapiro-Wilks test for

normality. Normally distributed data was analyzed using paired or unpaired t-tests as appropriate. Non-normally distributed data was analyzed using Mann-Whitney tests (unpaired data) or Wilcoxon matched-pairs signed rank test (paired data). For repeated measure experiments, an ANOVA (with a Dunnett's post-hoc test) or Friedman's test (with a Dunn's post-hoc test) was performed. Sample sizes were chosen to detect an effect size of 20% and a power of 0.8. In all experiments, alpha was set to $p<0.05$ and adjusted for multiple comparisons following post-hoc tests.

Results:

Characterization and Validation of ChR2 expression:

To ensure that channelrhodopsin was properly targeted to dopaminergic short axon cells, we counterstained tissue from $DAT^{IREScre/WT}$;$Rosa26^{LSL\text{-}ChR2\text{-}YFP/WT}$ mice with antibodies against tyrosine hydroxylase. As expected, ChR2 was expressed predominantly in the glomerular layer (Figure 1A; Gall et al, 1987; Maher and Westbrook, 2008), with 86.4±1.0% of $ChR2^+$ neurons colocalized with TH immunoreactivity (n=641 cells, 4 animals), and 83.0±1.1% of TH^+ neurons (same cohort) colocalized with ChR2 (Figure 1A). Consistent with the expression of TH in a subpopulation of external tufted cells (Gall *et al.*, 1987), some external tufted cells also expressed ChR2 (Figure 1A).

To determine how effectively ChR2 elicited spiking in $ChR2^+$ cells, we made cell-attached recordings from $ChR2^+$ short axon cells (Figure 1 B). A spike fidelity of 1 was defined as a single action potential per LED stimulus. At low

stimulation frequencies (0.1 Hz), LED stimulation elicited multiple action potentials (cell-attached: 2.5±0.5, n=6 cells, Figure 1 B). At higher frequencies (10 Hz), the spiking was closer to a spike fidelity of 1 (10 Hz: 1.6±0.3 spikes, n=7 cells, Figure 1 B). Therefore, for all subsequent experiments, we used an LED frequency of 10 Hz, to ensure a high fidelity of action potential generation.

Endogenous release of dopamine and GABA

To detect endogenous dopamine release from short axon cells we used fast scanning cyclic voltammetry (FSCV), which measures the cyclic oxidation and reduction of dopamine at characteristic voltages (Figure 1 C). Carbon fiber electrodes were placed in the tissue of interest using DIC optics; in the olfactory bulb, the electrode was placed in the center of a single glomerulus at an oblique angle. In both the olfactory bulb and dorsolateral striatum, optogenetic stimulation (20 pulses at 10 Hz) elicited cyclic voltammograms with oxidation peaks at 0.6 V and reduction peaks at -0.2 V, consistent with endogenous dopamine release (Figure 1 D). Interestingly, the voltammetric signals recorded in the olfactory bulb were much smaller (1.08±0.22 nA; n=12 slices from 3 animals) and slower (tau: 7.82±1.04 sec; n=12 slices from 3 animals) than in the dorsolateral striatum (amplitude: 21.4±4.4 nA; n=6 slices from 1 animal; Mann-Whitney test: p=0.001; tau: 1.2±0.1 sec; Mann-Whitney test: p=0.001; Figure 1 E, F).

To detect GABA release, we made whole cell recordings from external tufted cells or mitral cells. Optogenetic activation of short axon cells elicited an

inward current in external tufted cells (41.1±12.1 pA n=5 cells), which was blocked by the $GABA_A$ receptor antagonist SR95531 (2.2±0.4 pA, n=5 cells, Wilcoxon matched-pairs signed rank test: p=0.031). The kinetics of the GABAergic IPSC were consistent with monosynaptic GABAergic transmission (10% onset latency: 6.3±0.8 ms). Interestingly, in 5 of 6 mitral cells examined, optogenetically-evoked GABAergic currents were not detected (Mann-Whitney test (comparing ETC and MC IPSCs): p=0.043; Figure 1 G), consistent with previous reports (Whitesell *et al.*, 2013; Banerjee *et al.*, 2015; Liu *et al.*, 2016). Together, these data indicate that short axon cells release both dopamine and GABA, but that dendrodendritic activation of postsynaptic $GABA_A$ receptors is primarily restricted to external tufted cells.

Presynaptic $GABA_B$ and D_2 attenuation by intraglomerular short axon cells

D_2 and $GABA_B$ receptors are expressed on presynaptic terminals of olfactory receptor neurons, and exogenous agonist application can reduce release probability (Hsia *et al.*, 1999; Ennis *et al.*, 2001; Wachowiak *et al.*, 2005; Maher and Westbrook, 2008). To determine if endogenous release from short axon cells can access the axodendritic glomerular compartment and alter ORN-evoked EPSCs, we paired optogenetic stimulation (5 pulses at 10 Hz) of short axon cells centered around the target glomerulus with theta electrode stimulation of ORN axons (0.1 ms, 100 V) at a delay of 300 ms to allow for sufficient G-protein coupled receptor activation (Figure 2 A). In mitral cells, ORN stimulation elicited a biphasic EPSC with a fast peak of 433.0±76.7 pA (n=8 cells), which

was reversibly attenuated by optogenetic activation of short axon cells (10 Hz LED: 289.5±48.4 pA, 67.4±1.3% of control; Dunnett's post-hoc test: $p<0.01$; recovery: 382.7±60.1 pA, 90.6±4.7% of control, Dunnett's post-hoc test: $p>0.05$, Figure 2 B, C). Similarly, in external tufted cells, ORN stimulation elicited an EPSC (930.1±136.6 pA) that was reversibly attenuated by optogenetic activation of short axon cells (752.4±116.6 pA, 80.2±3.6% of control, n=8 cells, Dunnett's post-hoc test: $p<0.01$; recovery: 932.7±128.9 pA; 101.2±4.1% of control, Dunnett's post test: $p>0.05$, Figure 2 D, E). Interestingly, optogenetic stimulation of short axon cells did not significantly reduce the slow component (measured at 200 ms post stimulus) of the mitral cell EPSC (10 Hz LED: 88.9±4.1% control, Dunnett's post-hoc test: $p>0.05$; recovery: 93.9±3.4% control, Dunnett's post-hoc test: $p>0.05$) or external tufted cell EPSC (10 Hz LED: 10 Hz LED: 84.6±8.8% control, Dunnett's post-hoc test: $p>0.05$; recovery: 105.5±7.4% control; Dunnett's post-hoc test: $p>0.05$). The selective attenuation of the peak EPSC suggests that D_2 and $GABA_B$ activation alters the afferent ORN synapse without altering dendrodendritic release, which is consistent with the idea that the slow dendrodendritic current is all-or-none given sufficient afferent input (Carlson *et al.*, 2000).

In mitral cells, the peak attenuation was blocked by $GABA_B$ and D_2 receptor antagonists CGP55845 (200 nM) and sulpiride (500 nM), respectively (LED: 63.7±4.6 % of control, Dunnett's post-hoc test: $p<0.001$; LED+CPG55845/sulpiride: 106.2±5.6% of control, Dunnett's post-hoc test: $p>0.05$, n=7 cells, Figure 2 F, G). Both receptors contributed to inhibition as

EPSCs were also reduced in either CGP55845 (LED+CGP55845: 85.9±2.6% of control; Wilcoxon matched-pairs signed rank test: p=0.0002, n=13 cells, Figure 2 H), or sulpiride (LED+sulpiride: 76.6±5.7% of control; Wilcoxon matched-pairs signed rank test: p=0.008, n=8 cells, Figure 2 H). Consistent with a presynaptic site of action, optogenetic stimulation of short axon cells significantly increased the paired pulse ratio (control: 0.46±0.04, LED: 0.67±0.08, paired t-test: p=0.002, n=8 cells, Figure 2 I, J).

Short axon cell activation elicits post-synaptic rebound firing in external tufted cells (Liu *et al.*, 2013), which could activate periglomerular neurons, resulting in GABA release. To ensure that the presynaptic ORN inhibition observed was not a result of polysynaptic activation of periglomerular neurons, we repeated the experiments in the presence of the D_1 receptor antagonist SCH23390 (1 μM), which blocks rebound spiking in external tufted cells. The presence of the D_1 antagonist did not reduce the attenuation following short axon cell activation (65.1±3.7% of control; n=3 external tufted cells), suggesting that the GABAergic inhibition observed is a not a result of polysynaptic pathways involving periglomerular cells.

To examine the time-course of the endogenous attenuation, we optogenetically activated short axon cells (5 pulses at 10 Hz) then waited a variable time before stimulating the ORN afferents (50 ms – 4500 ms; Figure 3A). The onset of inhibition was fully developed by 50 ms, the shortest interval used. Consistent with a metabotropic response, the EPSC attenuation persisted for

many hundreds of milliseconds (recovery time constant: 1533.2±335 ms; Figure 3B, C).

To determine the relative strength of the endogenous inhibition, we compared endogenous inhibition with pharmacological activation of either D_2 or $GABA_B$ receptors (Quinpirole or SKF97541, respectively). Quinpirole produced a maximal inhibition of 69.7±4.5% (Figure 3D), whereas SKF97541 produced a maximal inhibition of 81.4±3.6% (Figure 3E). Therefore the maximal inhibition via presynaptic receptors is approximately 80%, as both D_2 and $GABA_B$ are $G_{i/o}$ coupled receptors, and likely act through the same presynaptic signaling cascade (Wachowiak et al., 2005). This data suggests that the endogenous inhibition (~40%) in our slice experiments is sub-maximal.

Effect of ORN attenuation on spiking patterns in mitral cells

Activation of short axon cells *in vivo* can suppress action potential generation in mitral cells (Banerjee *et al.*, 2015), which has been attributed to reductions in disynaptic activation of mitral cells. To determine if presynaptic inhibition of ORNs also affects spiking in mitral cells, we utilized an optogenetic protocol (300 ms between LED and ORN stimulation) following the full decay of $GABA_A$ receptor-mediated currents (Figure 4 A). In external tufted cells, optogenetically evoked GABAergic IPSPs decayed with a time constant of 34.7±2.8 ms and 5 IPSPs at 10 Hz decayed back to baseline within 107.3±6.5 ms (n=3 cells), well short of the 300 ms interval between optogenetic and electrical stimulation. Therefore, this optogenetic protocol was well suited to

isolate the effects of metabotropic receptor-mediated responses on cell spiking. In mitral cells, optogenetic stimulation reduced the number of action potentials from 22.3±6.3 action potentials to 16.9±6.2 (44.4±11.7% reduction; n=8 cells; Wilcoxon matched-pairs signed rank test: 0.016; Figure 4 B, D), and was accompanied by a shift in the first spike latency (control: 4.6±0.2 ms; 10 Hz LED: 7.8±1.1 ms; Wilcoxon matched-pairs signed rank test: 0.031; Figure 4 E, G).

Similarly, in external tufted cells, optogenetic stimulation reduced the number of action potentials from 4.6±1.3 to 3.6±1.4 (32.0±14.6% reduction; n=5 cells, Wilcoxon matched-pairs signed rank tests: 0.031; Figure 4 C, D). This was accompanied by a trend towards a longer first spike latency, however this was not statistically significant (control: 4.2±0.5 ms; 10 Hz LED: 5.3±1.1 ms, n=7 cells; Wilcoxon matched-pairs signed rank test: 0.094, Figure 4 F, G) Together these results suggest that endogenous short axon cell activation can result in reduced ORN-evoked spiking in mitral and external tufted cells.

Discussion:

Our results demonstrate that short axon cells directly inhibit the presynaptic ORN terminal via metabotropic D_2 and $GABA_B$ receptors as well as inhibit external tufted cells via $GABA_A$R-mediated currents (Whitesell *et al.*, 2013; Liu *et al.*, 2013). These two forms of inhibition are distinct because of their location of expression, predicted effects on circuit dynamics, and kinetic profiles. In summary, short axon cell activation may potently control the strength of afferent input, both through dendrodendritic and axodendritic synapses.

Short axon cell inhibition across timescales

Short axon cell activation can inhibit the olfactory bulb circuit over multiple timescales. Ionotropic GABAergic inhibition of external tufted cells persists for a few tens of milliseconds. Functionally, external tufted cells not only project to higher areas of olfactory cortex (Igarashi *et al.*, 2012), but also provide extensive feedforward excitation to local glomerular interneurons and mitral cells (Hayar *et al.*, 2005). Therefore, the rapid, $GABA_A$ receptor-mediated inhibition of external tufted cells, not only inhibits external tufted cell output directly, but may also reduce disynaptic activation of mitral cells, a critical component of synaptic amplification within the circuit. On a timescale of hundreds of milliseconds, our experiments show that endogenous dopamine and GABA release can activate presynaptic D_2 and $GABA_B$ metabotropic receptors, reducing glutamate release from the presynaptic terminal, most likely by reducing calcium currents in ORNs (Wachowiak *et al.*, 2005). Our data suggests that presynaptic inhibition of the ORN reduces spike generation in both mitral and external tufted cells. By inhibiting monosynaptic responses in both mitral and external tufted cells, presynaptic inhibition provides a distinct form of inhibition on a longer timescale than ionotropic GABA conductances.

This temporal disparity may be further accentuated by the long-lasting vesicular release of dopamine from short axon cells, which, in cultured short axon cells, lasts for many hundreds of milliseconds (Borisovska *et al.*, 2013). The extended time course of dopamine release may explain the slow kinetics of

voltammetric dopamine signals observed in the olfactory bulb. Whether dopamine acts via point-to-point or volume transmission in the olfactory bulb is not known, however, the slow envelope of the voltammetric signal suggests that dopamine may inhibit the circuit for many seconds, prolonging presynaptic inhibition. Furthermore, in the olfactory bulb, dopamine uptake may be minimal and clearance may be mediated by catechol-O-methyltransferase (COMT), further slowing the dopamine signal (Cockerham *et al.*, 2016).

The strength of presynaptic inhibition by short axon cells may be dynamically modulated over slow time scales. The expression level of tyrosine hydroxylase in short axon cells is dependent on olfactory activity (Baker *et al.*, 1983, 1993), suggesting that the overall dopamine tone within the olfactory bulb may serve as a mechanism to control the gain of afferent olfactory input on the timescale of days to weeks. Consistent with this hypothesis, increases in dopamine cell density in sporadic Parkinson's disease are accompanied by olfactory deficits including anosmia (Huisman *et al.*, 2004; Mundiñano *et al.*, 2011; Doty, 2012*a*). Our data suggests that the endogenous short axon cell inhibition is not saturated, at least under our experimental conditions. Although endogenous release may never fully saturate presynaptic receptors, these data suggest that the dynamic range of presynaptic inhibition may be quite large. Future studies examining whether short axon cell inhibition is larger when the density of TH^+ short axon cells is higher, as found in Parkinson's disease patients, could provide novel insights into the mechanism of anosmia in Parkinson's disease.

Short axon cell inhibition in multiple glomerular compartments

Multiple experimental factors may account for the relatively modest presynaptic inhibition seen in our experiments. Although individual short axon cells connect between 5 and 100 glomeruli (Kiyokage *et al.*, 2010), some have hypothesized that functionally short axon cells form an all-to-all inhibitory network by heavily interconnecting multiple glomeruli (Cleland, 2010). Such an arrangement may provide a neurophysiological mechanism to produce odorant decorrelation, by inhibiting inputs of weakly activated glomeruli, thereby increasing the odorant evoked signal to noise ratio across glomeruli. Such a circuit arrangement has been proposed, in part, because odorant chemotopy at the level of individual glomeruli is not present (Soucy *et al.*, 2009; Cleland, 2010). Therefore, a neurophysiological mechanism other than nearest-neighbor lateral inhibition may account for odorant decorrelation (Yokoi, 1995; Cleland, 2010). More work is needed to determine whether short axon cells form a functional, all-to-all inhibitory network, or if short axon cell inhibition produces more targeted inhibition to specific glomeruli.

Consistent with the activation of multiple short axon cells across glomeruli, activation of single short axon cells has little effect on the ORN evoked EPSC amplitude (unpublished observation); thus activation of a large ensemble of short axon cells may be necessary for maximizing inhibition. Therefore, in our experiments, limitations from slice preparation, namely severing dendritic arbors, and the number of labeled and activated $ChR2^{+}$ cells may underestimate the extent of presynaptic inhibition achieved *in vivo*. It is also worth noting that in our

experiments the optogenetic stimulation was centered above the target glomerulus, therefore we predominately activated intraglomerular circuitry. Other studies, both *in vitro* and *in vivo* have examined the function of short axon cells in inhibition across glomeruli (Whitesell *et al.*, 2013; Liu *et al.*, 2013; Banerjee *et al.*, 2015). It will be important for future experiments to determine the relative contribution of inter- and intra-glomerular presynaptic inhibition mediated by short axon cells.

Short axon cells can be activated by feedforward excitation by external tufted cells or by direct ORN input (Kiyokage *et al.*, 2010). Dendrodendritic and axodendritic synapses, however, occupy distinct compartments of the glomerulus: dendrodendritic synapses are in the core of the glomerulus whereas axodendritic synapses are localized to the shell (Pinching and Powell, 1971; Kasowski *et al.*, 1999). Because short axon cells can inhibit both external tufted cells and ORN presynaptic terminals, the dendrites of short axon cells either exist in both glomerular compartments, or neurotransmitters released in the dendrodendritic core can diffuse into the axodendritic shell. Despite their name, short axon cells release neurotransmitter from dendrites (Schoppa and Urban, 2003), therefore it is reasonable to assume that external tufted cell-driven short axon cells form reciprocal dendrodendritic synapses whereas ORN-driven short axon cells make dendroaxonic synapses back to the ORN. Such an arrangement may explain why short axon cells only inhibit external tufted cells (but see Liu *et al.*, 2016).

Physiological impact of activation short axon cells

The ability of short axon cells to inhibit principal neurons via two temporally and mechanistically distinct pathways may result in divergent effects on the glomerular circuit. The functional impact of short axon cell activation on external tufted cells involves more than GABAergic inhibition, as D_1 receptor activation in external tufted cells enhances rebound spiking by modulating I_h currents (Liu *et al.*, 2013). This pause-burst firing pattern is predicted to affect glomerular circuitry by engaging inhibitory periglomerular neurons, and producing feedforward excitation (Kiyokage *et al.*, 2010; Najac *et al.*, 2011). Some recent evidence also suggests that short axon cells may directly inhibit mitral cells (Liu *et al.*, 2016), however, we (and others) have failed to detect this current (i.e. (Whitesell *et al.*, 2013; Banerjee *et al.*, 2015)). Our results are consistent with previous reports that short axon cell activation robustly inhibits mitral cell responses both *in vitro* and *in vivo*, suggesting powerful inhibitory control over principal neuron firing (Banerjee *et al.*, 2015; Liu *et al.*, 2016).

The impact of short axon cells on the presynaptic ORN has not been as well characterized. Although bath application of D_2 and $GABA_B$ receptor agonists reduces presynaptic glutamate release (Hsia *et al.*, 1999; Aroniadou-Anderjaska *et al.*, 2000; Ennis *et al.*, 2001; Wachowiak *et al.*, 2005; Maher and Westbrook, 2008), the extent and magnitude to which this occurs has not been explored using physiological stimulation of short axon cells. Although there is *in vivo* evidence to suggest that interglomerular inhibition of the ORN may be modest (McGann *et al.*, 2005), these results used a combination of two odorants to

examine interglomerular inhibition. Such limited odorant mixtures may not be strong enough to engage robust interglomerular inhibition, because the connection probability of any two glomeruli chosen at random is presumably low. Conversely, more recent *in vivo* experiments, have demonstrated that short axon cell activation in distant glomeruli strongly inhibits odorant-evoked responses in mitral cells (Banerjee *et al.*, 2015). Whether this suppression involved presynaptic inhibition was not evaluated. It is worth noting that mitral cells and external tufted cells have unique cellular morphologies and responses to ORN input. External tufted cells, located around each glomerulus, have a much smaller cell body than mitral cells. Furthermore, mitral cells are connected to glomeruli via a long apical dendrite. Therefore, the relative strength of presynaptic inhibition may also vary between cell types, as mitral cells have a smaller monosynaptic ORN current (Vaaga and Westbrook, 2016), and therefore may be more sensitive to small changes in glutamate release.

Acknowledgements: We thank the members of the Westbrook lab for their helpful comments. This work was supported by NS26494 (GLW), National Science Foundation Graduate Research Fellowship DGE-0925180 (CEV), DA040409 (JTY), DA004523 (JTW), and a P30 imaging grant (NS061800)

Figure Legends

Figure 1 Optogenetic activation of short axon cells elicits endogenous dopamine and GABA release. (**A**) Expression of channelrhodopsin (ChR2, green) in short axon cells counterstained with tyrosine hydroxylase (magenta). Double-labeled cells (white, indicated by arrows) were primarily located in the glomerular layer, with some TH^+ external tufted cells in the juxtaglomerular external plexiform layer. (**B**) Cell attached recordings from $ChR2^+$ short axon cells. Optical stimulation (2 ms) reliably evoked spiking in cell attached recordings at frequencies up to 10 Hz. (**C**) Electrochemical reaction demonstrating the cyclic oxidation and reduction of dopamine (top) to dopamine-*o*-quinone at characteristic voltages, which can be detected as a current using fast-scanning cyclic voltammetry. (**D**) Average cyclic voltammograms in olfactory bulb and dorsolateral striatum with oxidation and reduction peaks typical of dopamine. (**E, F**) Average oxidation current as a function of time in the olfactory bulb (**E**) and dorsolateral striatum (**F**) following 20 LED pulses at 10 Hz. Both responses are plotted on the same time scale. (**G**) Optogenetic activation of short axon cells elicits a $GABA_A$ receptor mediated IPSC in external tufted cells (top, black) but not mitral cells (bottom, black). The IPSC is blocked the $GABA_A$ receptor antagonist SR95531 (red).

Figure 2 Short axon cells inhibit the presynaptic ORN terminal via D_2 and $GABA_B$ metabotropic receptors. (**A**) Optogenetic protocol: 5 LED pulses at 10 Hz followed by ORN stimulation (300 ms ISI). This stimulation protocol was used for all subsequent experiments. (**B-E**) Diary plot of the normalized ORN-evoked fast EPSC amplitude (10 second inter-stimulus interval; LED stimulation as in **A**). Activation of short axon cells elicits a reversible attenuation in the ORN-evoked EPSC in mitral cells (**B, C**) and external tufted cells (**D, E**). (**F, G**) Short axon cell inhibition of ORN-evoked currents was blocked by $GABA_B$ and D_2 receptor antagonists (100 nM CGP55845 and 500 nM sulpiride). (**H**) Short axon cell activation was capable of eliciting inhibition in the presence of either CGP55845 or sulpiride. (**I, J**) Activation of short axon cells alters the paired pulse ratio, suggesting changes in release probability from the ORN. Scale bar in (**B**) 100 pA; 20 ms. Scale bar in (**D**) 200 pA; 20 ms.

Figure 3: Timecourse of endogenous inhibition and maximal pharmacological inhibition. (**A**) Optogenetic stimulation protocol: 5 LED pulses at 10 Hz followed by ORN stimulation at various intervals (50 ms – 4500 ms). (**B**, **C**) Timecourse of attenuation by optogenetic stimulation of short axon cells. Inhibition was maximal at the shortest intervals tested (50 ms), and recovered with a single exponential with a time constant of 1533.2±335 ms. Attenuation recovered to baseline levels by approximately 4500 ms. (**D**) Pharmacological inhibition of afferent input by the D_2 agonist quinpirole at various

concentrations. (**E**) Pharmacological inhibition of afferent input by the $GABA_B$ agonist SKF97541.

Figure 4 Presynaptic inhibition of mitral cell and external tufted cell afferents reduces spiking. (**A**) Optogenetic protocol: 5 LED pulses at 10 Hz followed by ORN stimulation (300 ms ISI). (**B**) Mitral cell spiking induced by ORN stimulation in control (top, black) and following short axon cell activation (bottom, blue). (**C**) External tufted cell spiking induced by ORN stimulation in control (top, black) and following short axon cell activation (bottom, blue). (**D**) Optogenetic stimulation of short axon cells significantly reduced the ORN evoked spiking in both mitral and external tufted cells. (**E, F**) Higher temporal resolution of the first couple of spikes elicited in control (black) and following LED stimulation (blue) in mitral cells (**E**) and external tufted cells (**F**). Optogenetic stimulation of short axon cells significantly shifted the first spike latency in mitral cells, but not external tufted cells.

Figure 1:

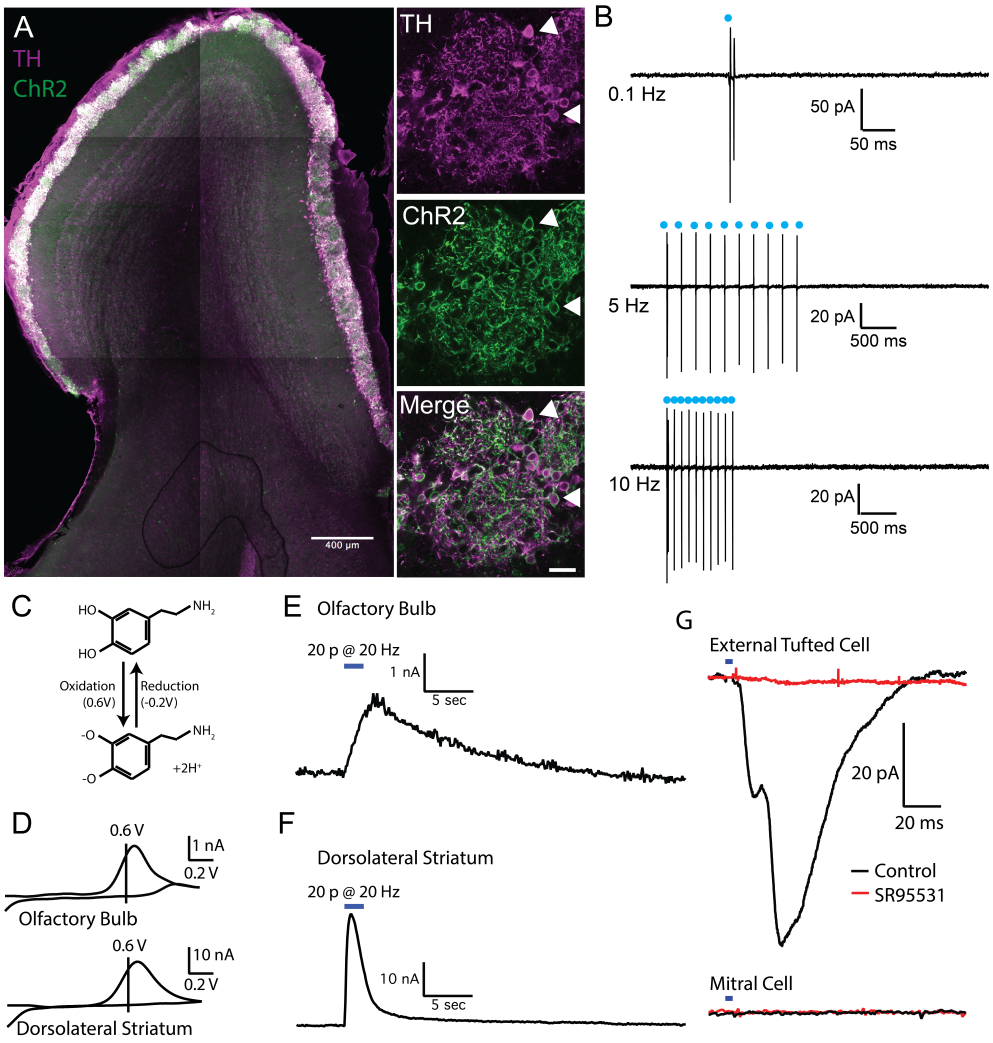
A
TH
ChR2
400 µm
TH
ChR2
Merge
B
0.1 Hz
50 pA
50 ms
5 Hz
20 pA
500 ms
10 Hz
20 pA
500 ms
C
HO
HO
NH2
Oxidation
(0.6V)
Reduction
(-0.2V)
-O
-O
NH2
+2H+
D
0.6 V
1 nA
0.2 V
Olfactory Bulb
0.6 V
10 nA
0.2 V
Dorsolateral Striatum
E
Olfactory Bulb
20 p @ 20 Hz
1 nA
5 sec
F
Dorsolateral Striatum
20 p @ 20 Hz
10 nA
5 sec
G
External Tufted Cell
20 pA
20 ms
Control
SR95531
Mitral Cell

Figure 2:

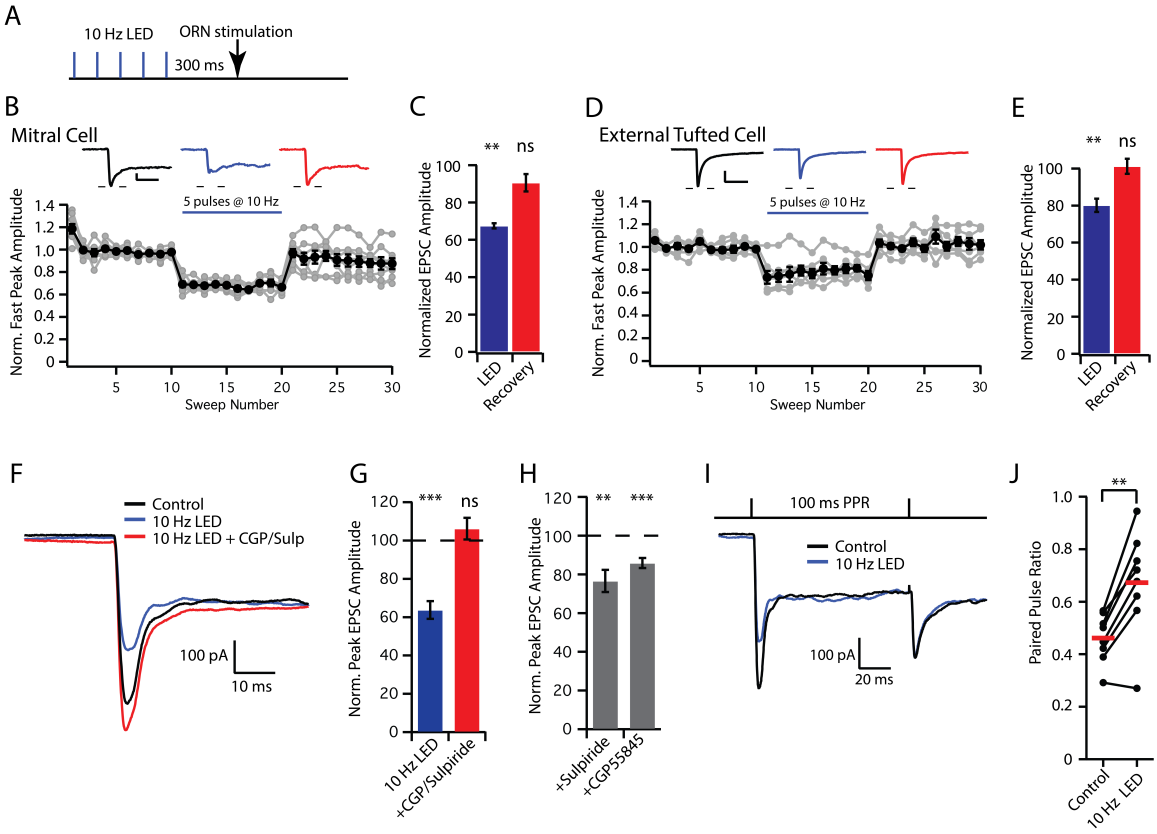
A
10 Hz LED
ORN stimulation
300 ms
B
Mitral Cell
5 pulses @ 10 Hz
Norm. Fast Peak Amplitude
Sweep Number
C
**
ns
Normalized EPSC Amplitude
LED
Recovery
D
External Tufted Cell
5 pulses @ 10 Hz
Norm. Fast Peak Amplitude
Sweep Number
E
**
ns
Normalized EPSC Amplitude
LED
Recovery
F
Control
10 Hz LED
10 Hz LED + CGP/Sulp
100 pA
10 ms
G
***
ns
Norm. Peak EPSC Amplitude
10 Hz LED
+CGP/Sulpiride
H
**
***
Norm. Peak EPSC Amplitude
+Sulpiride
+CGP55845
I
100 ms PPR
Control
10 Hz LED
100 pA
20 ms
J
**
Paired Pulse Ratio
Control
10 Hz LED

Figure 3:

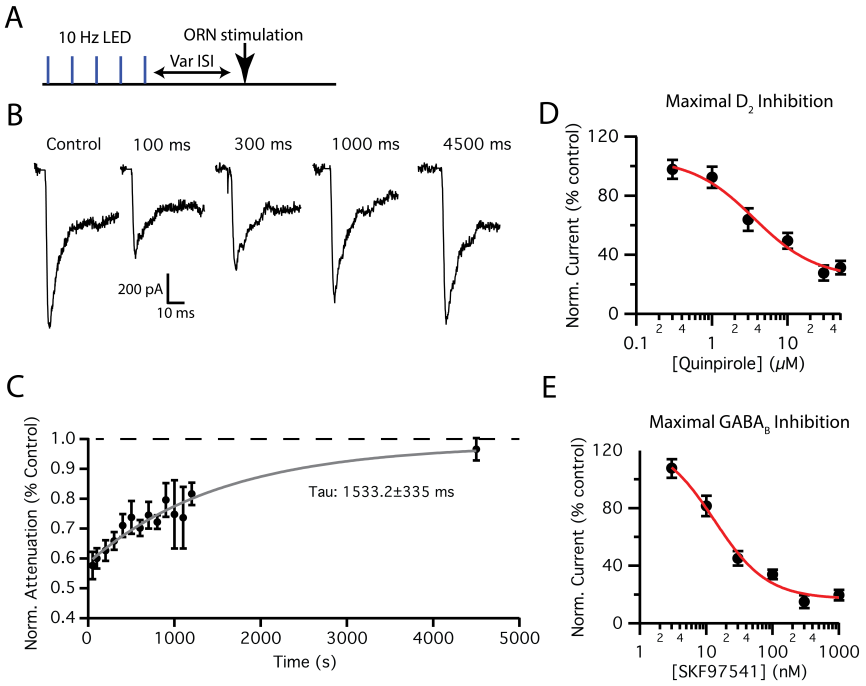
A
10 Hz LED
ORN stimulation
Var ISI
B
Control
100 ms
300 ms
1000 ms
4500 ms
200 pA
10 ms
C
Norm. Attenuation (% Control)
Tau: 1533.2±335 ms
Time (s)
D
Maximal D2 Inhibition
Norm. Current (% control)
[Quinpirole] (μM)
E
Maximal GABAB Inhibition
Norm. Current (% control)
[SKF97541] (nM)

Figure 4:

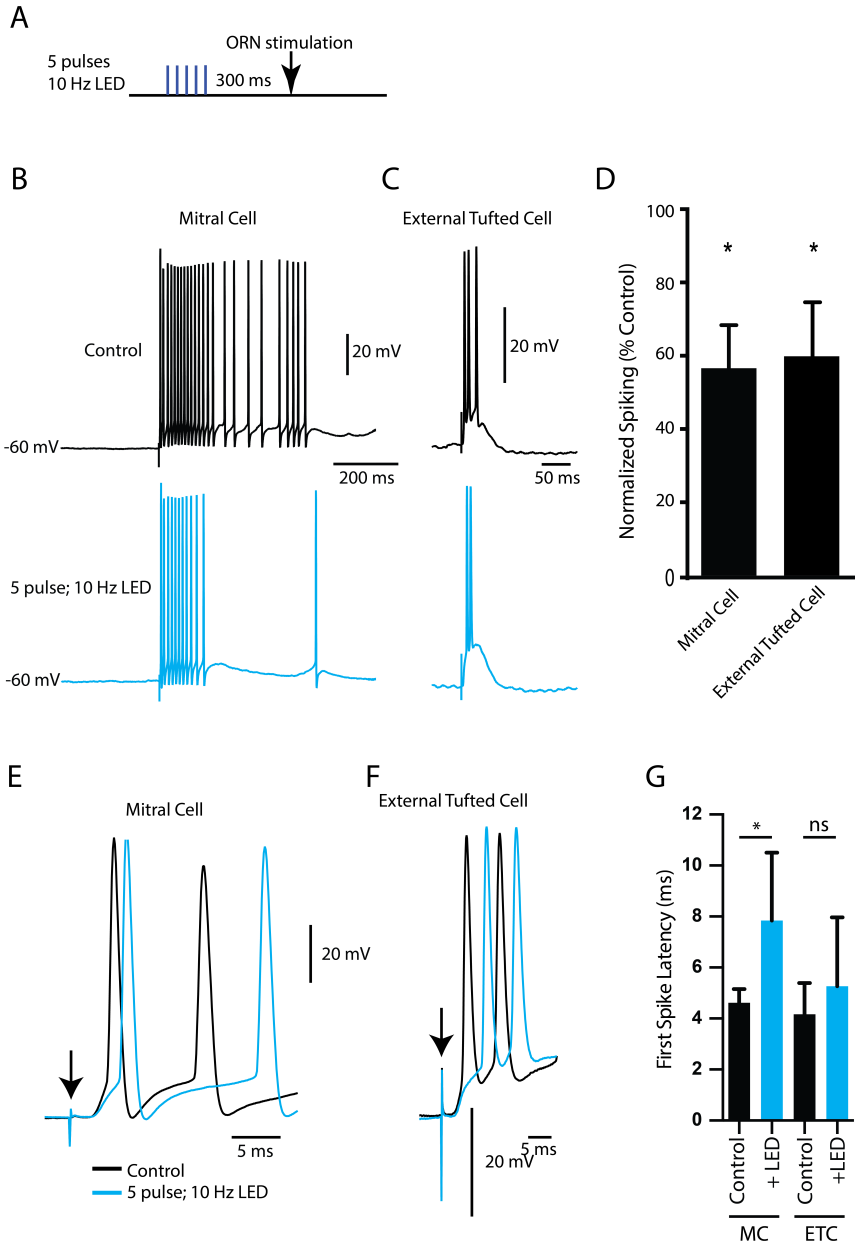
A
5 pulses
10 Hz LED
300 ms
ORN stimulation
B
Mitral Cell
Control
20 mV
-60 mV
200 ms
5 pulse; 10 Hz LED
-60 mV
C
External Tufted Cell
20 mV
50 ms
D
Normalized Spiking (% Control)
100
80
60
40
20
0
*
*
Mitral Cell
External Tufted Cell
E
Mitral Cell
20 mV
5 ms
Control
5 pulse; 10 Hz LED
F
External Tufted Cell
20 mV
5 ms
G
First Spike Latency (ms)
12
10
8
6
4
2
0
*
ns
Control
+ LED
Control
+LED
MC
ETC

Chapter 2

Parallel processing of afferent olfactory sensory information

Christopher E Vaaga[1,2], Gary L Westbrook[1]

[1]Vollum Institute, Oregon Health and Science University, Portland OR, USA 97239

[2]Neuroscience Graduate Program, Oregon Health and Science University, Portland OR, USA 97239

Published in Journal of Physiology, November 2016 (DOI: 10.1113/JP272755)

Abstract:

Primary olfactory receptor neurons terminate in anatomically and functionally discrete cortical modules known as olfactory bulb glomeruli. The synaptic connectivity and postsynaptic responses of mitral and external tufted cells within the glomerulus may involve both direct and indirect components. For example, it has been suggested that sensory input to mitral cells is indirect through feedforward excitation from external tufted cells. We also observed feedforward excitation of mitral cells with weak stimulation of the olfactory nerve layer, however, focal stimulation of an axon bundle entering an individual glomeruli, revealed that mitral cells receive monosynaptic afferent inputs. Although external tufted cells had a 4.1 fold larger peak EPSC amplitude, integration of the evoked currents showed that the synaptic charge was 5 fold larger in mitral cells, reflecting the prolonged response in mitral cells. Presynaptic afferents onto mitral and external tufted cells had similar quantal amplitude and release probability, suggesting that the larger peak EPSC in external tufted cells resulted from more synaptic contacts. Our results indicate that the monosynaptic afferent input to mitral cells depends on the strength of odorant stimulation. The enhanced spiking we observed in response to brief afferent input provides a mechanism to amplify sensory information and contrasts with the transient response in external tufted cells. These parallel input paths may have discrete functions in processing olfactory sensory input.

Key Points:

- The functional synaptic connectivity between olfactory receptor neurons and principal cells within the olfactory bulb is not well understood.
- One view suggests that mitral cells, the primary output neuron of the olfactory bulb, are solely activated by feedforward excitation.
- Using focal, single glomerular stimulation we demonstrate that mitral cells receive direct, monosynaptic input from olfactory receptor neurons.
- Compared to external tufted cells, mitral cells have a prolonged afferent-evoked EPSC, which serves to amplify the synaptic input.
- The properties of presynaptic glutamate release from olfactory receptor neurons are similar between mitral and external tufted cells.
- Our data suggest that afferent input enters the olfactory bulb in a parallel fashion.

Introduction:

The olfactory bulb is organized into anatomically and functionally discrete cortical modules known as glomeruli. Each glomerulus receives afferent sensory innervation from olfactory receptor neurons (ORNs) expressing the same odorant receptor from a large multi-gene family (Buck and Axel, 1991; Vassar *et al.*, 1994; Ressler *et al.*, 1994; Mombaerts *et al.*, 1996; Treloar *et al.*, 2002). Therefore the spatial map of activated glomeruli across the olfactory bulb surface is representative of odorant identity(Rubin and Katz, 1999; Mori *et al.*, 1999; Wachowiak and Cohen, 2001). Principal neurons send their dendrites to a single glomerulus, thereby preserving the one-to-one connectivity. Principal neurons are broadly categorized as mitral cells and tufted cells, with tufted cells further divided into internal, middle and external tufted cells depending on the position of their cell body (Pinching and Powell, 1971).

Recent studies suggest that external tufted cells play a major role in processing incoming olfactory sensory information. External tufted cells coordinate neuronal elements by providing feedforward excitation to intrinsic interneurons as well as drive activity in mitral/tufted cells through chemical synapses and electrical coupling (Hayar *et al.*, 2004*a*; De Saint Jan *et al.*, 2009; Najac *et al.*, 2011). Here, we define feedforward excitation as a circuit in which ORNs directly activate external tufted cells, which in turn activate mitral cells. This feedforward circuit arrangement has been proposed as the sole means of activating mitral cells (De Saint Jan and Westbrook, 2007; De Saint Jan *et al.*, 2009; Gire and Schoppa, 2009; Najac *et al.*, 2011; Gire *et al.*, 2012). In this view,

mitral cells respond to sensory input via slow disynaptic responses mediated solely by dendrodendritic synapses (Carlson *et al.*, 2000; Schoppa and Westbrook, 2001; De Saint Jan and Westbrook, 2007; De Saint Jan *et al.*, 2009; Gire and Schoppa, 2009; Gire *et al.*, 2012). Although early ultrastructural evidence indicates ORN axon terminals contact mitral cell dendrites (Pinching and Powell, 1971; White, 1973; Kosaka *et al.*, 2001), it remains controversial whether mitral cells receive physiologically relevant input from ORN axon terminals (De Saint Jan *et al.*, 2009; Gire and Schoppa, 2009; Najac *et al.*, 2011; Gire *et al.*, 2012). This is an important issue as mitral cells constitute the majority of principal neurons innervating the glomerular layer, and project extensively to areas of higher olfactory cortex (Igarashi *et al.*, 2012).

To address this question, we used focal stimulation of axon bundles innervating single glomeruli to probe the synaptic connectivity between ORN terminals and their glomerular targets. Whole-cell recordings from mitral and external tufted cells showed that both cell types receive unambiguous, direct afferent input, however, stimulating fewer afferents with diffuse stimulation in the olfactory nerve layer produced slow, polysynaptic currents in mitral cells. In response to focal stimulation, the synaptic charge was substantially larger in mitral cells than external tufted cells. Despite these differences in postsynaptic responses, the paired pulse ratio, an indicator of presynaptic release probability, and the quantal amplitude were similar in both cell types. The distinct properties of external tufted and mitral cell responses to afferent stimuli indicate that glomerular processing involves the integration of these two pathways.

Furthermore, whether a mitral cell shows monosynaptic, polysynaptic, or both, responses will depend on the relative number of activated afferent fibers.

Methods:

Animals. We used adult male and female mice (p21-p42) from WT C57Bl6/J mice, as well as three transgenic mouse strains: Tg(Thy1-YFP) GJrs heterozygous mice, Cx36-/-;mGluR2-GFP+/- mice, and OMP-cre;Rosa26(lsl-ChR2-YFP) mice. The Tg(Thy1-YFP)GJrs (Thy1-YFP mice; (Feng *et al.*, 2000)) mice were on a mixed C57Bl6/CBA background, which did not alter the physiological or morphological properties of neurons within the olfactory bulb (Bartel *et al.*, 2015). Thus experiments from both genetic backgrounds were grouped, where appropriate. The Oregon Health and Science University Institutional Animal Care and Use Committee (IACUC) approved all animal use and procedures.

Slice Preparation. Olfactory bulb slices were obtained as described previously (Schoppa and Westbrook, 2001). Briefly, animals were anesthetized with an intraperitoneal injection of 2% avertin (2, 2, 2-tribromoethanol), and transcardially perfused with 10 mL of 4°C sucrose-based cutting solution oxygenated with 95% O_2 and 5% CO_2 followed by decapitation. The cutting solution contained (in mM): 83 NaCl, 2.5 KCl, 1 NaH_2PO_4, 26.2 $NaHCO_3$, 22 dextrose, 72 sucrose, 0.5 $CaCl_2$, 3.3 $MgSO_4$ (300-310 mOsm, pH: 7.3). The brain was removed and coronally blocked at the level of the striatum. Horizontal sections (250 μm) were cut using a Leica 1200s vibratome. Sections were

recovered for 20-30 minutes in 34-36°C ACSF, which contained (in mM): 125 NaCl, 25 $NaHCO_3$, 1.25 NaH_2PO_4, 3 KCl, 2.5 dextrose, 2 $CaCl_2$, 1 $MgCl_2$ (300-310 mOsm, pH: 7.3). Sections were stored in ACSF at room temperature until being transferred to the recording chamber.

Electrophysiology. Whole-cell voltage clamp and current clamp recordings were made from mitral cells and external tufted cells under visual control using DIC optics and an ORCA II camera system (Hamamatsu). Patch pipettes (3-4 MΩ) contained (in mM): 130 K-gluconate, 20 KCl, 10 HEPES, 0.1 EGTA, 4 MgATP, 0.3 NaGTP, 0.07-0.1 Alexa-594 hydrazide (osmolality adjusted to 295, pH adjusted to 7.21 with KOH). The liquid junction potential of the internal solution was -7 mV and was not corrected. The sodium channel blocker Qx-314-Cl (5 mM) was included in the patch pipette for voltage clamp experiments to block unclamped action potentials. To record NMDA receptor responses, a cesium based internal was used, which included (in mM): 113 CsGluconate, 10 HEPES, 10 EGTA, 17.5 CsCl, 8 NaCl, 2 MgATP, 0.3 NaGTP (osmolality adjusted to 290, pH adjusted to 7.3 with CsOH). All recordings were done at 32-34°C. Data were acquired using a Multiclamp 700B amplifier (Molecular Devices, Sunnyvale CA, USA) and Axograph X acquisition software. Data were low-pass Bessel filtered at 4 kHz and digitized at 10 kHz. The series resistance, generally < 10 MΩ for mitral cells and < 25 MΩ for external tufted cells, was not compensated. Series resistance was continuously monitored with a -10 mV hyperpolarizing step. Cells with greater than 30% change in series resistance were excluded from analysis. Unless otherwise noted, for all voltage clamp

experiments, the holding potential was -70 mV. For current clamp experiments, a hyperpolarizing bias current (usually <200 pA) was injected to maintain the membrane voltage at -60±5 mV.

Mitral cells and external tufted cells were identified morphologically as described previously (Pinching and Powell, 1971; Hayar *et al.*, 2004*a*). Mitral cells were identified by their soma position within the mitral cell layer, the presence of a single apical dendrite innervating a glomerulus, as well as lateral dendrites extending into the external plexiform layer. Mitral cells had an average input resistance of 63.8±5.1 MΩ (min: 32 MΩ, max: 130 MΩ, n=25 cells). External tufted cells were identified by their pear-shaped, large cell bodies located within the outer 1/3 of the glomerular layer. External tufted cells were further distinguished from juxtaglomerular interneurons by the presence of a thick apical tuft ramifying into a single glomerulus and the lack of lateral dendrites (Kiyokage *et al.*, 2010). The average input resistance of external tufted cells was 225.3±19.5 MΩ (min: 52 MΩ, max: 477 MΩ, n=40 cells). We also used YFP expression in the Thy1-YFP transgenic line, which labeled both cell types. All cells were filled with Alexa-594 during the recording, allowing for identification of both cell type and dendritic targeting.

EPSCs were evoked using a constant voltage stimulator (100 μs, 5-100V) in conjunction with a small-bore theta glass electrode (theta electrode) filled with 2M NaCl, or with a bipolar electrode placed in the olfactory nerve layer. The tip diameter of the theta electrode (1-2 μm), provided precise, spatial stimulation because ORN axons innervating a glomerulus fasciculate into tight bundles just

prior to entering the glomerulus (Mombaerts *et al.*, 1996; De Saint Jan *et al.*, 2009; Borisovska *et al.*, 2011; Najac *et al.*, 2011). Although the stimulation voltage used for the theta electrode appears high, the effective current is greatly attenuated by the high impedance of the theta electrode, especially at higher intensities. All recordings were performed on the medial aspect of the olfactory bulb, where the ORN bundle topography is better defined. Recordings were only made if the innervated glomerulus was near the slice surface with a visibly identifiable ORN axon bundle entering from the olfactory nerve layer. Theta electrodes were placed within 20-30 μm of the glomerulus border to avoid stimulating fibers of passage. It is worth noting that our stimulation did not saturate responses, indicating that we were not stimulating every axon in a bundle. In optogenetic stimulation experiments, 2 ms wide-field LED illumination was centered at the glomerulus containing the apical dendrite of the recorded cell.

All drugs were bath applied to the slice via a recirculating pump. The drugs included: 10 μM NBQX to block AMPA receptors, 5-10 μM (R)-CPP to block NMDA receptors, 20 μM CPCCOEt to block mGluR1 receptors, and 3 mM strontium chloride to desynchronize vesicle release. All drugs were purchased from either Tocris Biosciences (Ellisville, MO, USA) or Ascent Scientific (Bristol, UK).

Imaging. Validation of the channelrhodopsin (ChR2) expression patterns following the OMP-cre;Ai32 genetic cross was performed on a Zeiss LSM 780 confocal microscope. Briefly, animals were deeply anesthetized with 2% avertin

(2, 2, 2-tribromoethanol) then transcardially perfused with 4% paraformaldehyde followed by a 24-hour drop fixation. The tissue was then sectioned (100 μm) on a vibratome. Intrinsic ChR2-YFP expression was boosted with a 488-conjugated secondary antibody (Rabbit anti-GFP 488; 2 hours, room temperature). Before mounting onto glass a slide, the tissue was counterstained with DAPI (Sigma-Aldrich, 1:10,000).

Data analysis. Electrophysiological data was analyzed in AxographX or imported into IGOR Pro (Vers. 6.22A, WaveMetrics, Inc., Lake Oswego, OR, USA). Confocal data was analyzed and prepared in ImageJ (imagej.nih.gov). Unless otherwise noted, all voltage clamp traces represent the average of 10 sweeps after baseline subtraction. Peak EPSC amplitude, 10% onset time, peak location, and charge transfer were calculated using built-in routines in AxographX. The total charge transfer was calculated by integrating the current until the EPSC amplitude recovered to 10% of the original peak amplitude (time to 90% recovery). For current clamp recordings, action potentials were detected using a threshold criterion (0 mV) in AxographX. The total number of spikes in each trial as well as the latency to the first spike were calculated then averaged across trials. To measure the time course of AMPA receptor block in paired recordings, a sigmoidal curve was fit to a diary plot of normalized peak EPSC amplitudes using a built-in Igor routine. The time at half-maximal (x_{half}) block was recorded and averaged across cells. Quantal EPSC events were detected using an AxographX scanning template, consisting of a single exponential (-30 pA amplitude, 0.5 ms rise time, 2 ms decay time constant). Miniature EPSCs were

manually reviewed and any events with half-widths > 2 ms were excluded to prevent GABAergic contamination. AMPA/NMDA ratios were calculated using fast AMPA receptor amplitudes at -70 mV and NMDA receptor amplitudes at +40 mV (at 50 ms post-stimulus).

Statistics. All data are reported as means ± SE unless otherwise noted. Statistical analyses were performed in Prism 6 (GraphPad Software Inc., La Jolla, CA, USA). Unless otherwise noted, data were considered as normally distributed and analyzed using paired or un-paired Student's t-test as appropriate. For sequential drug application experiments and paired pulse ratio experiments, a one-way repeated measure ANOVA was used with a Holm-Sidak's multiple comparison post-hoc test. We used two-way repeated measure ANOVAs for experiments in which responses to increasing stimulus intensity were compared, in which the repeated measures represented cell type and stimulus intensity. To determine a cell type interaction, a Holm-Sidak post-hoc test was used to compare mitral cell and external tufted cell responses at a given stimulus intensity. In non-parametric data sets, Mann-Whitney rank comparison tests were used to assess significance. In all experiments, alpha was set to $p<0.05$.

Results:

Single glomerulus stimulation evoked a monosynaptic afferent response in mitral cells

The current view that mitral cells receive indirect, polysynaptic input from external tufted cells is based on perithreshold stimulation in the olfactory nerve layer, designed to avoid directly stimulating dendritic glutamate release (Gire and Schoppa, 2009; Gire *et al.*, 2012). With weak distal bipolar stimulation of the olfactory nerve layer (bipolar electrode placed 6-10 glomeruli anterior to target glomerulus), we also observed a slow current in mitral cells (peak amplitude: 96.9±21.0 pA; time-to-peak: 489.8±106.1 ms post stimulus, n=5 cells) without a significant fast current (peak amplitude measured within 6 ms: 32.7±13.1 pA; one sample t-test p=0.066, Figure 1 A, B). In the same cells, however, focal theta electrode stimulation of an ORN bundle innervating a single glomerulus produced a biphasic EPSC with a prominent fast component (fast peak amplitude: 355.96±59.4 pA, p=0.005; time-to-peak: 4.2±0.2 ms, one sample t-test: p=0.004, paired student's t-test: p=0.01, n=5 cells, Figure 1 A, B).

To ensure that the fast current elicited with theta electrode stimulation was not an artifact of directly stimulating glutamate release from mitral cell dendrites (Schoppa and Westbrook, 2001; Urban and Sakmann, 2002; De Saint Jan and Westbrook, 2007; Najac *et al.*, 2011), a primary concern using this stimulation technique, we placed the bipolar electrode more proximal to the target glomerulus (2-3 glomeruli anterior to the innervated glomerulus) within the olfactory nerve layer. Bipolar stimulation (30-80 V) elicited biphasic EPSCs in

mitral cells, which were indistinguishable from EPSCs elicited with the theta electrode (bipolar fast peak amplitude: 495.3±33.5 pA, theta fast peak amplitude: 356.0±59.4 pA, p=0.08; bipolar time-to-peak: 4.8±0.8 ms, theta time-to-peak: 4.2±0.2 ms, p=0.52, n=5 cells each group, Figure 1 C, D). Together, this data strongly suggests that the monosynaptic current elicited with the theta electrode is not a result of dendritic glutamate release, and further suggests that the relative contributions of the slow and fast currents in mitral cells differ depending on the number of afferents stimulated.

To characterize the spatial spread of stimulation using the theta electrode, mitral cells were filled with Alexa 594, which provided direct identification of the glomerulus innervated by the apical dendrite. When the theta electrode was placed in the center of the ORN bundle approximately 30-50 μm from the edge of the glomerulus (Figure 2 A, B), brief stimulation (0.1 ms) elicited a large, two-component EPSC in all mitral cells examined (n=6 cells). With lateral movement of the theta electrode (10 μm steps), the fast EPSC decayed with a space constant of 11.4 μm (Figure 2 C, D), and was nearly abolished at 30 μm (7.0±5.4% of control), indicating that focal stimulation was limited to the diameter of the axon bundle and also likely did not spread to the dendritic arbor of principal neurons within the glomerulus. We next made paired recordings of external tufted cells innervating neighboring glomeruli separated by at most a single intervening glomerulus (Figure 2 E). Stimulation in the “target” glomerulus evoked a large amplitude EPSC (0.9±0.2 nA; n=12 cells, 6 pairs; Figure 2 F) but failed to elicit an EPSC in cells projecting to the neighboring or “off target”

glomerulus (6.9±1.7 pA; n=12 cells, 6 pairs; p=0.0012; Figure 2 F). In all pairs, moving the theta electrode to the other glomerulus reversed these results (Figure 2 F). Together these data suggest that the theta electrode stimulation produced spatially restricted, single glomerulus stimulation.

To determine if the fast component of the EPSC in mitral cells results from a monosynaptic connection, we stimulated the ORN while monitoring synaptic latency and jitter. Monosynaptic EPSCs are characterized by their short latency (<2 ms) and low synaptic jitter (Berry and Pentreath, 1976). Using theta electrode stimulation at 5 Hz, EPSCs in both mitral cells and external tufted cells showed a short synaptic latency (mitral cell: 1.5±0.07 ms, n=5 cells; external tufted cell: 1.7±0.01 ms, n=4 cells; p=0.27; Figure 3 A, B). Similarly, the synaptic jitter (standard deviation of the EPSC onset times) was not significantly different between mitral cells and external tufted cells (mitral cell: 0.08±0.004, n=5 cells; external tufted cell: 0.07±0.007, n=4 cells; p=0.18; Figure 3 A, B). These latencies are consistent with monosynaptic chemical transmission following axonal stimulation and strongly suggest that both cell types receive monosynaptic input from the olfactory nerve.

If mitral cells only received input from feedforward excitation by external tufted cells, then block of feedforward excitation with an AMPA receptor antagonist should prevent an EPSC in mitral cells. As expected, application of NBQX (10 μM) nearly abolished the ORN-evoked EPSC in external tufted cells by (3.4±0.8% of control; control: 1.3±0.3 nA; NBQX: 0.05±0.01 nA; n=4 cells; p=0.02). However, a monosynaptic EPSC in mitral cells was still present as

measured by the NMDA-receptor current at positive membrane potentials (V_H +70 mV: 212.9±61.7 pA; n=7 cells; Figure 3 C), which was blocked by bath application of the NMDA receptor antagonist, R-CPP (5-10 μM; 5.6±1.5% of control; p=0.017; Figure 3 C, D). The NMDA receptor current had a rise time of 6.9±4.7 ms and a latency of 2.9±0.2 ms consistent with slow activation kinetics of synaptic NMDA receptors. Furthermore, if mitral cells and external tufted cells receive monosynaptic input, the rate of AMPA receptor antagonist block should be similar across both cell types. In paired mitral and external tufted cell recordings, bath application of NBQX reduced the ORN-evoked EPSC in parallel (time to half maximal response amplitude: mitral cell: 125.3±8.9 s; external tufted cell: 129.1±8.4 s; paired Student's t-test p=0.79, NBQX block: mitral cell: 5.9±5.3% of control; external tufted cell: 4.7±1.2% of control, paired Student's t-test: p=0.79, n=4 pairs).

To further validate that the fast current elicited by theta electrode stimulation was not a result of dendritic glutamate release, we also compared activation of mitral and external tufted cells using optical stimulation. Using an OMP-cre;Rosa26(lsl-hChR2-YFP) mouse that expresses the light activated channelrhodopsin selectively in olfactory receptor neurons (Figure 4 A), 2 ms optical stimulation (Figure 4 B) elicited a fast EPSC in both mitral and external tufted cells (mitral cell: 1.2±0.2 nA, n=7 cells; external tufted cell: 1.9±0.6 nA, n=7 cells; Figure 4 C, D). Compared to electrical stimulation, optical stimulation elicited larger fast currents, likely reflecting the optical activation of more ORN fibers. Furthermore, although the synaptic latency and jitter from optical

stimulation were longer than electrical stimulation, due to the intrinsically slower kinetics of channelrhodopsin, there were no statistically significant differences in the synaptic latency or jitter across the two cell types (latency: mitral cell: 5.2±0.2 ms, external tufted cell: 5.0±0.5 ms, p=0.73; jitter: mitral cell: 0.2±0.04, external tufted cell: 0.2±0.04, p=0.78). The fast component of the optically-stimulated EPSC in mitral cells indicates that the response results from monosynaptic input from olfactory nerve axons and not from dendritic glutamate release.

Mitral cells and external tufted cells differentially respond to afferent input

It is well know that afferent stimulation causes a long lasting depolarization in mitral cells (Carlson *et al.*, 2000; Schoppa and Westbrook, 2001), which is mediated, in part, by NMDA-receptor-dependent dendritic release of glutamate (Nicoll and Jahr, 1982; Aroniadou-Anderjaska *et al.*, 1999; Carlson *et al.*, 2000; Christie and Westbrook, 2006; De Saint Jan and Westbrook, 2007; Pimentel and Margrie, 2008; Najac *et al.*, 2011). Theta electrode stimulation also elicited a biphasic EPSC in mitral cells, with a prominent slow component. The monosynaptic currents in both mitral and external tufted cells are larger than reported elsewhere (mitral cell: 322.8±25.4 pA; external tufted cell: 3.1±0.8 nA), however, this larger amplitude reflects stimulation of more axons using the focal, theta electrode stimulation. In mitral cells, the ORN-evoked EPSC duration was 1014.1±126.5 ms (n=8 cells) whereas stimulation elicited a much faster EPSC in external tufted cells (EPSC duration: 27.7±6.9 ms, n=6 cells; p<0.001). To compare the fractional contribution of the slow component, we measured the

amplitude of the slow current at 200 ms post-stimulus. This amplitude was 125.8±26.3 pA or 39.5±3.3% of the peak EPSC in mitral cells (n=8) compared to 27.9±40.6 pA or 0.8±0.5% of the peak EPSC in external tufted cells (n=6; unpaired Student's t-test: p=0.013). Therefore, although a small slow current is present in external tufted cells, the relative contribution of this current to the EPSC is much smaller than in mitral cells.

We next compared the receptor profiles of the two EPSCs by sequentially blocking NMDA, mGluR1 and AMPA receptors. In mitral cells, bath application of CPP reduced the synaptic charge to 24.5±1.1% of control (control: 99.2±8.4 pC; CPP: 24.3±1.1 pC; Holm-Sidak post-hoc test: $p<0.05$; n=8 cells; Figure 5 A, B) without altering the fast peak EPSC amplitude (control: 322.8±25.4 pA; CPP: 286.3±16.5 pA; Holm-Sidak post-hoc test: $p>0.05$; Figure 5 A (inset), C). Addition of CPCCOEt further reduced the synaptic charge to 9.9±0.6% of control (CPP/CPCCOEt: 9.9±0.6 pC; Holm-Sidak post-hoc test: $p<0.05$; Figure 4 A, B) and NBQX abolished the synaptic charge (0.6±0.2% of control; CPP/CPCCOEt/NBQX: 0.6±0.2 pC; Holm-Sidak post-hoc test: $p<0.01$; Figure 5 A, B) and the peak EPSC amplitude (1.8±0.4% of control; -5.9±1.3 pA; Holm-Sidak post-hoc test: $p<0.01$; Figure 5 A (inset), C).

In contrast, bath application of CPP in external tufted cells only produced a non-significant decrease in synaptic charge (control: 26.4±8.1 pC; CPP: 18.4±5.4 pC; Holm-Sidak post-hoc test: $p>0.05$; n=6 cells; Figure 5 D, E) and CPCCOEt had no effect on the synaptic charge (CPP/ CPCCOEt: 17.8±5.1 pC; Holm-Sidak post-hoc test: $p>0.05$; Figure 5 D, E). As in mitral cells, CPP had no

effect on the fast peak EPSC amplitude (92.3±10.5% of control; Holm-Sidak post-hoc test: $p>0.05$; Figure 5 D (inset), F). Consistent with the AMPA receptors producing the majority of the external tufted cell EPSC, NBQX reduced the synaptic charge to 2.1±0.4% of control (control: 26.4±8.1 pC; NBQX: 0.6±0.3 pC; Holm-Sidak post-hoc test: $p<0.05$; Figure 5 D, E;) and the peak amplitude to 0.8±0.1% of control (control: 3.1±0.9 nA; NBQX: 0.02±0.006 nA; Holm-Sidak post-hoc test: $p<0.05$; Figure 5 D (inset), F). These data demonstrate the vastly different kinetic and pharmacological profiles of the two monosynaptic EPSCs.

The slow component of the mitral cell EPSC is thought to result from the NMDA-receptor dependent dendritic glutamate release and not from NMDA receptors apposing afferent nerve terminals (Nicoll and Jahr, 1982; Isaacson, 1999; Aroniadou-Anderjaska *et al.*, 1999; Carlson *et al.*, 2000; Friedman and Strowbridge, 2000; Christie *et al.*, 2001; Schoppa and Westbrook, 2001; De Saint Jan and Westbrook, 2007). We tested this directly in Cx36-/- mice, which eliminates dendrodendritic release (Christie *et al.*, 2005; Christie and Westbrook, 2006; Maher *et al.*, 2009; Gire *et al.*, 2012). The AMPA/NMDA ratio did not differ between mitral cells (4.67±0.27, n=7 cells, Figure 5 G, I) and external tufted cells (4.49±0.82, n=7 cells; $p=0.83$, Figure 5 H, I), indicating that the complement of postsynaptic receptors at afferent synapses within the shell of the glomerulus does not explain the different EPSC timecourses.

Paired recording of mitral and external tufted cells

To directly compare responses to afferent stimulation, we recorded from pairs of mitral and external tufted cells innervating the same glomerulus at a variety of stimulus intensities (Figure 6 A, B). As shown in the stimulus-evoked input-output curve, external tufted cells had a larger fast EPSC amplitude at all stimulus intensities (amplitude at 100 V: external tufted cell: 3.0±0.6 nA; mitral cell: 0.9±0.2 nA; n=6 pairs; $p<0.001$; Figure 6 C-E). Despite a smaller fast EPSC amplitude (Figure 6 C, inset), mitral cells had a roughly 5-fold larger synaptic charge compared to external tufted cells (synaptic charge at 100 V: mitral cell: 120.5±14.9 pC; external tufted cell: 29.3±6.6 pC; $p<0.001$; Figure 6 C, D, F). It is worth noting that the synaptic responses did not saturate, suggesting sub-maximal stimulation of ORN fibers using the theta electrode. There was no significant difference in the synaptic latency between mitral cells and external tufted cells at either high intensity (100 V; ETC: 1.02±0.2 ms; MC: 1.5±0.4 ms, n=6 pairs, $p=0.12$) or low intensity (10 V; ETC: 1.2±0.2 ms; MC: 1.3±0.09 ms, n=6 pairs, $p=0.96$). Low stimulation intensities failed to produce unitary EPSC events, presumably due to the high density of ORN fibers in any given bundle, however, unitary events were elicited in later experiments by desynchronizing release with strontium (Figure 10).

To examine the afferent evoked spiking patterns in both cell types, responses were recorded in current clamp. Cells were injected with bias current (usually <200 pA) to maintain a holding potential of -60±5 mV. Consistent with the higher synaptic charge, brief afferent stimulation in current clamp recordings

generated significantly more spikes in mitral cells (Figure 7 A). At maximal stimulation intensity, ORN stimulation produced 10.5±3.5 action potentials in mitral cells, compared to 4.0±1.6 in external tufted cells ($p<0.001$, n=6 pairs). This trend persisted across stimulation intensities, but was only statistically significant above 10 V (Figure 7 A, B). There was no significant difference in the first spike latency between cell types at maximal stimulation intensity (mitral cell: 2.7±0.78 ms; external tufted cell: 2.4±0.4 ms; $p=0.78$, n=6 pairs) or at low stimulation intensity (10 V; mitral cells: 3.7±0.7 ms; external tufted cells: 3.3±0.8 ms; $p=0.21$, n=6 pairs).

Because Cx36 gap junctions in apical dendrites are required for dendritic glutamate release (Christie *et al.*, 2005; Christie and Westbrook, 2006; Maher *et al.*, 2009), we used Cx36-/- animals to examine the impact of the slow EPSC on mitral and external tufted cell responses. In mitral cells from Cx36-/- animals, ORN stimulation produced a fast EPSC (Figure 8 A), which completely lacked the typical slow phase; reducing the total charge transfer (WT: 99.2±23.8 pC, n=8 cells; Cx36-/-: 14.0±0.8 pC, n=9 cells; $p=0.002$; Figure 8 A, B) and shortening the EPSC duration accordingly (WT: 1014.1±126.5 ms; Cx36-/-: 26.7±3.1 ms; $p<0.0001$; Figure 8 A, C). In external tufted cells from Cx36-/- mice the total charge transfer was also reduced (WT: 26.4±8.1 pC, n=6 cells; Cx36-/- 8.8±0.4 pC, n=7 cells; $p=0.04$; Figure 8 D, E) without a significant change in the EPSC duration (WT: 27.7±6.9 ms; Cx36-/-: 16.88±2.2; $p=0.14$; Figure 7 D, F). The impact of the Cx36-/- on the peak amplitude of the EPSC was quite variable. The peak ESPC amplitude appeared to be larger in mitral cells, but did not reach

statistical significance (WT: 374.5±75.8 pA; Cx36-/-: 629.0±132.32 pA; p=0.13). However, in external tufted cells there was a decrease in the peak EPSC amplitude (WT: 3.2±1.0 nA; Cx36-/-: 1.3±0.2 nA; p=0.04). These differences may result from changes in shunting inhibition in the circuit lacking gap junctions. In current clamp, elimination of the slow component in Cx36-/- mice made the mitral cell spiking phenotype very similar to external tufted cells, producing at most 1-2 action potentials even at maximal stimulation intensities (WT: 10.5±3.5 action potentials, n=5 cells; Cx36-/-: 1.7±0.8, n=7 cells; p=0.016, Figure 8 G, H, I). These results indicate that the monosynaptic current in mitral cells is sufficient to drive both synaptic responses and action potentials, but the slow component dramatically boosts generation of action potentials in mitral cells.

Comparing presynaptic properties

Given the different properties of mitral and external tufted cell responses to afferent stimulation, we examined possible presynaptic mechanisms using paired recordings of mitral and external cells. It is well established that the ORN is a high release probability synapse (Murphy *et al.*, 2004). As expected, both cell types depressed with paired-pulse stimulation (100 ms ISI, 2 mM Ca^{2+}, paired pulse ratio: mitral cells: 0.5±0.05, external tufted cells: 0.6±0.04; p=0.11; n=6 pairs; Figure 9 A). Reducing the external Ca^{2+} to 1.5 mM similarly attenuated the EPSC amplitude in mitral and external tufted cells (mitral cell: 50.7±4.6% of control; external tufted cell: 56.1±5.0% of control; p=0.37; Figure 9 A, B) and increased the paired pulse ratio in parallel (mitral cell: 0.6±0.05; external tufted

cell: 0.7±0.03; Holm-Sidak post-hoc comparisons (2 mM: 1.5 mM Ca^{2+}) mitral cell $p<0.01$; external tufted cell $p<0.01$; n=6 pairs; Figure 9 A,C). The reduction in calcium increased the paired pulse ratio by 126.6±5.4% in mitral cells and by 119.4±4.15% in external tufted cells (p=0.31). Thus afferent inputs onto mitral and external tufted cells have similar release probabilities.

Given the similar release probabilities, the larger fast EPSC amplitude in external tufted cells could result from differences in quantal amplitude or number of synaptic contacts. To test this, we isolated quantal events originating from the afferent nerve terminal, using Cx36-/- mice (Christie *et al.*, 2005; Christie and Westbrook, 2006; Maher *et al.*, 2009). Asynchronous release events, representing quantal release, were elicited by replacing external calcium with strontium to desynchronize vesicle release (Xu-Friedman and Regehr, 1999, 2000; Babai *et al.*, 2014; Williams *et al.*, 2015). Application of strontium (3 mM Sr^{2+};2 mM Mg^{2+}) reduced the fast EPSC amplitude and resulted in asynchronous EPSCs (aEPSCs; Figure 10 A). As shown in Figure 10, the aEPSC amplitude histograms were not normally distributed therefore non-parametric analyses were utilized. There was no significant difference in median quantal amplitude between mitral cells (29.9 pA, n=4 cells, 395 events) and external tufted cells (30.8 pA, n=4 cells, 624 events, Mann-Whitney test, p=0.054, Figure 10 B). Mitral cells had a slightly slower decay (mitral cell: 2.3±0.02 ms; external tufted cell: 1.4±0.3 ms; p=0.03) likely due to dendritic filtering and reduced space clamp of the apical dendrite in mitral cells. Given the similar release probabilities and quantal amplitudes, the larger EPSC amplitude in external tufted cells likely results from

more synaptic contacts. Assuming that the release probability is 0.8 (Murphy et al., 2004), the average peak amplitude of a mitral cell EPSC with our stimulation conditions results from 38.4±4.9 synaptic contacts compared to 59.3±2.4 synaptic contacts for an external tufted cell.

Discussion:

One view of the flow of afferent information into the olfactory system is that olfactory receptor neurons exclusively contact external tufted cells, which then in turn feed forward onto mitral cells directly or via inhibitory interneurons, before projecting to cortical areas. Our results suggest a circuit organization in which both mitral cells and external tufted cells receive monosynaptic afferent input but differentially respond to brief stimulation. Purely feedforward excitation of mitral cells (as in (Gire and Schoppa, 2009; Gire *et al.*, 2012) was only observed in our experiments when weak stimuli were applied to the olfactory nerve layer, i.e. with stimulation of only a few axons to a particular glomerulus. Given that, in mice, ca. 11,000 axons innervate a glomerulus and make approximately 18 synaptic contacts each (Hálasz and Greer, 1993; Klenoff and Greer, 1998; McCormick and Shepherd, 2004), it seems unlikely that only a few ORNs will be activated by odorants. Therefore, purely feedforward excitation is likely not the only means of activating mitral cells. Our data is in agreement with recent computational studies, which suggest that multiple, parallel input pathways accurately predict *in vivo* mitral cell response properties (Carey *et al.*, 2015).

Defining single glomerular inputs

It has long been known that odorants or electrical stimulation of the olfactory nerve trigger responses in both mitral and external tufted cells (Carlson *et al.*, 2000; Schoppa and Westbrook, 2001; Hayar *et al.*, 2004*a*; De Saint Jan and Westbrook, 2007; Griff *et al.*, 2008; Gire and Schoppa, 2009; Najac *et al.*, 2011; Igarashi *et al.*, 2012; Fukunaga *et al.*, 2012; Wachowiak *et al.*, 2013). However, whether mitral cells receive functional monosynaptic input from the olfactory nerve has been controversial. Although initial ultrastructural studies in both the rat and mouse (Pinching and Powell, 1971; White, 1973; Kosaka *et al.*, 2001; Najac *et al.*, 2011) observed synaptic structures between olfactory nerve axons and mitral cell dendrites, physiologically stimulating a monosynaptic current has yielded mixed results. Macroscopic, perithreshold stimulation of the nerve fiber layer in olfactory bulb slices failed to elicit clear monosynaptic currents in mitral cells (Gire and Schoppa, 2009; Gire *et al.*, 2012). However, given that entering axons coursing through the cribriform plate do not organize into glomerular-specific bundles until just prior to entering the glomerulus (Mombaerts *et al.*, 1996), nerve layer stimulation inevitably results in stimulation of only a few axons innervating any given glomerulus, leading to weak activation of many glomeruli. Conversely, more focal stimulation techniques have revealed a direct monosynaptic current (De Saint Jan *et al.*, 2009; Najac *et al.*, 2011), however, direct electrical stimulation of dendritic glutamate release has been raised as a concern(Gire *et al.*, 2012). Therefore, the nature of the synaptic

connectivity between primary sensory neurons and projection neurons in the olfactory bulb has remained contentious. Our results, using spatially restricted, single glomerulus stimulation, demonstrate that monosynaptic mitral cell currents can be elicited by ORN activation (De Saint Jan *et al.*, 2009; Najac *et al.*, 2011). These results confirm a circuit diagram in which mitral cells receive parallel direct and indirect input via the ORN and external tufted cells, respectively.

A few apparent discrepancies with prior studies deserve discussion. The rationale for using peri-threshold stimulation in previous studies was that more direct stimulation of afferent nerve bundles entering individual glomeruli would inadvertently stimulate mitral and external tufted cell dendrites (Gire and Schoppa, 2009; Gire *et al.*, 2012). Our results, however, clearly define the spatial spread of theta electrode stimulation, and preclude this possibility. Furthermore, Gire et al., (2012) suggested that mitral cell monosynaptic contacts, which they observed in Cx36-/- animals, are not functionally relevant because electrical coupling across mitral cell dendrites shunts the fast EPSC current. However, even at low stimulation intensities mitral cells had a monosynaptic component that was sufficient to drive spiking, which is inconsistent with a purely feedforward activation mechanism. Gire and colleagues (2012) also reported predominantly slow currents in mitral cells using optogenetic techniques, however ChR2-mediated activation of ORNs in our experiments always included a monosynaptic component. These differences are likely explained by differences in the expression of ChR2 as well as the ChR2 variants used.

Taken together, these results suggest that mitral cells have two distinct activation patterns: a purely feedforward EPSC and a biphasic EPSC with a prominent monosynaptic response, both of which may be activated depending on the strength of the odorant. Although *in vivo*, sniff-activated odorant responses in mitral cells lag responses in tufted cells (Igarashi *et al.*, 2012; Fukunaga *et al.*, 2012), these differences are on much slower time scales than either monosynaptic or disynaptic activation by afferents, and are more likely due to the efficacy of odor stimulation than to the presence or absence of monosynaptic inputs to mitral cells. Furthermore, computational models in which ORNs form parallel direct and indirect inputs onto mitral cells accurately predict the *in vivo* response properties of mitral cells (Carey *et al.*, 2015), which suggests that a parallel circuit arrangement is sufficient to explain the in vivo responses.

Comparing the response properties of mitral and external tufted cells

Our results confirm that mitral cells as well as external tufted cells have monosynaptic components that originate in the axodendritic shell of the glomerulus (Kasowski *et al.*, 1999; Kim and Greer, 2000; De Saint Jan *et al.*, 2009; Najac *et al.*, 2011). However, the postsynaptic responses in these two pathways were quite different. The EPSC in mitral cells was 35-fold longer because of a slow synaptic current generated by dendritic glutamate release (Nicoll and Jahr, 1982; Carlson *et al.*, 2000; Christie and Westbrook, 2006; De Saint Jan and Westbrook, 2007; Pimentel and Margrie, 2008; Najac *et al.*, 2011), which was 4.5 fold larger in mitral cells. Why external tufted cells lack a more

prominent slow current is unclear, as their dendrites also occupy the core of the glomerulus, which contains the majority of dendrodendritic synapses (Pinching and Powell, 1971; Kasowski *et al.*, 1999; Kim and Greer, 2000; Kosaka and Kosaka, 2005). External tufted cell dendrites are also capable of releasing glutamate (Hayar *et al.*, 2004*a*; De Saint Jan *et al.*, 2009; Najac *et al.*, 2011), and can initiate slow currents in mitral cells (De Saint Jan *et al.*, 2009). Classical dendrodendritic synapses between mitral cells and inhibitory granule cells are reciprocal (Nowycky *et al.*, 1981; Jahr and Nicoll, 1982; Isaacson and Strowbridge, 1998; Schoppa *et al.*, 1998; Bartel *et al.*, 2015) . However, defining excitatory dendrodendritic synapses as reciprocal is difficult because vesicles are not clustered around discrete active zones, but rather dispersed along the dendrite (Pinching and Powell, 1971). In fact in paired recordings, De Saint Jan et al., (2009) demonstrated that action potentials in external tufted cells could drive dendrodendritic EPSCs in mitral cells, but mitral cells were unable to drive EPSCs in external tufted cells, suggesting a unidirectional interaction. Functionally, external tufted cells potently activate inhibitory juxtaglomerular interneurons (Hayar *et al.*, 2004*a*; De Saint Jan *et al.*, 2009; Najac *et al.*, 2011); therefore the brief time course of activation likely contributes to coordination of inhibitory neurons within the circuit.

Despite differences in postsynaptic responses, presynaptic release properties onto mitral cells and external tufted cells were similar. This pattern is perhaps not surprising as olfactory receptor neurons serve primarily as relays between the sensory epithelium and the olfactory bulb, a fact reflected in, for

example, their high turnover rate, simple complement of ion channels, and high transmitter release probability (Graziadei and Graziadei, 1979; Simmons and Getchell, 1981; Trombley and Westbrook, 1991; Murphy *et al.*, 2004). Whether natural stimuli alter the presynaptic properties in these two principal cells has not been examined. Olfactory receptor neurons respond to natural odorants with high frequency bursts of action potentials (Gesteland and Sigwart, 1977; Getchell and Shepherd, 1978; Sicard, 1986; Duchamp-Viret *et al.*, 1999; Savigner *et al.*, 2009; Tan *et al.*, 2010; Martelli *et al.*, 2013), which likely reduces the effective release probability as a result of synaptic depression. For example, auditory nerve fibers have a high initial release probability, however, natural stimulation patterns engage both pre- and post-synaptic depression (Zhang and Trussell, 1994; Borst and Sakmann, 1996; Oleskevich *et al.*, 2000). Given the exclusively monosynaptic responses in external tufted cells, one might expect that synaptic depression would preferentially affect external tufted cell activation more than mitral cell activation.

Mitral and external tufted cells as parallel input pathways

The different response properties between mitral and external tufted cells suggest that these two principal neurons serve as distinct, but parallel, input pathways. It has been suggested that tufted cells serve as a labeled line, encoding odorant identity (Nagayama *et al.*, 2010; Igarashi *et al.*, 2012; Fukunaga *et al.*, 2012). This hypothesis is supported by *in vivo* experiments suggesting that tufted cells fire earlier in the sniff cycle, respond to lower odorant

concentrations, and have more consistent responses across odorant concentrations (Igarashi *et al.*, 2012; Fukunaga *et al.*, 2012; Kikuta *et al.*, 2013). Furthermore, tufted cells *in vivo* have higher odorant evoked firing rates than mitral cells (Nagayama *et al.*, 2004; Griff *et al.*, 2008). However, mitral cells have a more narrowly tuned molecular receptive range resulting from stronger afferent-evoked disynaptic inhibition (Shao *et al.*, 2012; Kikuta *et al.*, 2013), which may allow more effective discrimination between qualitatively similar odorants.

Although external tufted cells have been primarily viewed as local excitatory interneurons, recent evidence suggests that they do in fact project to higher areas of cortex (Nagayama *et al.*, 2010; Igarashi *et al.*, 2012). Interestingly, mitral cells and external tufted cells (in fact, all tufted cells) project to distinct, non-overlapping regions of olfactory cortex (Nagayama *et al.*, 2010; Igarashi *et al.*, 2012), suggesting discrete functions in higher olfactory processing. Mitral cells project broadly to the piriform cortex, entorhinal cortex and amygdala; whereas external tufted cells make extensive local connections within the glomerulus and project to a much more circumscribed regions of anterior piriform cortex and anterior olfactory nucleus (Hayar *et al.*, 2004*a*; De Saint Jan *et al.*, 2009; Kiyokage *et al.*, 2010; Nagayama *et al.*, 2010; Najac *et al.*, 2011; Igarashi *et al.*, 2012).

The robust amplification of brief afferent input in mitral ells compared to the transient response profile of external tufted cells is consistent with the view that mitral cells are important for odorant discrimination. This distinction may be

even more pronounced with natural ORN stimulation patterns (Duchamp-Viret *et al.*, 1999; Savigner *et al.*, 2009; Tan *et al.*, 2010). Overall our results suggest that large transient response of external tufted cells is well positioned to encode the presence of an odorant, and engage glomerular interneurons via feedforward excitation. Conversely, the robust amplification of brief afferent input by mitral cells is well suited to most effectively drive activity in downstream cortical areas.

Acknowledgements: This work was supported by NS26494 (GLW), National Science Foundation Graduate Research Fellowship DGE-0925180 (CEV) and a P30 imaging grant (NS061800). We thank the members of the Westbrook laboratory for their helpful comments. We would also like to thank Dr. Charles Greer for the Thy1-eYFP transgenic mice.

Figure Legends:

Figure 1: Comparing diffuse and focal stimulation. (A) Comparison of synaptic responses recorded in single mitral cells following either bipolar electrode stimulation or theta electrode stimulation (stimulus location indicated by black arrowhead). For bipolar stimulation, the electrode was placed approximately 6-10 glomeruli anterior to the target glomerulus in the olfactory nerve layer (stimulus intensity: 10-40 V). Conversely, for theta electrode stimulation, the electrode was placed in the center of the axon bundle entering the glomerulus. Inset demonstrates the lack of a fast current following bipolar stimulation. (B) Comparison of the fast EPSC amplitude (measured within 6 ms of the stimulus) and the peak EPSC. For theta electrode stimulation, the peak EPSC occurred within 6 ms of the stimulus, however, for bipolar stimulation, the peak EPSC occurred 489.9±106.1 ms after the stimulus. (C,D) Comparison of mitral cell responses to theta electrode and proximal bipolar electrode stimulation. The bipolar electrode was placed closer to the target glomerulus (3-5 glomeruli anterior; stimulus intensity: 30-80 V). Both stimulation paradigms elicited a biphasic EPSC waveform. (E) Comparison of the time-to-peak for bipolar and theta electrode stimulation.

Figure 2: Single glomerulus stimulation using theta glass electrodes. (A) Schematic of recording configuration. A two-barreled glass theta electrode with a tip diameter of 1-2 μm was placed in the center of a visibly identifiable ORN axon

bundle just prior to entering a glomerulus. (B) Mitral cell apical dendrite filled with Alexa 594 dye innervating the depicted glomerulus. Theta electrode (outlined in white) placement in an ORN bundle entering the innervated glomerulus. White dots represent approximately 10 μm steps laterally from ORN bundle. (C, D) Theta electrode stimulation elicited biphasic EPSCs when the theta electrode was placed in the center of the ORN bundle (arrowheads indicate time of stimulation). Moving the theta electrode laterally resulted in a rapid attenuation of the peak EPSC with a space constant of 11.4±1.09 μm (n=6 cells). (E) Paired external tufted cell recording configuration with each cell innervating distinct glomeruli. (F) Stimulation of the "target" glomerulus produced a large EPSC in the corresponding external tufted cell but failed to produce an EPSC in the external tufted cell innervating the "neighboring" glomerulus. Abbreviations: MC: mitral cell; ETC: external tufted cell; ORN: olfactory receptor neuron (axon bundle).

Figure 3: Monosynaptic EPSC in mitral cells, not just external tufted cells. (A,B) Overlay of 50 sweeps recorded in mitral cells and external tufted cells (100 V theta stimulation) demonstrate the short synaptic latency and low synaptic jitter typical of a monosynaptic connection. In mitral cells, NMDA and mGluR1 receptor antagonists (10 μM CPP and 20 μM CPCCOEt, respectively) were included to isolate the AMPA receptor-mediated current. Responses in both cells were peak scaled. The synaptic latency was measured as time to 10% of the peak EPSC response. (C,D) Block of feedforward excitation with AMPA receptor

antagonists (10 μM NBQX) failed to block an NMDA-receptor mediated EPSC in mitral cells when held at positive potentials. The ORN-evoked NMDA-receptor EPSC was blocked by bath application of CPP (10-20 μM). GABA and mGluR1 receptor antagonists (SR95531, 10 μM and CPCCOEt, 20 μM) were also included.

Figure 4: Optogenetic activation of ORNs elicits monosynaptic currents in mitral cells and external tufted cells. (A) Confocal image demonstrating expression of Channelrhodopsin2 in olfactory receptor neurons (green). Cell bodies are stained with DAPI and shown in blue. (B) Schematic illustrating LED illumination (488 nm light, 2 ms widefield LED illumination; 15 mW/mm^2) centered on the innervated glomerulus. (C) In mitral cells, 2 ms LED (denoted by blue arrowhead) illumination elicited a biphasic EPSC with a prominent fast component. The synaptic latency was 5.2 ±0.17 ms and the jitter was 0.2 ±0.03 ms, suggesting monosynaptic connectivity. (inset) overlay of raw traces (grey) and average (black) showing the fast peak of the optically evoked EPSC in mitral cells. (D) In external tufted cells, LED stimulation also elicited a fast EPSC. The synaptic latency was 5.0 ±0.47 ms and the synaptic jitter was 0.2 ±0.04 ms. (inset) overlay of raw traces (grey) and average (black) showing the fast peak of the optically evoked EPSC in external tufted cells. Scale bar 25 μm, Inset 200 pA, 10 ms.

Figure 5: Pharmacology of the slow phase EPSC. (A) Under control conditions, brief afferent stimulation elicited a biphasic, prolonged EPSC in mitral cells. The majority of the slow component was blocked by the NMDA receptor antagonist CPP, and further reduced by the sequential addition of the mGluR1 receptor antagonist CPCCOEt. Bath application of NBQX abolished the fast component of the EPSC. (B) Quantification of the synaptic charge transfer across drug conditions demonstrates the block of the slow EPSC component by NMDA and mGluR1 receptor antagonists. (C) Neither CPP nor CPCCOEt altered the peak EPSC amplitude. (D) Brief afferent stimulation elicited a fast EPSC in external tufted cells. (E) Unlike mitral cells, bath application of CPP and CPCCOEt had no significant effect on the synaptic charge. (F) As in mitral cells, CPP and CPCCOEt did not reduce the peak EPSC amplitude. (G,H) AMPA/NMDA ratio recorded from mitral cells (G) and external tufted cells (H) from Cx36-/- animals to isolate the ORN to principal neuron synapse. (I) There is no significant difference in the AMPA/NMDA ratio between mitral and external tufted cells.

Figure 6: Paired recording comparison of afferent stimulation in mitral cells and external tufted cells. (A) Schematic of recording configuration: paired recordings were obtained from mitral cells and external tufted cells projecting to the same glomerulus (confirmed with Alexa 594 dye fill) and stimulated with a theta electrode. (B) Skeletal reconstruction of cell fills of a typical paired recording. (C, D) Mitral cell (C) and external tufted cell (D) EPSCs evoked by

ORN stimulation. (E) Comparison of peak EPSC amplitudes between cell types across stimulus intensities. Across all stimulus intensities, external tufted cells had a larger peak EPSC amplitude († denotes $p<0.0001$). (F) Conversely, mitral cells had a larger synaptic charge across all stimulus intensities, reflecting the slow EPSC component unique to mitral cells. Scale bar 20 μm.

Figure 7: Slow mitral cell EPSC results in an increased spiking in response to afferent stimulation. (A) Comparison of the spiking responses in mitral cell and external tufted cell across three stimulation intensities (100 V, 60 V, 20 V). All cells were held at -60±5 mV with a bias current to isolate the synaptically evoked spiking responses. (B) Quantification of average number of action potentials as a function of cell type and stimulus intensity. At stimulation intensities greater than 10 V, mitral cells produced significantly more action potentials than external tufted cells.

Figure 8: Synaptic responses in connexin-36 knockout animals. (A) Mitral cell response in wildtype (black) and Cx36-/- animal (red) demonstrating vastly different kinetics and charge redistribution. In mitral cells, EPSCs evoked in Cx36-/- animals had smaller synaptic charge transfer (B) and a shorter EPSC duration (C). (D) Afferent evoked responses in external tufted cells from Cx36-/- animals. (E) External tufted cells from Cx36-/- animals had reduced synaptic charge. (F) There was no significant change in external tufted cell EPSC duration. (G,H) Current clamp recordings from mitral cells in wildtype (G) and

Cx36 -/- (H) animals. (I) The loss of the slow current reduced the total number of spikes produced in mitral cells.

Figure 9: Homogeneous ORN release probability across cellular targets. (A) Paired recording from mitral cell and external tufted cell projecting to the same glomerulus. Paired stimuli (100 ms interval) elicited synaptic depression. Reducing extracellular calcium from 2 mM to 1.5 mM similarly altered the paired pulse ratio in both cell types. (B) Reducing external calcium reduced the fast EPSC peak amplitude to the first stimulus in both mitral cells and external tufted cells. (C) Across pairs, there was no significant difference in the paired pulse ratio between cell types at 2 mM Ca^{2+}. However, decreasing external calcium similarly increased the paired pulse ratio in both cell types.

Figure 10: ORN synapses have similar quantal amplitudes in mitral cells and external tufted cells. (A) Example mitral cell recording from Cx36-/- animal to isolate ORN-evoked currents. Replacing extracellular calcium with 3 mM strontium (red trace) significantly reduced the fast, synchronous EPSC and resulted in asynchronous release events (arrows). (B) Comparison of asynchronous, quantal EPSCs recorded in mitral cells and external tufted cells. Raw traces (C) and histograms (D) of collected asynchronous EPSCs in mitral cell. Slower EPSC kinetics reflects dendritic filtering. Raw traces (E) and histograms (F) of collected asynchronous EPSCs in external tufted cells.

Figure 1:

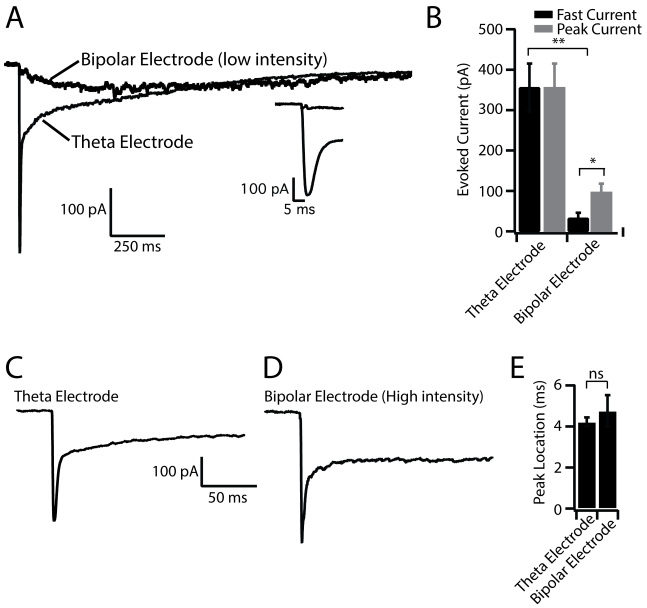
A
Bipolar Electrode (low intensity)
Theta Electrode
100 pA
250 ms
100 pA
5 ms
B
Fast Current
Peak Current
**
*
Evoked Current (pA)
500
400
300
200
100
0
Theta Electrode
Bipolar Electrode
C
Theta Electrode
100 pA
50 ms
D
Bipolar Electrode (High intensity)
E
ns
Peak Location (ms)
6
4
2
0
Theta Electrode
Bipolar Electrode

Figure 2:

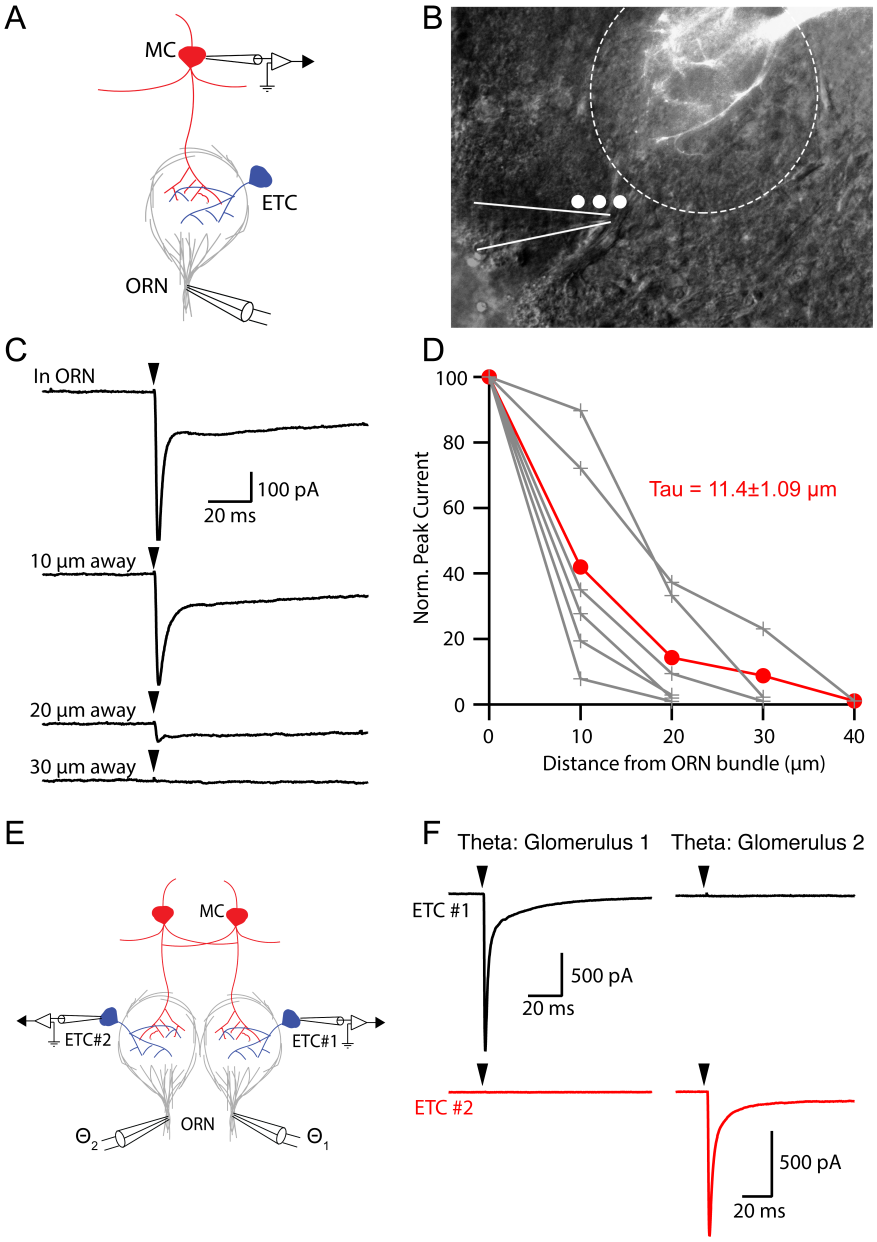
A
MC
ETC
ORN
B
C
In ORN
100 pA
20 ms
10 µm away
20 µm away
30 µm away
D
Norm. Peak Current
Tau = 11.4±1.09 µm
Distance from ORN bundle (µm)
E
MC
ETC#2
ETC#1
ORN
Θ2
Θ1
F
Theta: Glomerulus 1
Theta: Glomerulus 2
ETC #1
500 pA
20 ms
ETC #2
500 pA
20 ms

Figure 3:

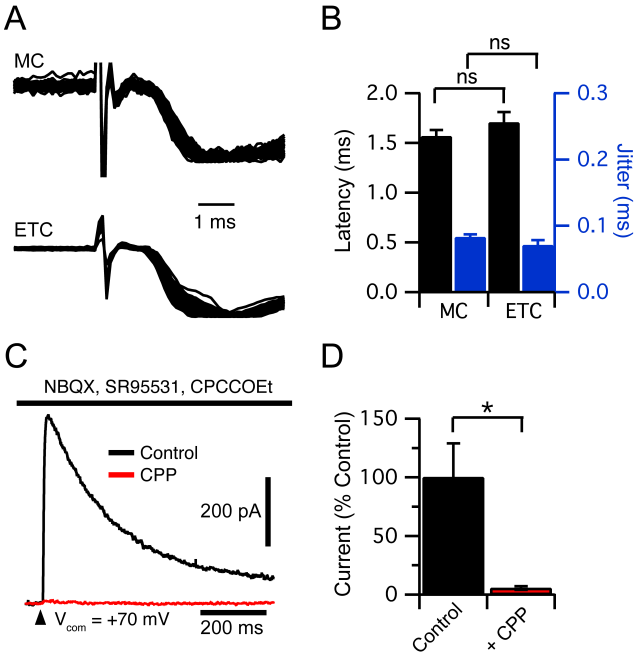
A
MC
ETC
1 ms
B
ns
ns
2.0
1.5
1.0
0.5
0.0
Latency (ms)
0.3
0.2
0.1
0.0
Jitter (ms)
MC
ETC
C
NBQX, SR95531, CPCCOEt
Control
CPP
200 pA
V com = +70 mV
200 ms
D
*
150
100
50
0
Current (% Control)
Control
+ CPP

Figure 4:

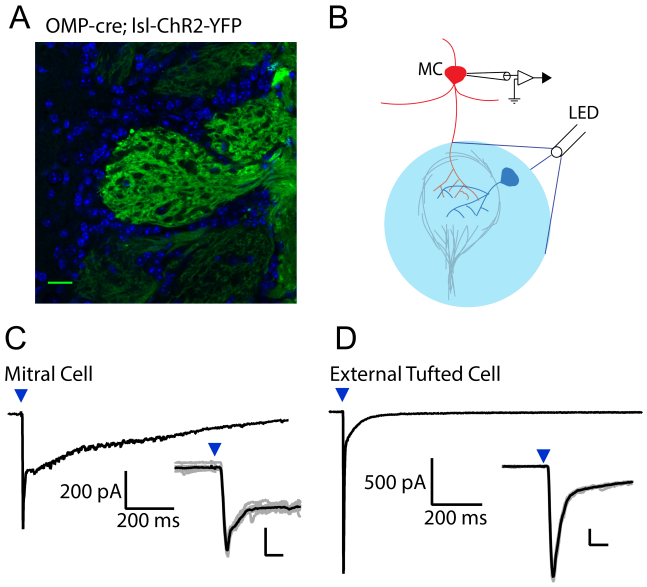
A
OMP-cre; Isl-ChR2-YFP
B
MC
LED
C
Mitral Cell
200 pA
200 ms
D
External Tufted Cell
500 pA
200 ms

Figure 5:

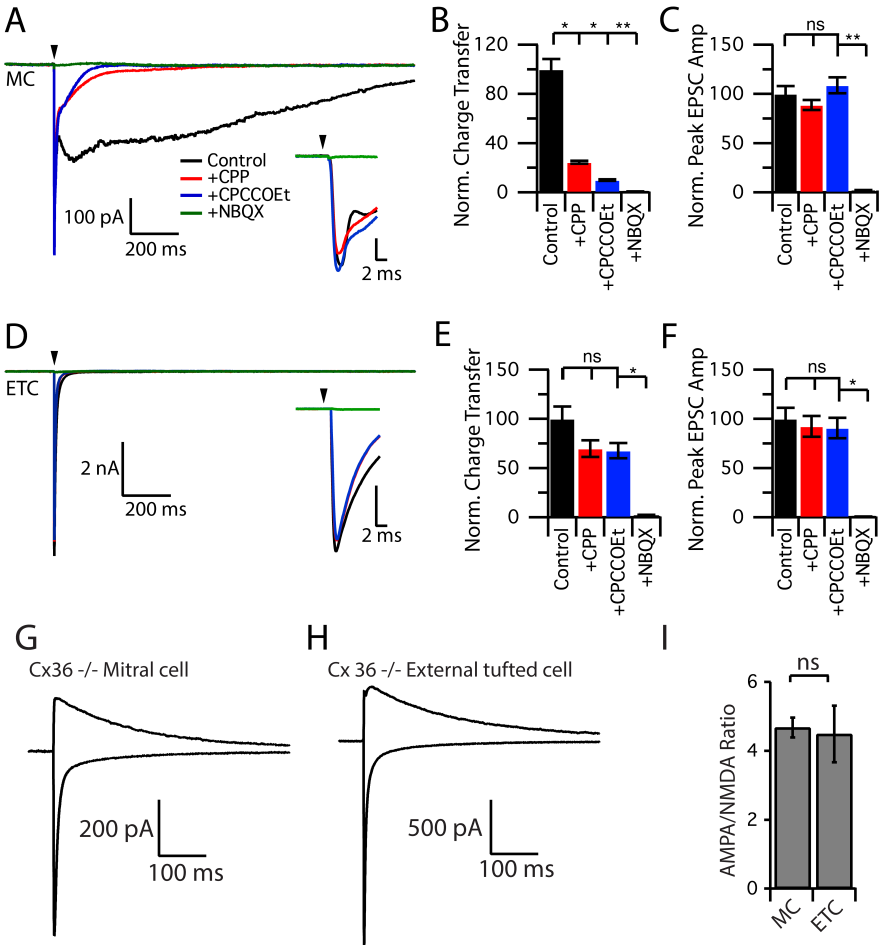
A
MC
Control
+CPP
+CPCCOEt
+NBQX
100 pA
200 ms
2 ms
B
Norm. Charge Transfer
120
80
40
0
*
*
**
Control
+CPP
+CPCCOEt
+NBQX
C
Norm. Peak EPSC Amp
150
100
50
0
ns
**
Control
+CPP
+CPCCOEt
+NBQX
D
ETC
2 nA
200 ms
2 ms
E
Norm. Charge Transfer
150
100
50
0
ns
*
Control
+CPP
+CPCCOEt
+NBQX
F
Norm. Peak EPSC Amp
150
100
50
0
ns
*
Control
+CPP
+CPCCOEt
+NBQX
G
Cx36 -/- Mitral cell
200 pA
100 ms
H
Cx 36 -/- External tufted cell
500 pA
100 ms
I
AMPA/NMDA Ratio
6
4
2
0
ns
MC
ETC

Figure 6:

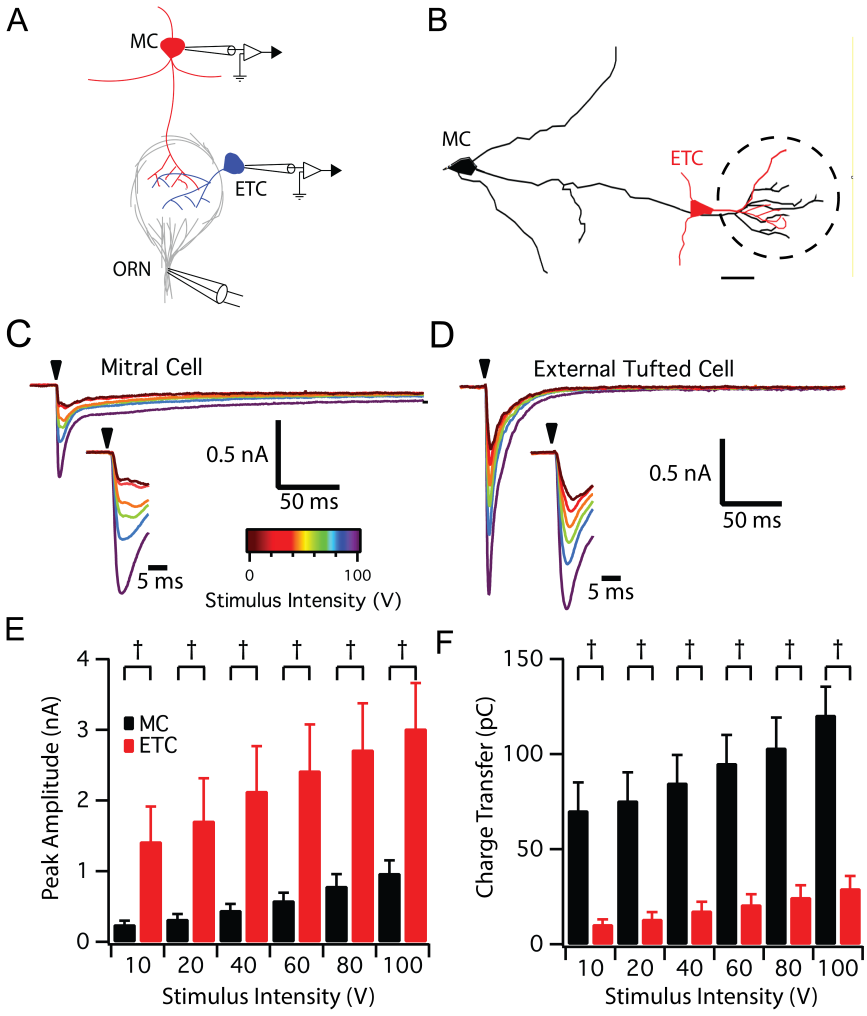
A
MC
ETC
ORN
B
MC
ETC
C
Mitral Cell
0.5 nA
50 ms
5 ms
0
100
Stimulus Intensity (V)
D
External Tufted Cell
0.5 nA
50 ms
5 ms
E
Peak Amplitude (nA)
MC
ETC
0
1
2
3
4
10
20
40
60
80
100
Stimulus Intensity (V)
F
Charge Transfer (pC)
0
50
100
150
10
20
40
60
80
100
Stimulus Intensity (V)

Figure 7:

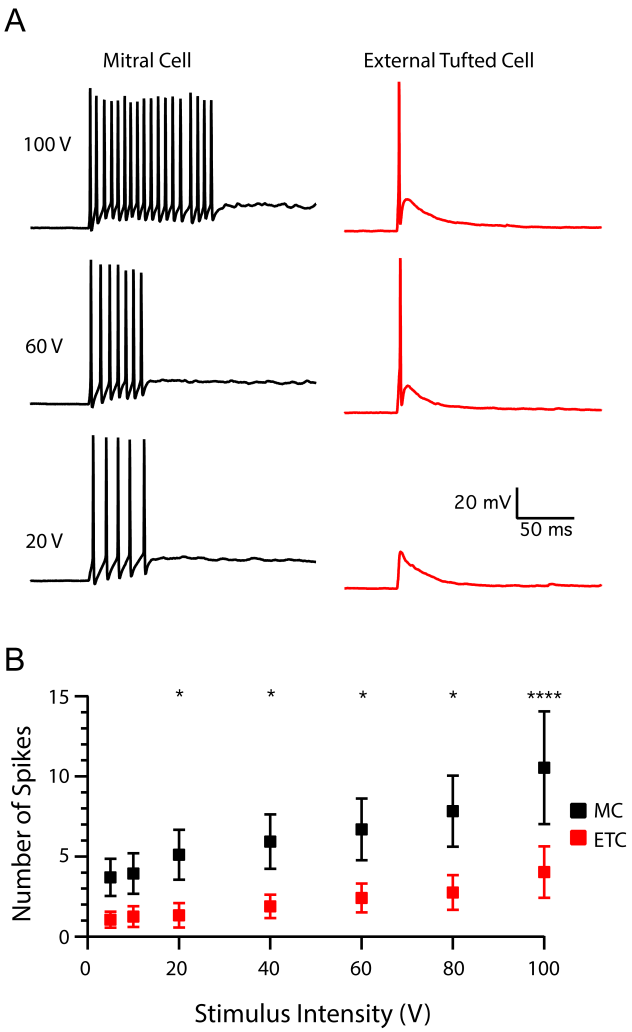
A
Mitral Cell
External Tufted Cell
100 V
60 V
20 V
20 mV
50 ms
B
Number of Spikes
15
10
5
0
*
*
*
*
****
0
20
40
60
80
100
Stimulus Intensity (V)
MC
ETC

Figure 8:

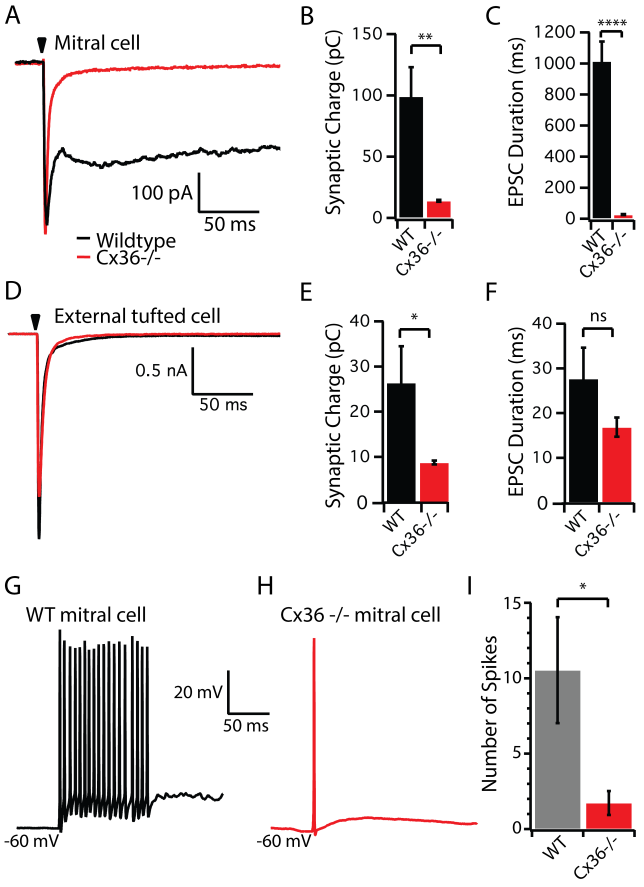
A
Mitral cell
100 pA
50 ms
Wildtype
Cx36-/-
B
Synaptic Charge (pC)
150
100
50
0
**
WT
Cx36-/-
C
EPSC Duration (ms)
1200
1000
800
600
400
200
0
****
WT
Cx36-/-
D
External tufted cell
0.5 nA
50 ms
E
Synaptic Charge (pC)
40
30
20
10
0
*
WT
Cx36-/-
F
EPSC Duration (ms)
40
30
20
10
0
ns
WT
Cx36-/-
G
WT mitral cell
20 mV
50 ms
-60 mV
H
Cx36 -/- mitral cell
-60 mV
I
Number of Spikes
15
10
5
0
*
WT
Cx36-/-

Figure 9:

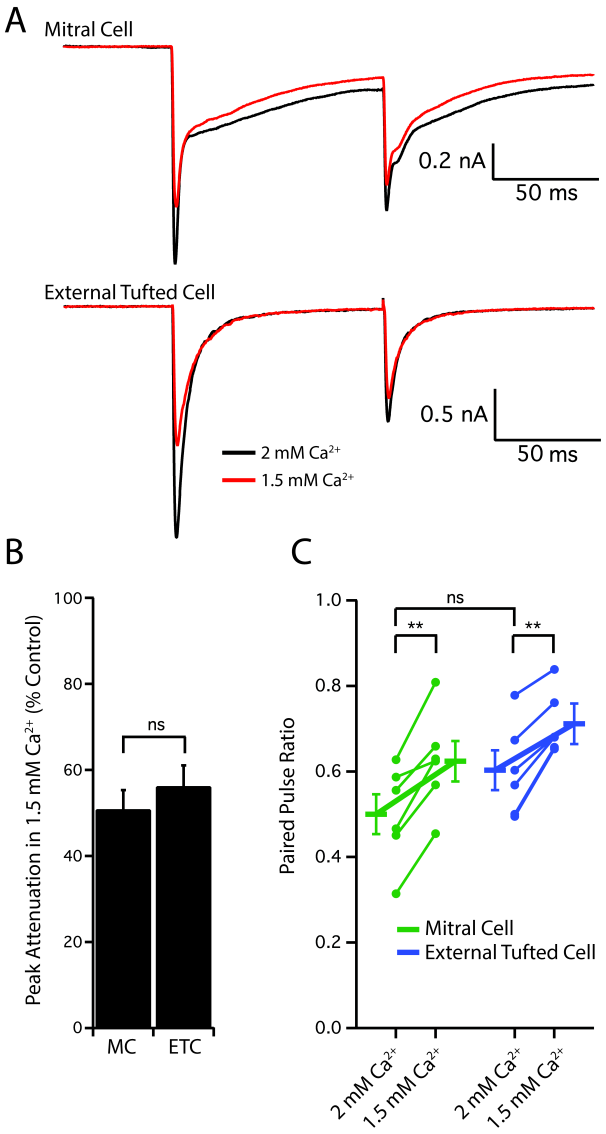
A
Mitral Cell
0.2 nA
50 ms
External Tufted Cell
0.5 nA
50 ms
2 mM Ca2+
1.5 mM Ca2+
B
Peak Attenuation in 1.5 mM Ca2+ (% Control)
100
80
60
40
20
0
ns
MC
ETC
C
Paired Pulse Ratio
1.0
0.8
0.6
0.4
0.2
0.0
ns
**
**
Mitral Cell
External Tufted Cell
2 mM Ca2+
1.5 mM Ca2+
2 mM Ca2+
1.5 mM Ca2+

Figure 10:

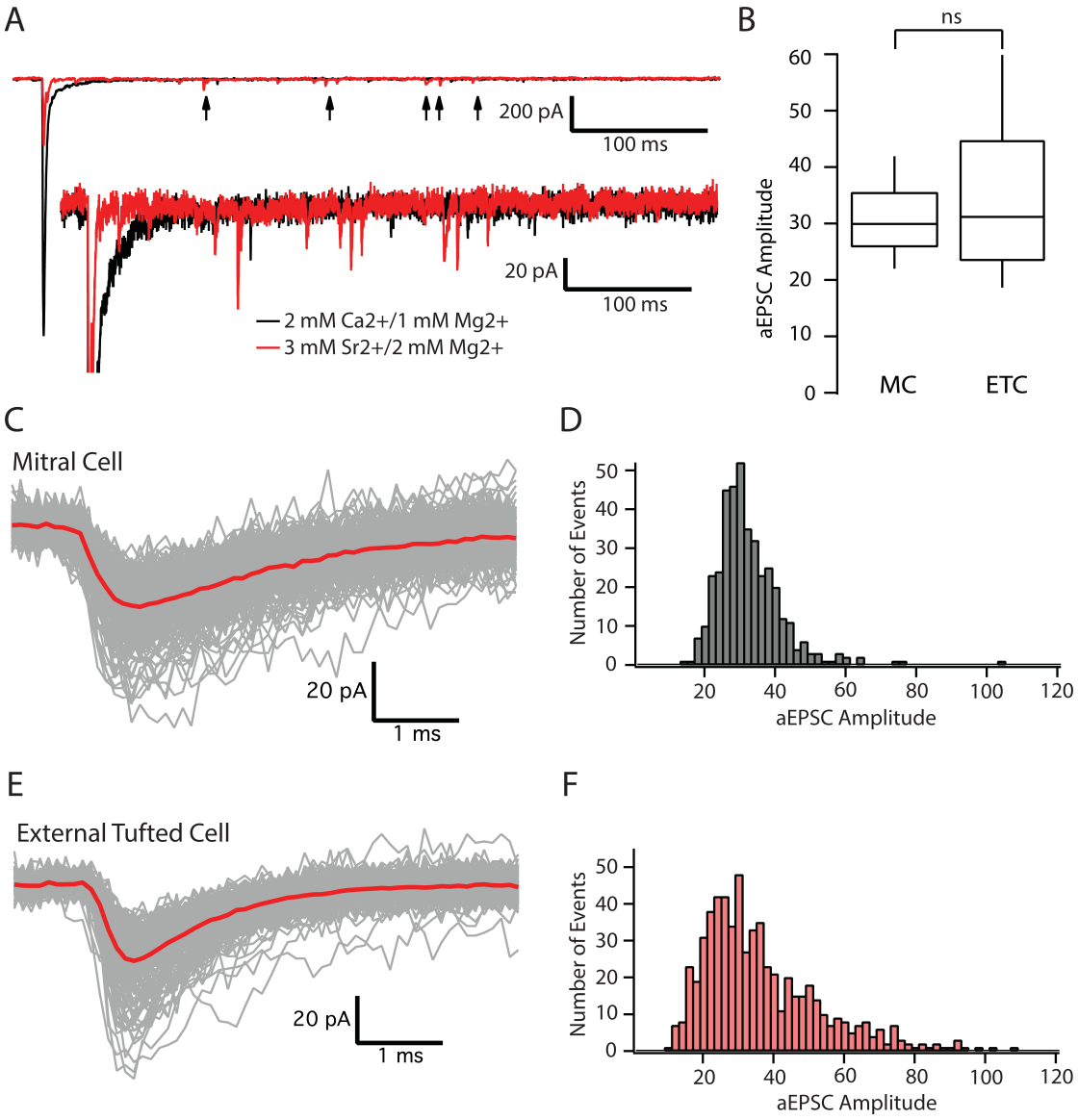
A
200 pA
100 ms
20 pA
100 ms
2 mM Ca2+/1 mM Mg2+
3 mM Sr2+/2 mM Mg2+
B
ns
aEPSC Amplitude
MC
ETC
C
Mitral Cell
20 pA
1 ms
D
Number of Events
aEPSC Amplitude
E
External Tufted Cell
20 pA
1 ms
F
Number of Events
aEPSC Amplitude

Chapter 3

Distinct temporal filters in mitral cells and external tufted cells in response to high frequency afferent stimulation

Christopher E Vaaga[1,2], Gary L Westbrook[1]

[1] Vollum Institute, Oregon Health and Science University, Portland OR, USA

[2] Neuroscience Graduate Program, Oregon Health and Science University, Portland OR, USA

Manuscript in preparation for submission to Journal of Physiology

Abstract:

Short-term synaptic plasticity is a critical component of neural circuits, and largely determines how information is processed. In the olfactory bulb, afferent olfactory receptor neurons respond to increasing concentrations of odorants with high frequency action potentials, and have an extraordinarily high release probability (Sicard, 1986; Murphy *et al.,* 2004). These features suggest that during naturalistic stimuli, afferent input to the olfactory bulb will be dominated by strong synaptic depression, resulting in transient responses in postsynaptic cells. Here, we use single glomerular stimulation in olfactory bulb slices to examine the synaptic dynamics of afferent evoked input at physiological frequencies. In cell attached recordings, mitral cells responded to high frequency stimulation with sustained responses, whereas external tufted cells responded only transiently. Consistent with previous reports (Murphy *et al.*, 2004), olfactory nerve terminals had a high release probability (0.7), measured using high frequency stimulus trains, which did not differ across cell types and consisted of a single pool of slowly recycling vesicles. The distinct temporal response profiles in mitral cells and external tufted cells resulted from enhanced dendrodendritic currents in mitral cells, as blocking the slow current in mitral cells revealed transient response profiles, mimicking those seen in external tufted cells. Our results suggest that despite strong axodendritic synaptic depression, the relative balance of axodendritic and dendrodendritic circuitry differentially tunes the postsynaptic responses to high frequency, naturalistic stimulation in distinct cell populations.

Key Points:

- The release probability of the ORN is reportedly one of the highest in the brain, which is predicted to impose a transient temporal filter on postsynaptic cells.
- Mitral cells responded to high frequency ORN stimulation with sustained transmission, whereas external tufted cells responded transiently.
- Using high frequency trains of stimulation, we find that the release probability of the ORN (0.7) was homogeneous across principal cells and could be explained single pool of slowly recycling vesicles.
- The sustained response in mitral cells was supported by dendrodendritic amplification in mitral cells; block by NMDA and mGluR1 receptor antagonists converted mitral cell responses to transient response profiles.
- Our results suggest that although the afferent ORN synapse shows strong synaptic depression, the dendrodendritic circuitry in mitral cells produces robust amplification of brief afferent input, and the relative strength of axodendritic and dendrodendritic input determines the postsynaptic response profile.

Introduction:

The computational capacity of neural circuits is largely determined by the short-term synaptic dynamics at play within the circuit (Abbott and Regehr, 2004), which result from pre- and postsynaptic mechanisms. Short-term synaptic depression results in a net decrease in postsynaptic responses upon repeated stimulation, which is often attributed to depletion of the readily of releasable pool of synaptic vesicles at high release probability terminals (Liley and North, 1953; Betz, 1970; von Gersdorff and Borst, 2002; Regehr, 2012). However, at some high release probability synapses, there are multiple pools of synaptic vesicles, with distinct release probabilities, which can protect the circuit from synaptic depression during high frequency stimulation (Lu and Trussell, 2016; Taschenberger *et al.*, 2016; Turecek *et al.*, 2016).

In the olfactory bulb, principal neurons receive monosynaptic input from olfactory receptor neuron afferents (Najac *et al.*, 2011; Vaaga and Westbrook, 2016). Odorant receptor neurons (ORNs) respond to increasing odorant concentrations with monotonic increases in firing frequency (Sicard, 1986; Duchamp-Viret *et al.*, 1999; Rospars *et al.*, 2003), which can reach up to 100 Hz (Sicard, 1986; Duchamp-Viret *et al.*, 1999; Carey *et al.*, 2009; Tan *et al.*, 2010). Furthermore, the release probability of the afferent synapse between the ORN and its postsynaptic targets is one of the highest reported in the brain, at approximately 0.8 to 0.9 (Murphy *et al.*, 2004). Together, these features suggest that the transmission between ORNs and principal neurons would be subject to robust short-term depression. However, *in vivo,* mitral cells respond to olfactory

input with sustained responses (Giraudet *et al.*, 2002; Nagayama *et al.*, 2004; Leng *et al.*, 2014), suggesting either that release probability during trains isn't as high as has been reported, or other circuit mechanisms maintain sustained transmission.

To examine the synaptic dynamics between ORN afferents and principal neurons in response to physiologically relevant stimulation frequencies we recorded the postsynaptic responses of mitral cells and external tufted cells during high frequency afferent stimulation. We demonstrate that mitral cells respond to high frequency ORN stimulation with sustained spiking responses, whereas the spiking responses in external tufted cells were transient. Using high frequency stimulation, we demonstrate that the release probability at the afferent ORN terminal is approximately 0.7, and is mediated by a single pool of synaptic vesicles which recycle unusually slowly. Such high release probability contributes to strong synaptic depression of the axodendritic input, and is responsible for the transient responses in external tufted cells. However, in mitral cells, the strong axodendritic depression is compensated for by robust dendrodendritic amplification. Pharmacological block of dendrodendritic currents in mitral cells elicited transient response profiles, similar to those in external tufted cells. Our results suggest that the high release probability and slow vesicle dynamics within the ORN are optimized for faithful transmission, but that dendrodendritic amplification in mitral cells compensates for the strong synaptic depression and strongly amplifies afferent input.

Materials and Methods:

Animals: We used adult (>p24) male and female C57Bl6/J as well as Tg(Thy1-YFP) GJrs heterozygous mice. All animal procedures were approved by the Oregon Health and Sciences University Institutional Animal Care and Use Committee.

Slice Preparation: Olfactory bulb slices were obtained as described previously (Schoppa and Westbrook, 2001). Animals were given an intraperitoneal injection of 2,2,2-tribromoethanol and monitored until fully anesthetized. Animals were then transcardially perfused with oxygenated 4º C modified ACSF solution, which contained (in mM): 83 NaCl, 2.5 KCl, 1 NaH_2PO_4, 26.2 $NaHCO_3$, 22 dextrose, 72 sucrose, 0.5 $CaCl_2$, 3.3 $MgSO_4$ (300-310 mOsm, pH: 7.3). The brain was quickly removed and coronally blocked at the level of the striatum. Horizontal sections (300 µm) through the olfactory bulb were made using a Leica 1200S vibratome. Slices were recovered in warm (32-36º C) ACSF for 30 minutes then stored at room temperature until being transferred to the recording chamber. Unless otherwise noted, the ACSF contained (in mM): 125 NaCl, 25 $NaHCO_3$, 1.25 NaH_2PO_4, 3 KCl, 2.5 dextrose, 2 $CaCl_2$, 1 $MgCl_2$ (300-310 mOsm, pH: 7.3).

Electrophysiology: Whole cell voltage clamp and current clamp recordings were made from mitral cells and external tufted cells under DIC optics. Mitral cells and external tufted cells were identified as described previously (Hayar *et al.*, 2005; Vaaga and Westbrook, 2016). Patch pipettes (3-5 MΩ) contained (in mM): 120 K-gluconate, 20 KCl, 10 HEPES, 0.1 EGTA, 4 Mg-ATP, 0.3 Na-GTP,

0.05 Alexa-594 hydrazide, and 5 QX-314. We made no correction for the liquid junction potential (-7 mV). During cell-attached recordings, the membrane patch was held at -70 mV after achieving a gigaohm seal. Data were acquired using a Multiclamp 700b amplifier (Molecular Devices, Sunnyvale CA, USA) and AxographX acquisition software. Data was digitized at 10 kHz and low pass Bessel filtered at 4 KHz. For cell attached recordings, the data was filtered post-hoc at 1 kHz. During whole-cell recordings the series resistance was continually monitored with a -10 mV hyperpolarizing step. Series resistance was generally <25 MΩ and was not compensated. Cells with greater than 30% change in series resistance during the recording were excluded from analysis. All recordings were made at 34-36º C.

EPSCs were elicited using single glomerulus theta stimulation, as described previously (Vaaga and Westbrook, 2016). Stimulation was provided by a constant current stimulator (100 μs, 3.2 - 32 mA) in conjunction with a small bore theta electrode (2 μm) placed directly in the axon bundle entering the target glomerulus. All recordings were made along the medial aspect of the olfactory bulb, and recordings were only made if the ORN bundle entering the target glomerulus was clearly identifiable under DIC optics. Stimulation frequencies (10, 25 and 50 Hz) were chosen to represent the approximate firing rate of ORNs in response to odorant presentation (Sicard, 1986; Duchamp-Viret *et al.*, 1999; Carey *et al.*, 2009; Tan *et al.*, 2010). ORN stimulation was repeated once every 60 seconds, to prevent rundown. All drugs were made from stock solutions according to manufacturer specifications and applied via a gravity fed perfusion

system. The drugs used in this study included: 2 mM kynurenic acid, 500 nM sulpiride, 200 nM CGP55845, 10 μM CPP and 20 μM CPCCOEt. All drugs were purchased from Abcam biochemical or Tocris Biosciences.

Data Analysis. Electrophysiology data were analyzed using AxographX and IGOR Pro (version 6.22A, Wavemetrics). Spike waveforms in cell attached recordings were detected using a threshold detection criteria in AxographX, which was used to calculate the total spike number and generate raster plots. Voltage clamp traces represent the average of 5-10 sweeps after baseline subtraction. Fast EPSC amplitude measurements were made foot-to-peak, to eliminate any contribution of the slow current. To directly measure the slow current we recorded the EPSC amplitude just prior to each stimulus within the train. The total charge transfer (0 – 2.5 seconds after stimulus onset) was measured using a built-in AxographX routine. Data was normalized to the first fast peak EPSC amplitude, unless otherwise noted.

To estimate release probability, two methods of estimating the size of the readily releasable pool were used, each of which utilizes a different set of assumptions (Neher, 2015; Thanawala and Regehr, 2016). In the train method (SMN method), the cumulative fast EPSC amplitude (at 50 Hz stimulation) was plotted as a function of stimulus number and a linear fit was made with the last 5 responses in the train using IGOR Pro. The readily releasable pool size was estimated as the y-intercept of the linear fit (Schneggenburger *et al.*, 1999, 2002). Finally, release probability was calculated by dividing the initial EPSC amplitude by the size of the readily releasable pool. In the Elmqvist-Quastal

method (EQ method; Elmqvist and Quastel, 1965), the fast EPSC amplitude was plotted as a function of the cumulative EPSC amplitude. A linear fit to the first 3 EPSCs was used to calculate the size of the readily releasable pool (x-intercept). Release probability was then calculated as in the SMN method.

Statistics: All data is reported as mean±SEM unless otherwise indicated. Statistical analysis was performed in Prism6 (GraphPad Software, La Jolla, CA). The data was assumed to be normally distributed, and was analyzed using parametric statistics. Student's paired and unpaired t-tests were used as appropriate. One-way and two-way repeated measure experiments were analyzed using ANOVA with Holm-Sidak post-hoc pairwise comparisons as indicated in the text. To compare the exponential fit across data sets, an extra sum of squares F-test was performed to compare lines of best fit. Sample sizes were chosen to detect an effect size of 20%, based on prior, similar experiments, with a power of 0.8. In all experiments, the initial value for α was set to $p<0.05$, and was adjusted for multiple comparisons as appropriate.

Results:

Different temporal response profiles in mitral and external tufted cells

To determine the synaptic dynamics of principal neuron activity in response to high frequency afferent stimulation, we first examined the spiking of principal neurons using cell-attached recordings. Both mitral cells and external tufted cells responded to 50 Hz ORN stimulation with spikes throughout the stimulus train (Figure 1 A-D). Mitral cells and external tufted cells produced

similar numbers of spikes early in the train, however, action potentials produced in external tufted cells gradually decreased, such that by the 7th stimulus, mitral cells produced significantly more action potentials per stimulus than external tufted cells (two-way ANOVA; $p<0.01$; n=7 mitral cells, 8 external tufted cells; Figure 1 E). Mitral cells also continued spiking well after cessation of the stimulus train, contributing to the higher total number of spikes produced (2.5 second window, mitral cells: 161.8±27.2 spikes per trial, n=7 cells; external tufted cells: 45.2±9.0 spikes per trial, n=8 cells, unpaired t-test: $p=0.009$, Figure 1 F).

In order to quantify the temporal filter in mitral cells and external tufted cells, we calculated the percentage of total spikes within 20 ms (50 Hz interstimulus interval) of each stimulus within the 50 Hz train. Using this metric, a steep input-output curve indicates a transient temporal filter. In both mitral cells and external tufted cells, the input-output curve was fit by a single exponential decay. In mitral cells, this relationship was relatively shallow (τ=5.2 stimuli), consistent with sustained transmission. On average, mitral cells produced 7.8±2.7% of total spikes immediately after the first stimulus and 3.8±1.0% of spikes following the final stimulus (n=7 cells). In comparison, external tufted cells had a significantly steeper input-output relationship (τ=3.2 stimuli, extra sum of squares F test: $p<0.0001$), producing 13.7±4.0% of total spikes after the first stimulus and 2.8±0.47% following the final stimulus (n=8 cells). Thus the two principal cells have distinct response properties with mitral cells responding to high frequency stimulation with sustained responses, whereas external tufted cells respond only transiently.

High release probability from a single pool of synaptic vesicles

Differences in release probability could underlie the distinct responses of mitral cells and external tufted cells. To determine the release probability of the ORN, we stimulated at high frequencies to estimate the size of the readily releasable pool (Elmqvist and Quastel, 1965; Schneggenburger *et al.*, 1999; Neher, 2015; Thanawala and Regehr, 2016). Consistent with a high release probability synapse, 50 Hz trains of stimuli elicited robust depression of the phasic EPSC amplitude in mitral cells (Figure 2 A_1) and external tufted cells (Figure 2 B_1). We estimated the release probability of the ORN in response to 50 Hz stimulation using two methods, the SMN (Figure 2 A_2, B_2) and EQ methods (Figure 2 A_3, B_3), each of which have a different set of assumptions (Elmqvist and Quastel, 1965; Schneggenburger *et al.*, 1999; Neher, 2015; Thanawala and Regehr, 2016). There was no significant difference in the release probability between cell types (SMN: mitral cells: 0.67±0.02, n=7 cells, external tufted cells: 0.71±0.06, n=8 cells, p=0.51; EQ: mitral cells: 0.66±0.02, external tufted cells: 0.73±0.03, p=0.14; Figure 2 C), therefore data from mitral cells and external tufted cells were pooled. Estimates of the release probability were also not significantly different between the two methods (SMN: 0.69±0.03; EQ: 0.70±0.2, p=0.7, Figure 2 C).

The somewhat lower release probability estimates using high frequency trains of stimuli likely reflect the activation of presynaptic D_2 and $GABA_B$ receptors in our experiments (Nickell *et al.*, 1994; Aroniadou-Anderjaska *et al.*, 2000; Ennis *et al.*, 2001; Wachowiak *et al.*, 2005; Maher and Westbrook, 2008;

Shao *et al.*, 2009; Vaaga *et al.*, 2017). Consistent with this hypothesis, measurements of the release probability in D_2 and $GABA_B$ receptor antagonists (500 nM sulpiride and 200 nM CGP55845, respectively) increased the release probability to 0.95±0.06 (SMN method, n=4 cells, unpaired t-test: p=0.008). These data suggest that although the basal release probability of the ORN is near 1, tonic and/or phasic activation of presynaptic D_2 and/or $GABA_B$ receptors reduces the release probability by approximately 30%.

To confirm that the synaptic depression following ORN stimulation resulted purely from presynaptic mechanisms, we compared the paired pulse ratio in control and 2 mM kynurenic acid, which blocks receptor saturation and desensitization (Trussell *et al.*, 1993; Wadiche and Jahr, 2001; Foster *et al.*, 2002; Wong *et al.*, 2003; Chanda and Xu-Friedman, 2010; Wong *et al.*, 2003). Kynurenic acid did not significantly change the paired pulse ratio (control: 0.24±0.05; 2 mM kynurenic acid: 0.25±0.05, n=5 cells, paired t-test: 0.70; Figure 2 D, E), suggesting that at the ORN afferent synapse, synaptic depression is primarily mediated by presynaptic factors (Murphy *et al.*, 2004).

We next wanted to determine if other aspects of vesicle dynamics contribute to sustained transmission in mitral cells and external tufted cells. One possibility is that, as in other circuits (Kennewick and Matthews, 1996; Sakaba and Neher, 2001; Lu and Trussell, 2016; Turecek *et al.*, 2016), there are multiple pools of synaptic vesicles, with heterogeneous release probabilities, which, if present, may obscure our measurements of release probability and support sustained transmission high stimulation frequencies (Neher, 2015; Turecek *et al.*,

2016). To test for multiple pools of synaptic vesicles, we stimulated at 10 Hz (20 pulses) to deplete the high release probability pool then switched to 50 Hz stimulation (20 pulses). Such a depletion protocol has been used to reveal a transient facilitation resulting from the low release probability of the remaining synaptic vesicles (Lu and Trussell, 2016; Turecek *et al.*, 2016). In external tufted cells this stimulation protocol failed to reveal facilitation (Figure 3 A); transitioning to high frequency stimulation elicited further depression of the ORN-evoked phasic EPSC ($EPSC_{21}$: 25.3±0.4% of control, $EPSC_{22}$: 14.7±0.2% of control; Figure 3 B), suggesting a single pool of synaptic vesicles.

As a second measure of whether two pools of synaptic vesicles exists in ORNs, we plotted the phasic EPSC amplitude of external tufted cells as a function of stimulus number (Figure 3 C). Consistent with a single pool of vesicles, the decay was best fit with a single exponential function (τ: 0.68; extra sum of squares F test: p=0.49; Figure 3 C). Together, these data suggest that a single pool of high release probability vesicles can explain vesicle release from afferent olfactory nerve terminals.

It is also possible that the sustained responses in mitral cells are maintained despite high release probability by fast vesicle replenishment (Wang and Kaczmarek, 1998; Saviane and Silver, 2006). To examine the vesicle replenishment rate, we stimulated at 50 Hz then examined the time course of EPSC recovery (Figure 3 D). The phasic EPSC amplitude recovered surprisingly slowly, following a double exponential time course (τ_1: 0.79 seconds; τ_2: 8.23

seconds, Figure 3 E, F), suggesting that fast vesicle replenishment does not contribute to the sustained responses in the glomerular microcircuit.

Dendrodendritic excitation maintains sustained transmission

Our results suggest that the properties of the afferent presynaptic terminal alone cannot explain the sustained transmission observed in mitral cells. To determine what mechanisms support sustained transmission we next examined the voltage clamp responses of mitral cells and external tufted cells following stimulation at various frequencies (10 Hz, 25 Hz, 50 Hz; Figure 4 A, B). Across stimulus frequencies, the phasic EPSC showed robust depression, reaching steady state levels after approximately 5 stimuli (Figure 4 D, E). Surprisingly, even relatively low stimulus frequencies (10 Hz) elicited robust depression in both cell types, consistent with the slow vesicle replenishment rates and unusually high release probability. In both cell types, there was a significant effect of stimulus frequency on the total degree of phasic EPSC depression (One way ANOVA: mitral cell: $p=0.0003$; external tufted cell: $p<0.0001$; Figure 4 G). In both cells, the depression increased from 10 Hz to 25 Hz (mitral cells: 10 Hz: 16.4±1.3% of $EPSC_1$, n=6 cells; 25 Hz: 9.4±2.1% of $EPSC_1$ n=5 cells, Holm-Sidak post-hoc comparison: $p<0.05$; external tufted cells: 10 Hz: 14.8±2.0, n=7 cells; 25 Hz: 5.8±0.9% of control, n=7, Holm-Sidak post-hoc comparison: $p<0.001$), but was not significantly different between 25 Hz and 50 Hz (mitral cell: 25 Hz: 9.4±2.1% of $EPSC_1$ n=5 cells, 50 Hz: 5.4±0.9% of $EPSC_1$, n=6 cells, Holm-Sidak post-hoc comparison: $p>0.05$; external tufted cell: 25 Hz: 5.8±0.9%

of $EPSC_1$, n=7, 50 Hz: 4.4±0.6% of $EPSC_1$, n=8 cells, Holm-Sidak post-hoc comparison: p>0.05). There was no significant difference in the total degree of phasic depression between mitral cells and external tufted cells at any stimulus frequency tested (Figure 4 G), consistent with the similar presynaptic properties of mitral cells and external tufted cells.

However, one prominent difference between the responses to high frequency stimulation in mitral cells and external tufted cells was the amplitude of the slow, envelope current. In mitral cells, phasic EPSCs were superimposed on a large slow current, reflecting the larger dendrodendritic currents in mitral cells (Figure 4 C; Vaaga and Westbrook, 2016). Across all stimulus frequencies, the total charge transfer was significantly larger in mitral cells (10 Hz: mitral cell: 219.9±50.6 pC, n=6 cells, external tufted cell: 84.4±23.25 pC, n=6 cells, Holm-Sidak post-hoc comparison: p<0.05; 25 Hz: mitral cell: 268.0±43.4 pC, n=5 cells, external tufted cell: 75.5±24.7 pC, n=7 cells, Holm-Sidak post-hoc comparison: p<0.01; 50 Hz: mitral cell: 309.9±50.1 pC, n=7 cells, external tufted cell: 78.3±12.3 pC, n=7 cells; Holm-Sidak post-hoc comparison: p<0.001, Figure 4 F). Interestingly, the charge transfer did not change with stimulation frequency (mitral cell: One way ANOVA: p=0.43; external tufted cell: One-way ANOVA: p=0.96, Figure 4 F), consistent with an all-or-none dendrodendritic slow EPSC (Carlson *et al.*, 2000; De Saint Jan *et al.*, 2009; Gire and Schoppa, 2009). Unlike the phasic responses, the degree of depression of the slow envelope current was significantly different between mitral cells and external tufted cells (10 Hz: mitral cell: 57.1±3.2% of $EPSC_1$, external tufted cell 34.0±8.4% of $EPSC_1$, Holm-Sidak

post-hoc comparison: $p<0.05$; 25 Hz: mitral cell: 67.2±10.2% of $EPSC_1$, external tufted cell: 33.9±5.5% of $EPSC_1$, Holm-Sidak post-hoc comparison: $p<0.01$; 50 Hz: mitral cell: 79.5±4.8% of $EPSC_1$, external tufted cell: 26.8±4% of $EPSC_1$, Holm-Sidak post-hoc comparison: $p<0.0001$; Figure 4 H).

In both mitral cells and external tufted cells, the phasic depression was significantly larger than the depression of the slow, envelope current, and therefore all the data points fall above the unity line in a plot of phasic EPSC depression as a function of slow ESPC depression (Figure 4 I). Furthermore, the similarity of the phasic depression and distinct slow current depression across cell types produced two identifiable clusters when the phasic and slow current depression are directly compared (Figure 4 I). Together this data suggests that a robust slow current supports sustained transmission in mitral cells, which is relatively insensitive to depression throughout the stimulus train.

The mitral cell slow current is responsible for sustained transmission

To determine whether the difference in the slow current between mitral cells and external tufted cells was sufficient to explain the different spiking responses to 50 Hz stimulation, we blocked NMDA and mGluR1 receptors (10 μM CPP and 20 μM CPCCOEt, respectively), which reduced the slow current in mitral cells (Figure 5 A). Bath application of NMDA and mGluR1 antagonists also reduced the total charge transfer (mitral cell: 309.9±50.1 pC, n=7 cells; mitral cell + CPP/CPCCOEt: 42.3±8.5 pC, n=6 cells, Holm-Sidak post-hoc comparison: $p<0.0001$, Figure 5 B), which was not significantly different than the charge

transfer in external tufted cells (external tufted cell: 78.27±12.26, n=7 cells, Holm-Sidak post-hoc comparison: $p>0.05$, Figure 5 B). This data suggests that blocking the slow current converts the mitral cell response pattern to an external tufted cell pattern.

In cell attached recordings, blocking NMDA and mGluR1 receptors reduced the total number of spikes produced following 50 Hz stimulation (mitral cell: 161.8±27.2 spikes, n=7 cells; mitral cell + CPP/CPCCOEt: 37.62±7.3 spikes, n=5 cells, Holm-Sidak post-hoc comparison: $p<0.001$; external tufted cell: 45.2±9.0 spikes, n=8 cells; Holm-Sidak post-hoc comparison: $p>0.05$, Figure 5 D), suggesting that the difference in total number of spikes produced between cell types is a direct result of NMDA and mGluR1-dependent amplification in mitral cells. Furthermore, bath application of NMDA and mGluR1 receptor antagonists also altered the temporal patterning of spikes, converted the sustained responses of mitral cells to more transient responses (extra sum of squares F-test: $p<0.001$, Figure 5 E), which were not significantly different than the transient response of external tufted cells (extra sum of squares F-test: $p>0.05$, Figure 5 F). This data suggests that the differences in slow current between mitral cells and external tufted cells are responsible for the sustained transmission in mitral cells.

Long term synaptic depression following naturalistic stimulation frequencies

Given the extraordinarily high release probability of the ORN, we wondered if spike trains mimicking naturalistic inhalation patterns could alter the

strength of axodendritic input. mGluR1 dependent long-term depression of the ORN has been reported (Mutoh *et al.*, 2005), however, it is unclear whether such depression can be engaged using naturalistic stimulation patterns. We stimulated the ORN using theta burst pattern (5 pulses at 100 Hz, separated by 200 ms, Figure 6 A), which mimics the high ORN firing rate and the approximate inhalation frequency of mice. Theta burst ORN stimulation induced robust depression of synaptic responses in external tufted cells (average EPSC amplitudes 12-15 minutes post induction: control: 98.0±2.1% of control, n=4 cells, theta burst stimulation: 71.2±0.5% of control, n=6 cells, unpaired t-test: $p<0.0001$, Figure 6B, C), suggesting that repeated ORN stimulation can reduce presynaptic release probability, possibly through mGluR1 receptor-dependent mechanisms (Mutoh *et al.*, 2005).

Discussion:

In the glomerular microcircuit, the interplay of axodendritic and dendrodendritic synapses is critical to understanding the function of the circuit. Although the glomerulus has long been viewed as a cortical module whose primary function is to enhance the signal-to-noise ratio (Chen and Shepherd, 2005), the synaptic dynamics in response to high frequency, naturalistic ORN stimulation have not been examined. Here we demonstrate that mitral cells and external tufted cells respond to high frequency afferent input with distinct temporal filters; mitral cells produce sustained responses, whereas external tufted cells produce transient responses. Because external tufted cell responses

are dominated by axodendritic input (Vaaga and Westbrook, 2016), their responses to high frequency stimulation reflect the high release probability and slow vesicle replenishment of the ORN. Conversely, the dendrodendritic amplification present in mitral cells protects these cells from the axodendritic synaptic depression. Blocking the dendrodendritic slow current in mitral cells converted the sustained response to a transient response profile, indicating that NMDA and mGluR1 receptor mediated amplification produces sustained response profiles in mitral cells. Together, our results indicate that the axodendritic and dendrodendritic circuits are functionally separable, and the relative balance of the two circuits determines the temporal filter of the postsynaptic cell.

Axodendritic input is tuned to ensure faithful transmission

One of the most striking aspects of the glomerular microcircuit is the massive convergence of axons to a single glomerulus, with each axon carrying functionally redundant information (Mombaerts *et al.*, 1996). This unimodal input is critical for odorant identification, as each odorant mixture elicits a unique map of activated glomeruli, a so-called odor image (Xu *et al.*, 2000). However, from a computational perspective, the massive redundancy is a waste of information channels (Rieke, 1999; Chen and Shepherd, 2005). Furthermore, each olfactory receptor neuron responds to increases in odorant concentration with monotonic increases in firing frequency, reaching up to 100 Hz (Sicard, 1986; Duchamp-Viret *et al.*, 1999; Carey *et al.*, 2009; Tan *et al.*, 2010). Coupled with the high

ORN release probability (Murphy *et al.*, 2004), trains of ORN activity should produce strong synaptic depression, imposing a transient temporal filter in postsynaptic cells.

The primary function of olfactory receptor neurons is to accurately convey the presence of odorants in the periphery to the olfactory bulb. The olfactory system is exquisitely sensitive, capable of detecting 1 part per 10^{15} molecules (Julius and Katz, 2004). In the periphery, this is achieved through biochemical amplification downstream of G-protein coupled odorant receptors, such that a single odorant receptor-binding event can elicit an action potential in the ORN (Lynch and Barry, 1989). The high release probability of ORNs maintains the high sensitivity of the olfactory system, by ensuring that ORN activity is faithfully converted to a postsynaptic response. However, the high release probability and slow vesicle replenishment of ORNs suggests that individual nerve terminals can only transiently contribute to postsynaptic activation, therefore requiring an ensemble of functionally redundant channels to accurately convey information with high fidelity. Many synapses have recently been shown to utilize at least two pools of synaptic vesicles, each with different release probabilities (Mennerick and Matthews, 1996; Sakaba and Neher, 2001; Lu and Trussell, 2016; Turecek *et al.*, 2016). Such an arrangement is attractive in the olfactory bulb, because the high release probability pool ensures faithful transmission, whereas the low release probability pool maintains transmission during high frequency activity. However, our data suggest that this is not the case in ORNs, where there is a single pool of slowly recycling synaptic vesicles.

Previous estimates of release probability using steady state measurements have suggested that the release probability of the ORN is near 1 (Murphy *et al.*, 2004). However, such measurements may overestimate the release probability during naturalistic high frequency trains of activity. Furthermore, tonic and phasic activation of juxtaglomerular interneurons reduces the effective release probability within the circuit by reducing presynaptic calcium influx (Aroniadou-Anderjaska *et al.*, 2000; Ennis *et al.*, 2001; Wachowiak *et al.*, 2005; Vaaga *et al.*, 2017). Our results using high frequency trains of stimuli suggest that the release probability of the ORN is as high as 0.9 when presynaptic D_2 and $GABA_B$ receptors are blocked, however, tonic and/or afferent evoked activation of presynaptic D_2 and $GABA_B$ receptors reduces the release probability by approximately 30% in brain slices.

In vivo, the release probability of the ORN is likely dynamically regulated in response to activity. For example, short axon cells, which presynaptically inhibit afferent nerve terminals via D_2 and $GABA_B$ receptor activation, connect multiple glomeruli, and are therefore well positioned to modulate afferent nerve terminals in distributed glomeruli (Kiyokage *et al.*, 2010; Whitesell *et al.*, 2013; Banerjee *et al.*, 2015; Vaaga *et al.*, 2017). In fact, long term changes in the density of dopaminergic short axon cells in response to global changes in activity likely alters the strength of axodendritic synapses through changes in tonic and afferent evoked $GABA_B$ and D_2 activation (Baker *et al.*, 1983, 1993; Banerjee *et al.*, 2015; Vaaga *et al.,* 2017). Furthermore, within a single glomerulus, our data suggests that repeated naturalistic stimulation elicits long-term synaptic

depression, likely via mGluR1 receptor dependent mechanisms (Mutoh *et al.*, 2005). Interestingly, although long-term depression of the ORN is presynaptically expressed (Mutoh *et al.*, 2005), mGluR1 receptors are exclusively expressed postsynaptically (van den Pol, 1995). Such an arrangement suggests retrograde signaling, perhaps through endocannabinoid or nitric oxide synthesis, which has been reported elsewhere in the olfactory bulb (Wang *et al.*, 2012).

Dendrodendritic circuitry promotes sustained transmission

The ability of the axodendritic afferent input to maintain the sensitivity of ORNs comes at a cost: the "noisy" olfactory environment dramatically increases the total number of activated glomeruli in response to ambient air. The signal to noise ratio, therefore, is enhanced through dendrodendritic circuitry within the glomerulus (Carlson *et al.*, 2000; Chen and Shepherd, 2005; De Saint Jan and Westbrook, 2007; Vaaga and Westbrook, 2016). Dendritic glutamate release from mitral and tufted cell dendrites coordinates inhibitory interneurons and provides recurrent excitation (Hayar *et al.*, 2004*a*; De Saint Jan *et al.*, 2009; Gire and Schoppa, 2009; Vaaga and Westbrook, 2016).

The sustained responses of mitral cells in cell-attached recordings was perhaps surprising, as juxtaglomerular interneurons and granule cells provide strong inhibition of mitral cells (Jahr and Nicoll, 1980, 1982; Shao *et al.*, 2012, 2013). In fact, mitral cells receive stronger glomerular layer inhibition than tufted cells (Geramita and Urban, 2017), contributing to their delayed activation *in vivo* (Nagayama *et al.*, 2004). The majority of juxtaglomerular interneurons are

activated exclusively through polysynaptic pathways involving external tufted cells (Shao *et al.*, 2009; Kiyokage *et al.*, 2010), thus the inhibition onto mitral cells is also likely transient. Furthermore, the exact nature of dendrodendritic excitation within the glomerulus is still poorly understood. At the ultrastructural level, there are no *bona fide* synaptic contacts between principal cell dendrites (Pinching and Powell, 1971; Bourne and Schoppa, 2017), however, all mitral cells projecting to the same glomerulus are coupled by electrical synapses (Schoppa and Westbrook, 2002; Christie *et al.*, 2005; Christie and Westbrook, 2006). Therefore, the major substrate for dendrodendritic excitation may in fact be the electrical coupling of autoreceptor currents. The release probability and dynamics of dendritic vesicles are not well understood, however, our results suggest that in mitral cells there is little depression of the slow current even following prolonged stimulation. This relative lack of depression suggests that the release probability of dendritic vesicles in any one cell may be quite low.

The glomerulus as two circuits: axodendritic and dendrodendritic circuits perform unique computations

Multiple lines of evidence suggest that axodendritic and dendrodendritic synapses are in fact distinct circuits. Anatomically, axodendritic and dendrodendritic synapses are separated into the shell and core of the glomerulus, respectively (Kasowski *et al.*, 1999; Kim and Greer, 2000). Functionally, whether the postsynaptic cell responds to high frequency afferent stimulation with transient or sustained responses depends on the relative

balance of axodendritic and dendrodendritic synaptic input, which is not uniform across cell types (Vaaga and Westbrook, 2016). Although external tufted cells have larger fast, axodendritic synaptic responses, they lack dendrodendritic slow currents (Burton and Urban, 2014; Vaaga and Westbrook, 2016). As a result, external tufted cells transiently respond to high frequency afferent stimulation. Mitral cells, on the other hand, despite weaker, fast afferent evoked responses have strong dendrodendritic amplification (De Saint Jan *et al.*, 2009; Najac *et al.*, 2011; Gire *et al.*, 2012; Vaaga and Westbrook, 2016), allowing mitral cells to produce sustained responses to high frequency afferent stimulation. In fact, differences in the strength of dendrodendritic amplification directly correlated to the degree of sustained transmission, and blocking dendrodendritic amplification in mitral cells "converted" them to transient responses, similar to the responses in external tufted cells.

It is clear that different principal neuron subtypes in the olfactory bulb represent parallel input pathways. For example, *in vivo*, tufted cells respond to lower odorant concentrations, have concentration invariant responses, and respond to odorants earlier in the sniff cycle (Nagayama *et al.*, 2004; Igarashi *et al.*, 2012; Fukunaga *et al.*, 2012; Kikuta *et al.*, 2013). Mitral cells, on the other hand, are more narrowly tuned than tufted cells, and shift their responses relative to the sniff cycle in response to increasing odorant concentrations (Nagayama *et al.*, 2004; Kikuta *et al.*, 2013). Furthermore, mitral cells and tufted cells project to non-overlapping regions of olfactory cortex (Igarashi *et al.*, 2012), suggesting that they convey distinct information. These in vivo results are consistent with the

view that tufted cell responses maintain the sensitivity of the ORN, via strong afferent evoked responses, whereas mitral cells provide robust amplification, via strong dendrodendritic circuitry. Therefore, the distinct balance of axodendritic and dendrodendritic synaptic strength in each principal cell population likely contributes to the unique computations within these parallel input pathways, by imposing unique temporal filters in each cell type.

Acknowledgements: This work was supported by NS26494 (GLW), National Science Foundation Graduate Research Fellowship DGE-0925180 (CEV) and a P30 imaging grant (NS061800). We thank the members of the Westbrook laboratory for their helpful comments.

Figure Legends:

Figure 1: **Sustained transmission in mitral and external tufted cells** (**A**) Cell attached recording from mitral cell in response to 50 Hz ORN stimulation. (**B**) Raster plot of mitral cell response. Mitral cells responded to ORN stimulation with sustained responses, which outlasted the stimulus. (**C**) Cell attached recording and (**D**) associated raster plot of external tufted cell response to 50 Hz ORN stimulation. External tufted cells produced much more transient response profiles. (**E**) Plot of the average number of action potentials produced following each stimulus in the train. Mitral cells and external tufted cells produce similar numbers of action potentials at the beginning of the train. By the end of the train, however, mitral cells produce approximately twice as many action potentials as external tufted cells. (**F**) The total number of spikes produced (within 2.5 seconds) in mitral cells is significantly higher than in external tufted cells. (**G**) Plot of the fraction of total spikes in the train as a function of stimulus number. Mitral cells (black) have a more shallow relationship, consistent with sustained transmission. External tufted cells (red) have a significantly steeper relationship, indicative of transient response profiles.

Figure 2: **Olfactory receptor neurons have a high release probability** (**A_1, B_1**) Representative whole-cell voltage clamp responses to 50 Hz stimulation in mitral cells (**A_1**, black) and external tufted cells (**B_1**, red). (**A_2, B_2**) Estimates of the readily releasable pool size using the SMN train method in mitral cells (**A_2**) and

external tufted cells (**B_2**). (**A_3, B_3**) Estimate of readily releasable pool size using the EQ method in mitral cells (**A_3**) and external tufted cells (**B_3**). (**C**) Estimates of release probability do not differ between the Schneggenburger and Elmqvist-Quastal methods. There was also no significant difference between the release probability calculated in mitral cells (black) and external tufted cells (red). (**D**) Paired pulse ratio in external tufted cells before (black) and after (green) addition of 2 mM kynurenic acid to prevent receptor saturation and desensitization. Response in kynurenic acid scaled to control (red). (**E**) Summary of the paired pulse ratio in external tufted cells before and after 2 mM kynurenic acid, suggesting postsynaptic saturation and desensitization do not contribute to synaptic depression.

Figure 3: **Single pool of slowly recycling vesicles** (**A**) Representative external tufted cell recording showing 10 Hz stimulation followed by 50 Hz stimulation. (**B**) Group data shows immediate depression following 10 Hz stimulation, suggesting a single pool of synaptic vesicles. (**C**) Plot of the phasic EPSC amplitude as a function of stimulus number is fit by a single exponential, further suggesting a single pool of high release probability vesicles. (**D, E**) Recovery of phasic EPSC amplitude following 50 Hz stimulation suggests that vesicle replenishment is slow. (**F**) Recovery time course is best fit by a double exponential.

Figure 4: **Differential modulation of phasic and slow currents in mitral and external tufted cells** (**A, B**) Whole-cell voltage clamp responses of mitral cells

(**A**, black) and external tufted cells (**B**, red) to stimulation at various frequencies (10, 25, 50 Hz). (**C**) Comparison of the slow, envelope current measured in mitral cells (grey) and external tufted cells (pink) at each stimulus frequency. Mitral cells had consistently larger envelope currents. (**D**) Depression of the phasic EPSC amplitude as a function of stimulus number in mitral cells across stimulation frequencies (blue: 10 Hz, red: 25 Hz, black: 50 Hz). (**E**) Depression of phasic EPSC amplitude as a function of stimulus number in external tufted cells (colors as in **D**). (**F**) The total charge transfer (measured 2.5 seconds after stimulus onset) was significantly larger in mitral cells than external tufted cells across all stimulation frequencies. There was no significant difference across stimulus frequencies within either cell type. (**G**) Total phasic depression in mitral cells (black) and external tufted cells (red) across stimulation frequencies. There was no significant difference between cell types at any frequency tested. (**H**) Total slow current depression in mitral cells (black) and external tufted cells (red) across stimulation frequencies. Mitral cells had significantly less slow current depression at all stimulus frequencies tested. (**I**) Plot showing a direct comparison of phasic depression and tonic depression across cell types and frequencies (blue: 10 Hz, red: 25 Hz, black: 50 Hz). Although the phasic depression was similar between cell types and frequencies, the slow current was differentially regulated in mitral cells and external tufted cells.

Figure 5: **Blocking the slow current converts mitral cell responses into external tufted cell responses** (**A**) Peak scaled comparison of the whole cell

voltage clamp recordings from mitral cells in control (black) and 10 μM CPP/20 μM CPCCOEt (green) in response to 50 Hz ORN stimulation. As expected, CPP/CPCCOEt blocked a significant portion of the slow envelope current. (**B**) Comparison of the total charge transfer in mitral cells (black), external tufted cells (red) and mitral cells with CPP/CPCCOEt (green) shows that blocking the NMDA/mGluR1 receptor dependent current significantly reduces the total charge transfer to levels comparable to external tufted cells. (**C**) Cell-attached recording from mitral cell in response to 50 Hz ORN stimulation shows transient spiking profile mitral cells when NMDA and mGluR1 receptors are blocked. (**D**) The total number of action potentials produced in mitral cells with NMDA and mGluR1 receptors are similar to external tufted cell responses. (**E**) Comparison of the temporal profile of mitral cell spiking in control (black) and with CPP/CPCCOEt (green). Block of NMDA and mGluR1 receptors reveals transient response profile of mitral cells. (**F**) With NMDA and mGluR1 receptors blocked, the temporal profile of mitral cell spiking (green) is not significantly different than the responses of external tufted cells (red).

Figure 6 **Theta burst ORN stimulation elicits long-term depression** (A) Schematic of theta burst ORN stimulation. Five High frequency bursts of stimulation (100 Hz) were separated by 200 ms and repeated a total of 10 times. (B) Diary plot of the long-term depression evoked by theta burst stimulation (black, filled circles) compared to control experiments in which the induction

protocol was omitted (black, open circles). (C) Comparison ORN-evoked EPSCs before and after the theta burst stimulation induction protocol.

Figure 1:

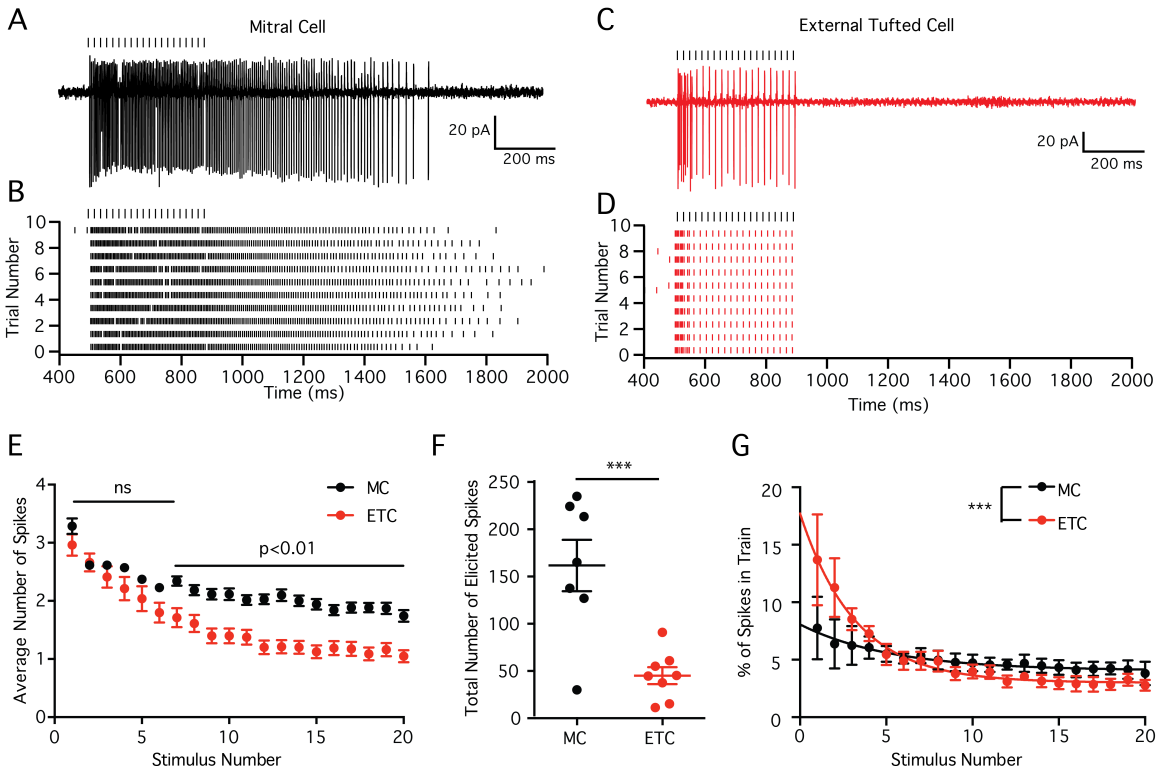
A
Mitral Cell
20 pA
200 ms
B
Trial Number
Time (ms)
C
External Tufted Cell
20 pA
200 ms
D
Trial Number
Time (ms)
E
ns
p<0.01
MC
ETC
Average Number of Spikes
Stimulus Number
F
***
Total Number of Elicited Spikes
MC
ETC
G
***
MC
ETC
% of Spikes in Train
Stimulus Number

Figure 2:

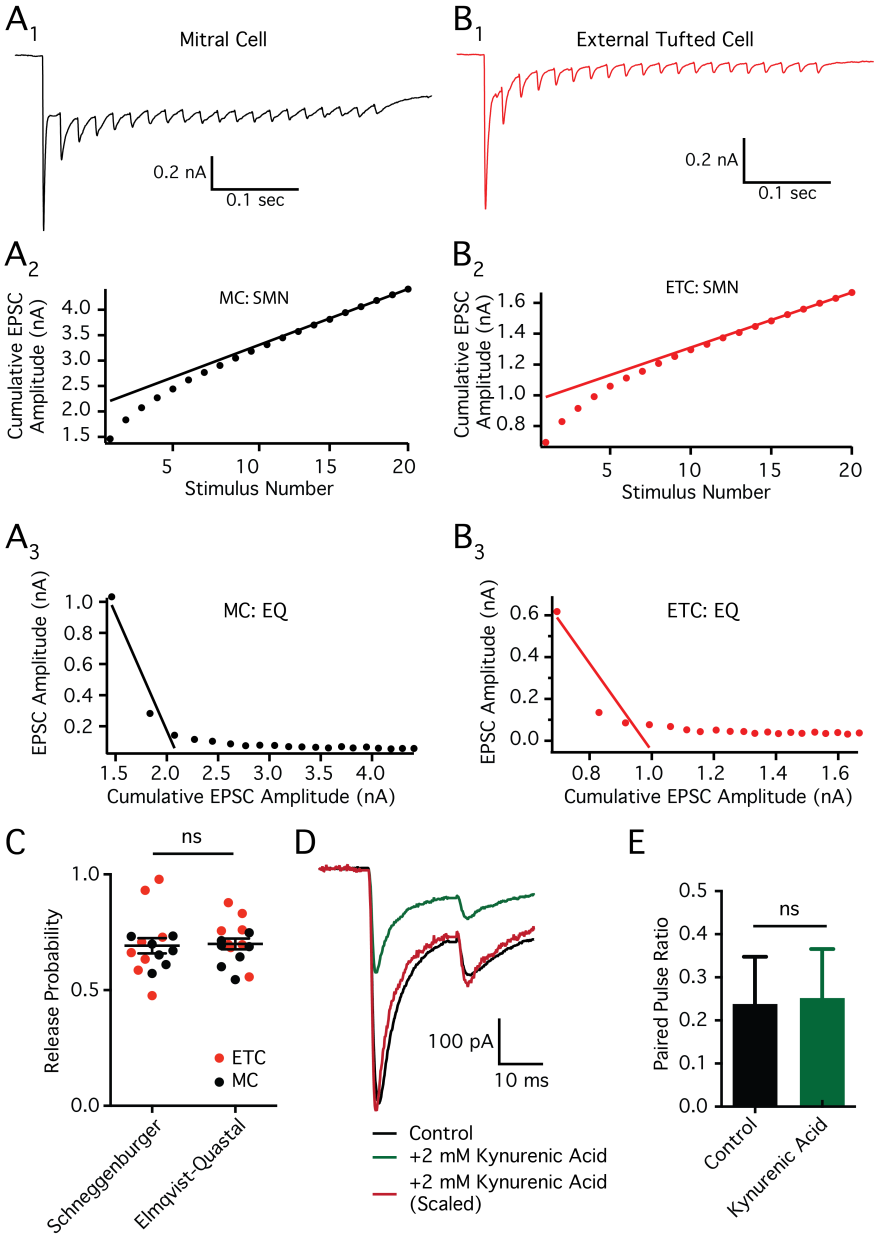
A1
Mitral Cell
0.2 nA
0.1 sec
B1
External Tufted Cell
0.2 nA
0.1 sec
A2
MC: SMN
Cumulative EPSC Amplitude (nA)
Stimulus Number
B2
ETC: SMN
Cumulative EPSC Amplitude (nA)
Stimulus Number
A3
MC: EQ
EPSC Amplitude (nA)
Cumulative EPSC Amplitude (nA)
B3
ETC: EQ
EPSC Amplitude (nA)
Cumulative EPSC Amplitude (nA)
C
ns
Release Probability
ETC
MC
Schneggenburger
Elmqvist-Quastal
D
100 pA
10 ms
Control
+2 mM Kynurenic Acid
+2 mM Kynurenic Acid (Scaled)
E
ns
Paired Pulse Ratio
Control
Kynurenic Acid

Figure 3:

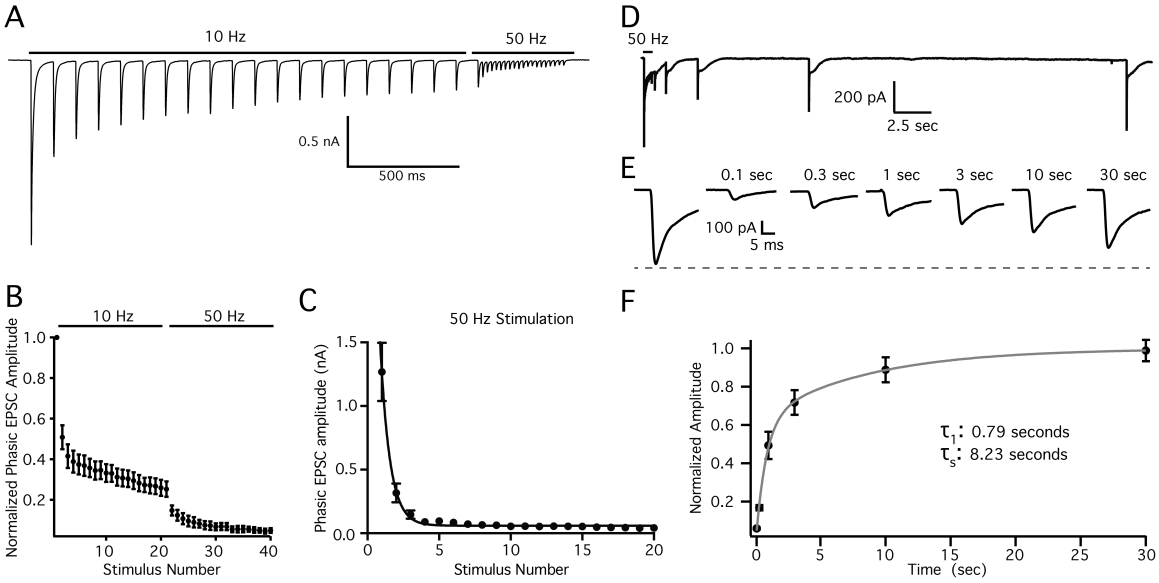
A
10 Hz
50 Hz
0.5 nA
500 ms
D
50 Hz
200 pA
2.5 sec
E
0.1 sec
0.3 sec
1 sec
3 sec
10 sec
30 sec
100 pA
5 ms
B
10 Hz
50 Hz
Normalized Phasic EPSC Amplitude
Stimulus Number
C
50 Hz Stimulation
Phasic EPSC amplitude (nA)
Stimulus Number
F
Normalized Amplitude
τf: 0.79 seconds
τs: 8.23 seconds
Time (sec)

Figure 4:

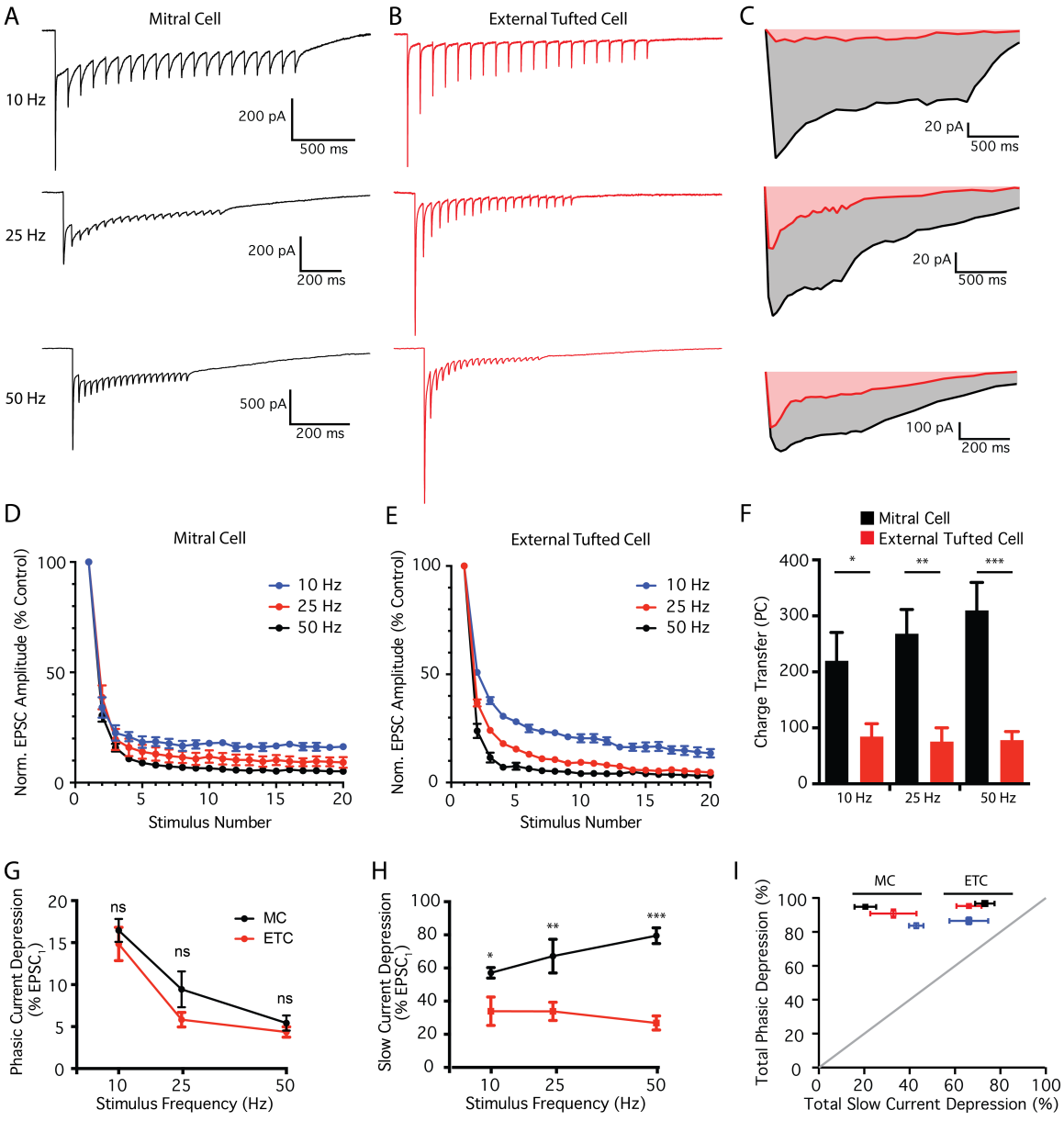
A
Mitral Cell
10 Hz
200 pA
500 ms
25 Hz
200 pA
200 ms
50 Hz
500 pA
200 ms
B
External Tufted Cell
C
20 pA
500 ms
20 pA
500 ms
100 pA
200 ms
D
Mitral Cell
Norm. EPSC Amplitude (% Control)
10 Hz
25 Hz
50 Hz
Stimulus Number
E
External Tufted Cell
Norm. EPSC Amplitude (% Control)
10 Hz
25 Hz
50 Hz
Stimulus Number
F
Mitral Cell
External Tufted Cell
Charge Transfer (PC)
10 Hz
25 Hz
50 Hz
G
Phasic Current Depression (% EPSC1)
MC
ETC
ns
Stimulus Frequency (Hz)
H
Slow Current Depression (% EPSC1)
Stimulus Frequency (Hz)
I
MC
ETC
Total Phasic Depression (%)
Total Slow Current Depression (%)

Figure 5:

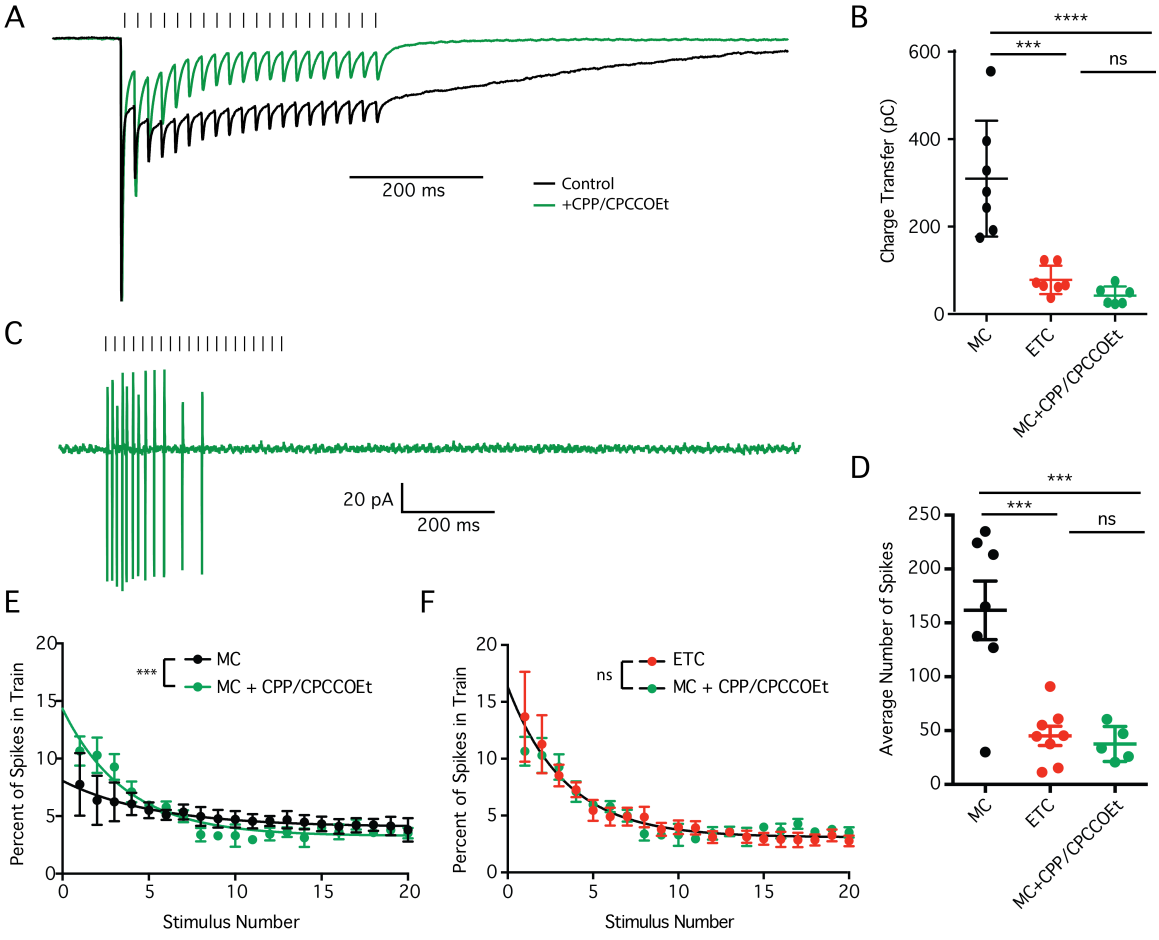
A
200 ms
Control
+CPP/CPCCOEt
B
****
***
ns
Charge Transfer (pC)
600
400
200
0
MC
ETC
MC+CPP/CPCCOEt
C
20 pA
200 ms
D
***
***
ns
Average Number of Spikes
250
200
150
100
50
0
MC
ETC
MC+CPP/CPCCOEt
E
***
MC
MC + CPP/CPCCOEt
Percent of Spikes in Train
20
15
10
5
0
0
5
10
15
20
Stimulus Number
F
ns
ETC
MC + CPP/CPCCOEt
Percent of Spikes in Train
20
15
10
5
0
0
5
10
15
20
Stimulus Number

Figure 6:

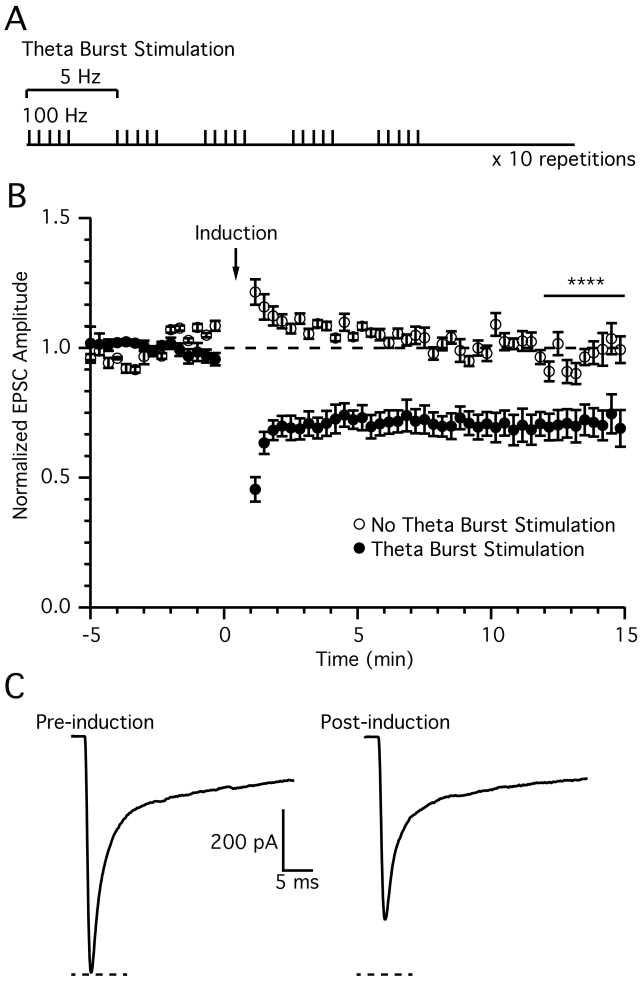
A
Theta Burst Stimulation
5 Hz
100 Hz
x 10 repetitions
B
Induction
****
Normalized EPSC Amplitude
1.5
1.0
0.5
0.0
-5
0
5
10
15
Time (min)
No Theta Burst Stimulation
Theta Burst Stimulation
C
Pre-induction
Post-induction
200 pA
5 ms

Discussion and Future Directions:

The work presented in this dissertation was aimed at understanding the connectivity as well as the presynaptic and postsynaptic transformations that occur in distinct principal cell populations within the glomerular microcircuit. In order to address these questions, I used whole cell voltage and current clamp recordings from acute olfactory bulb slices from wildtype and mutant mice. I also refined a single glomerular stimulation technique, which allows for the precise and focal stimulation of olfactory afferents innervating a single glomerulus. Broadly speaking, my results indicate that despite receiving common afferent olfactory input, which has an extraordinarily high release probability, mitral cells and external tufted cells have dramatic differences in the postsynaptic responses. Specifically, mitral cells have robust dendrodendritic amplification that significantly prolongs the EPSC in response to brief afferent stimulation, and increases the total charge transfer. In response to naturalistic, high frequency ORN stimulation the enhanced dendrodendritic amplification in mitral cells allows them to produce sustained spiking responses, whereas in external tufted cells the lack of dendrodendritic amplification results in transient responses to high frequency ORN stimulation. These distinct postsynaptic transformations may be critical in determining the parallel processing of afferent olfactory input.

Short axon cells modulate presynaptic release probability

Among juxtaglomerular interneurons, short axon cells are unique not only in their ability to release multiple transmitters, but also in their broad connectivity across multiple glomeruli (Maher and Westbrook, 2008; Kiyokage *et al.*, 2010; Borisovska *et al.*, 2013). Functionally, short axon cells produce inhibition-excitation coupling in external tufted cells (Whitesell *et al.*, 2013; Liu *et al.*, 2013), and may directly inhibit mitral cells as well (Liu *et al.*, 2016). The ability of short axon cells to modulate presynaptic release probability is perhaps not surprising given the expression of D_2 and $GABA_B$ receptors presynaptically (Nickell *et al.*, 1994; Bonino *et al.*, 1999; Hsia *et al.*, 1999; Aroniadou-Anderjaska *et al.*, 2000; Ennis *et al.*, 2001; Wachowiak *et al.*, 2005; Maher and Westbrook, 2008). However, given the anatomical segregation of axodendritic and dendrodendritic synaptic compartments, it was unclear whether synaptically released dopamine and GABA could act on presynaptic receptors. The work presented here demonstrates that short axon cells are capable of modulating the presynaptic release probability of olfactory receptor nerve terminals. The ability of short axon cells to release multiple neurotransmitters across distinct timescales and inhibit both pre and postsynaptic targets, suggests that short axon cells potently control the gain of afferent olfactory input (Whitesell *et al.*, 2013; Borisovska *et al.*, 2013; Liu *et al.*, 2013, 2016). In fact, *in vivo*, stimulation of short axon cells reduced the odorant-evoked responses in distant mitral cells; however, whether this resulted from pre- or postsynaptic inhibition was not addressed (Banerjee *et al.*, 2015).

The role of short axon cells in modulating the gain of afferent input is further supported by naris occlusion experiments, in which sensory deprivation dramatically reduces the expression of tyrosine hydroxylase in short axon cells (Baker *et al.*, 1983, 1993). On the other hand, increased tyrosine hydroxylase may reduce the gain of afferent input. For example, there is a near 100% increase in the density of tyrosine hydroxylase positive short axon cells in Parkinson's disease (Huisman *et al.*, 2004; Mundiñano *et al.*, 2011; Doty, 2012*a*), which is associated with a dramatic reduction in the sense of smell (Doty, 2012*a*). However, a causal link between increased dopamine cell density and olfactory function is lacking, especially given the relatively early presence of α-synuclein aggregation in the olfactory bulb (Doty, 2012*a*, 2012*b*).

Future Directions: It would be interesting, both scientifically and clinically, to directly determine whether the increase in dopamine cell density in the olfactory bulb results in reduced olfactory function. Experimentally, this could be achieved in multiple ways. One approach would be to utilize already established mouse models of Parkinson's disease, screening for increases in tyrosine hydroxylase expression in the olfactory bulb. Alternatively, 6-OHDA lesions in midbrain dopamine neurons has been shown to alter the density of neurons in the olfactory bulb, through changes in neurogenesis within the subventricular zone (Winner *et al.*, 2006; Sui *et al.*, 2012). Understanding the mechanistic underpinnings of olfactory dysfunction in Parkinson's disease is of particular importance as it is increasingly being used in the differential diagnosis for Parkinson's disease (Doty, 2012*a*).

Principal cell connectivity and synaptic transformations:

Defining the connectivity and postsynaptic responses of principal neurons is critical to understanding circuit function. My results indicate that mitral cells receive functionally relevant, monosynaptic input from afferent olfactory nerve terminals, supporting short latency responses in mitral cells. In the intact circuit, polysynaptic activation of mitral cells may be possible when only a few ORN axons are active. This suggests that mitral cells may have different modes of activation depending on the strength of afferent input, thereby reconciling the work of multiple labs (De Saint Jan *et al.*, 2009; Gire and Schoppa, 2009; Najac *et al.*, 2011; Gire *et al.*, 2012). The polysynaptic activation of mitral cells following sparse stimulation is perhaps not surprising, given that stimulation of a single external tufted cell can trigger slow currents in mitral cells (De Saint Jan *et al.*, 2009). Therefore, stimulation of a few afferent fibers may be sufficient to activate external tufted cells, which outnumber mitral cells, and drive the polysynaptic activation of mitral cells.

Despite receiving common afferent input, mitral cells and external tufted cells differed dramatically in their postsynaptic responses. Mitral cells responded to brief afferent stimulation with a prolonged biphasic EPSC that included a prominent slow current mediated by dendrodendritic glutamate release (Carlson *et al.*, 2000; Schoppa and Westbrook, 2001; De Saint Jan and Westbrook, 2007; De Saint Jan *et al.*, 2009; Gire and Schoppa, 2009; Najac *et al.*, 2011; Gire *et al.*, 2012). Interestingly, this slow current was completely absent in external tufted cells.

Future Directions: One of the most striking differences between the afferent evoked synaptic responses of mitral cells and external tufted cells is the complete lack of dendrodendritic currents in external tufted cells. External tufted cells are capable of triggering dendrodendritic slow currents in mitral cells (De Saint Jan *et al.*, 2009), have dendrites in the dendrodendritic glomerular core (Hayar *et al.*, 2004*a*), and form gap junctions with other principal cells (Gire *et al.*, 2012). One possibility, which is directly supported by my experiments, is that external tufted cells lack metabotropic glutamate receptors, which provide critical dendrodendritic amplification in mitral cells (De Saint Jan and Westbrook, 2007; Johnston and Delaney, 2010). The sequence of events necessary to generate the slow dendrodendritic current is still not well understood. Determining if the lack of mGluR1 receptor expression explains the lack of slow currents in external tufted cells may provide an important clue into the mechanisms responsible for generating the slow current.

Finally, whether or not external tufted cells project to olfactory cortex remains controversial. Anatomically, single cell axon tracing experiments suggest that external tufted cells project to a circumscribed region of olfactory cortex (Igarashi *et al.*, 2012), however, it is unclear whether these cells truly represent external tufted cells, which have unique synaptic and intrinsic properties (Hayar *et al.*, 2004*b*, 2004*a*; Najac *et al.*, 2011). Experimentally, this could be confirmed using monosynaptic labeling techniques, such as pseudorabies virus, to label cells projecting to different regions of olfactory cortex; followed by electrophysiological recordings to confirm their identity using synaptic and

intrinsic properties. If external tufted cells do project to higher areas of cortex, determining their odorant evoked responses would provide insight into the parallel processing of olfactory input.

Axodendritic and dendrodendritic synapses form distinct circuits

The differential response profiles of mitral cells and external tufted cells is particularly striking in response to high frequency ORN stimulation, as it contributes to distinct temporal filters in each cell type. These results suggest that the differential weighting of axodendritic and dendrodendritic input across cell types determines, at least in part, the parallel processing of common afferent input.

The results presented in this dissertation also examined the presynaptic release probability and vesicle dynamics of the olfactory receptor neuron. In agreement with previous literature, the ORN release probability in my experiments was high (near 1), however, in brain slices, the tonic and/or phasic activation of presynaptic D_2 and $GABA_B$ reduced the release probability to approximately 0.7, which is still one of the highest release probabilities reported in the brain. The high release probability of the ORN is consistent with the primary function of the ORN in faithfully transmitting odorant-binding events.

Future Directions: Behavioral experiments in which the strength of axodendritic and dendrodendritic synapses is directly modulated would provide critical insight into whether these two pathways contribute to different aspects of

olfactory processing. Experimentally, this could be accomplished with cell type specific knockouts of mGluR1 or connexin-36. Cell type specific knockouts are advantageous here as global knockouts of these proteins introduce additional behavioral complexities, which may confound the results. New cell-type specific cre-lines have been recently developed which specifically target mitral cells (e.g. protocadherin-21), making these experiments technically feasible

Implications for olfactory processing:

One potential hypothesis regarding the parallel processing of afferent input by mitral cells and external tufted cells is that they differentially contribute to the olfactory percept. For example, the robust amplification of afferent input in mitral cells has long been thought to contribute to enhancing the signal to noise ratio and contributing to the identification of odorants, especially at low concentrations (Chen and Shepherd, 2005). Additionally, *in vivo,* the temporal pattern of mitral cell responses varies in a concentration dependent manner (Fukunaga *et al.,* 2012); therefore mitral cells are well positioned to encode the concentration or intensity of the odorant.

The function of external tufted cells, however, is less well understood. One possibility is that the large afferent evoked responses in external tufted cells, coupled with the extraordinarily high afferent release probability, allows external tufted cells to maintain odorant sensitivity originally established in the olfactory periphery. Such high sensitivity, in theory, would produce similar responses in

external tufted cells across odorant concentrations, allowing external tufted cells to encode odorant identity. This interpretation is consistent with *in vivo* data, which suggest that tufted cells show concentration invariant responses (Nagayama *et al*., 2004; Igarashi *et a*l., 2012; Fukunaga *et a*l., 2012; Kikuta *et al.,* 2013).

Recent *in vivo* experiments in piriform cortex suggest that the odorant identity and concentration are differentially encoded (Bolding and Franks, 2017), which may reflect parallel inputs. Within piriform cortex, odorant identity is encoded by the ensemble activation of neurons, independent of odorant concentration. However, odorant concentration is best encoded by the relative timing of two response phases in piriform cortex cells, that is, as concentration increases, the latency of the second response phase is significantly shortened (Bolding and Franks, 2017). One possibility, is that the short latency responses in piriform cortex results from the transient, robust responses in external tufted cells, whereas the delayed response represents mitral cell activity, such that the relative timing between transient and sustained response profiles encodes odorant concentration. The work presented here highlights the distinct synaptic transformations that occur in two principal neuron subtypes within the olfactory bulb, and suggests that these two cells may differentially encode odorant features, thereby contributing to the parallel processing of olfactory information.

References:

Abbott LF and Regehr WG (2004). Synaptic computation. *Nature* **431,** 796–803.

Adler J (1969). Chemoreceptors in bacteria. *Science* **166,** 1588–1597.

Allison AC (1953). THE MORPHOLOGY OF THE OLFACTORY SYSTEM IN THE VERTEBRATES. *Biol Rev Camb Philos Soc* **28,** 195–244.

Antunes G and Simoes de Souza FM (2016). Olfactory receptor signaling. *Methods Cell Biol* **132,** 127–145.

Aroniadou-Anderjaska V, Ennis M and Shipley MT (1997). Glomerular synaptic responses to olfactory nerve input in rat olfactory bulb slices. *Neuroscience* **79,** 425–434.

Aroniadou-Anderjaska V, Ennis M and Shipley MT (1999). Dendrodendritic recurrent excitation in mitral cells of the rat olfactory bulb. *J Neurophysiol* **82,** 489–494.

Aroniadou-Anderjaska V, Zhou F-M, Priest CA, Ennis M and Shipley MT (2000). Tonic and Synaptically Evoked Presynaptic Inhibition of Sensory Input to the Rat Olfactory Bulb Via GABAB Heteroreceptors. *J Neurophysiol* **84,** 1194–1203.

Babai N, Kochubey O, Keller D and Schneggenburger R (2014). An Alien Divalent Ion Reveals a Major Role for Ca2+ Buffering in Controlling Slow Transmitter Release. *J Neurosci* **34,** 12622–12635.

Bäckman CM, Malik N, Zhang Y, Shan L, Grinberg A, Hoffer BJ, Westphal H and Tomac AC (2006). Characterization of a mouse strain expressing Cre recombinase from the 3′ untranslated region of the dopamine transporter locus. *Genesis* **44,** 383–390.

Bakalyar HA and Reed RR (1990). Identification of a specialized adenylyl cyclase that may mediate odorant detection. *Science* **250,** 1403–1406.

Baker H, Kawano T, Margolis FL and Joh TH (1983). Transneuronal regulation of tyrosine hydroxylase expression in olfactory bulb of mouse and rat. *J Neurosci* **3,** 69–78.

Baker H, Morel K, Stone DM and Maruniak JA (1993). Adult naris closure profoundly reduces tyrosine hydroxylase expression in mouse olfactory bulb. *Brain Res* **614,** 109–116.

Banerjee A, Marbach F, Anselmi F, Koh MS, Davis MB, Garcia da Silva P, Delevich K, Oyibo HK, Gupta P, Li B and Albeanu DF (2015). An Interglomerular Circuit Gates Glomerular Output and Implements Gain Control in the Mouse Olfactory Bulb. *Neuron* **87,** 193–207.

Bartel DL, Rela L, Hsieh L and Greer CA (2015). Dendrodendritic synapses in the mouse olfactory bulb external plexiform layer. *J Comp Neurol* **523,** 1145–1161.

Berry MS and Pentreath VW (1976). Criteria for distinguishing between monosynaptic and polysynaptic transmission. *Brain Res* **105,** 1–20.

Betz WJ (1970). Depression of transmitter release at the neuromuscular junction of the frog. *J Physiol* **206,** 629–644.

Bolding KA, Franks KM (2017). Complementary codes for odor identity and intensity in olfactory cortex. *Elife* DOI: 10.7554/eLife.22630.

Bonino M, Cantino D and Sassoè-Pognetto M (1999). Cellular and subcellular localization of γ-aminobutyric acid B receptors in the rat olfactory bulb. *Neurosci Lett* **274,** 195–198.

Borisovska M, Bensen AL, Chong G and Westbrook GL (2013). Distinct modes of dopamine and GABA release in a dual transmitter neuron. *J Neurosci* **33,** 1790–1796.

Borisovska M, McGinley MJ, Bensen A and Westbrook GL (2011). Loss of olfactory cell adhesion molecule reduces the synchrony of mitral cell activity in olfactory glomeruli. *J Physiol* **589,** 1927–1941.

Borst JG and Sakmann B (1996). Calcium influx and transmitter release in a fast CNS synapse. *Nature* **383,** 431–434.

Bourne JN and Schoppa NE (2017). Three-dimensional synaptic analyses of mitral cell and external tufted cell dendrites in rat olfactory bulb glomeruli. *J Comp Neurol* **525,** 592–609.

Buck L and Axel R (1991). A novel multigene family may encode odorant receptors: a molecular basis for odor recognition. *Cell* **65,** 175–187.

Burton SD and Urban NN (2014). Greater excitability and firing irregularity of tufted cells underlies distinct afferent-evoked activity of olfactory bulb mitral and tufted cells. *J Physiol* **592,** 2097–2118.

Bushdid C, Magnasco MO, Vosshall LB and Keller A (2014). Humans can discriminate more than 1 trillion olfactory stimuli. *Science* **343,** 1370–1372.

Carey RM, Sherwood WE, Shipley MT, Borisyuk A and Wachowiak M (2015). Role of intraglomerular circuits in shaping temporally structured responses to naturalistic inhalation-driven sensory input to the olfactory bulb. *J Neurophysiol* **113,** 3112–3129.

Carey RM, Verhagen JV, Wesson DW, Pírez N and Wachowiak M (2009). Temporal structure of receptor neuron input to the olfactory bulb imaged in behaving rats. *J Neurophysiol* **101,** 1073–1088.

Carlson GC, Shipley MT and Keller A (2000). Long-lasting depolarizations in mitral cells of the rat olfactory bulb. *J Neurosci* **20,** 2011–2021.

Carter AG and Regehr WG (2000). Prolonged synaptic currents and glutamate spillover at the parallel fiber to stellate cell synapse. *J Neurosci* **20,** 4423–4434.

Castro JB and Urban NN (2009). Subthreshold glutamate release from mitral cell dendrites. *J Neurosci* **29,** 7023–7030.

Chanda S and Xu-Friedman MA (2010). A low-affinity antagonist reveals saturation and desensitization in mature synapses in the auditory brain stem. *J Neurophysiol* **103,** 1915–1926.

Chao TI, Kasa P and Wolff JR (1997). Distribution of astroglia in glomeruli of the rat main olfactory bulb: exclusion from the sensory subcompartment of neuropil. *J Comp Neurol* **388,** 191–210.

Chatzi C, Schnell E and Westbrook GL (2015). Localized hypoxia within the subgranular zone determines the early survival of newborn hippocampal granule cells. *Elife* **4,** e08722.

Chen WR and Shepherd GM (1997). Membrane and synaptic properties of mitral cells in slices of rat olfactory bulb. *Brain Res* **745,** 189–196.

Chen WR and Shepherd GM (2005). The olfactory glomerulus: a cortical module with specific functions. *J Neurocytol* **34,** 353–360.

Chess A, Simon I, Cedar H and Axel R (1994). Allelic inactivation regulates olfactory receptor gene expression. *Cell* **78,** 823–834.

Christie JM, Bark C, Hormuzdi SG, Helbig I, Monyer H and Westbrook GL (2005). Connexin36 mediates spike synchrony in olfactory bulb glomeruli. *Neuron* **46,** 761–772.

Christie JM, Schoppa NE and Westbrook GL (2001). Tufted cell dendrodendritic inhibition in the olfactory bulb is dependent on NMDA receptor activity. *J Neurophysiol* **85,** 169–173.

Christie JM and Westbrook GL (2006). Lateral excitation within the olfactory bulb. *J Neurosci* **26,** 2269–2277.

Cleland TA (2010). Early transformations in odor representation. *Trends Neurosci* **33,** 130–139.

Clements JD (1996). Transmitter timecourse in the synaptic cleft: its role in central synaptic function. *Trends Neurosci* **19,** 163–171.

Cockerham R, Liu S, Cachope R, Kiyokage E, Cheer JF, Shipley MT and Puche AC (2016). Subsecond Regulation of Synaptically Released Dopamine by COMT in the Olfactory Bulb. *J Neurosci* **36,** 7779–7785.

Coddington LT, Nietz AK and Wadiche JI (2014). The contribution of extrasynaptic signaling to cerebellar information processing. *Cerebellum* **13,** 513–520.

Connors BW (2017). Synchrony and so much more: Diverse roles for electrical synapses in neural circuits. *Dev Neurobiol*; DOI: 10.1002/dneu.22493.

De Saint Jan D, Hirnet D, Westbrook GL and Charpak S (2009). External tufted cells drive the output of olfactory bulb glomeruli. *J Neurosci* **29,** 2043–2052.

De Saint Jan D and Westbrook GL (2005). Detecting activity in olfactory bulb glomeruli with astrocyte recording. *J Neurosci* **25,** 2917–2924.

De Saint Jan D and Westbrook GL (2007). Disynaptic amplification of metabotropic glutamate receptor 1 responses in the olfactory bulb. *J Neurosci* **27,** 132–140.

Dhallan RS, Yau KW, Schrader KA and Reed RR (1990). Primary structure and functional expression of a cyclic nucleotide-activated channel from olfactory neurons. *Nature* **347,** 184–187.

Doty RL (2012*a*). Olfactory dysfunction in Parkinson disease. *Nat Rev Neurol* **8,** 329–339.

Doty RL (2012*b*). Olfaction in Parkinson's disease and related disorders. *Neurobiol Dis* **46,** 527–552.

Duchamp-Viret P, Chaput MA and Duchamp A (1999). Odor response properties of rat olfactory receptor neurons. *Science* **284,** 2171–2174.

Egger V and Urban NN (2006). Dynamic connectivity in the mitral cell-granule cell microcircuit. *Semin Cell Dev Biol* **17,** 424–432.

Elmqvist D and Quastel DM (1965). A quantitative study of end-plate potentials in isolated human muscle. *J Physiol* **178,** 505–529.

Ennis M, Zhou F-M, Ciombor KJ, Aroniadou-Anderjaska V, Hayar A, Borrelli E, Zimmer LA, Margolis F and Shipley MT (2001). Dopamine D2 Receptor–Mediated Presynaptic Inhibition of Olfactory Nerve Terminals. *J Neurophysiol* **86,** 2986–2997.

Ennis M, Zimmer LA and Shipley MT (1996). Olfactory nerve stimulation activates rat mitral cells via NMDA and non-NMDA receptors in vitro. *Neuroreport* **7,** 989–992.

Fekete A, Johnston J and Delaney KR (2014). Presynaptic T-type Ca2+ channels modulate dendrodendritic mitral-mitral and mitral-periglomerular connections in mouse olfactory bulb. *J Neurosci* **34,** 14032–14045.

Feng G, Mellor RH, Bernstein M, Keller-Peck C, Nguyen QT, Wallace M, Nerbonne JM, Lichtman JW and Sanes JR (2000). Imaging neuronal subsets in transgenic mice expressing multiple spectral variants of GFP. *Neuron* **28,** 41–51.

Firestein S, Picco C and Menini A (1993). The relation between stimulus and response in olfactory receptor cells of the tiger salamander. *J Physiol* **468,** 1–10.

Firestein S, Shepherd GM and Werblin FS (1990). Time course of the membrane current underlying sensory transduction in salamander olfactory receptor neurones. *J Physiol* **430,** 135–158.

Ford CP (2014). The role of D2-autoreceptors in regulating dopamine neuron activity and transmission. *Neuroscience* **282,** 13–22.

Ford CP, Gantz SC, Phillips PEM and Williams JT (2010). Control of extracellular dopamine at dendrite and axon terminals. *J Neurosci* **30,** 6975–6983.

Foster KA, Kreitzer AC and Regehr WG (2002). Interaction of postsynaptic receptor saturation with presynaptic mechanisms produces a reliable synapse. *Neuron* **36,** 1115–1126.

Friedman D and Strowbridge BW (2000). Functional role of NMDA autoreceptors in olfactory mitral cells. *J Neurophysiol* **84,** 39–50.

Fukunaga I, Berning M, Kollo M, Schmaltz A and Schaefer AT (2012). Two distinct channels of olfactory bulb output. *Neuron* **75,** 320–329.

Gall CM, Hendry SH, Seroogy KB, Jones EG and Haycock JW (1987). Evidence for coexistence of GABA and dopamine in neurons of the rat olfactory bulb. *J Comp Neurol* **266,** 307–318.

Gardner EP and Johnson KO (2013). Sensory coding. In Principals of Neural Science, 5th edn, ed. Kandel ER, Schwartz JH, Jessel TM, Siegelbaum SA, Hudspeth AJ, pp. 449-474. McGraw Hill, New York.

Geramita MA, Burton SD and Urban NN (2016). Distinct lateral inhibitory circuits drive parallel processing of sensory information in the mammalian olfactory bulb. *Elife*; DOI: 10.7554/eLife.16039.

Geramita M and Urban NN (2017). Differences in Glomerular-Layer-Mediated Feedforward Inhibition onto Mitral and Tufted Cells Lead to Distinct Modes of Intensity Coding. *J Neurosci* **37,** 1428–1438.

von Gersdorff H and Borst JGG (2002). Short-term plasticity at the calyx of Held. *Nat Rev Neurosci* **3,** 53–64.

Gesteland RC and Sigwart CD (1977). Olfactory receptor units—a mammalian preparation. *Brain Res* **133,** 144–149.

Getchell TV and Shepherd GM (1978). Responses of olfactory receptor cells to step pulses of odour at different concentrations in the salamander. *J Physiol* **282,** 521–540.

Giraudet P, Berthommier F and Chaput M (2002). Mitral cell temporal response patterns evoked by odor mixtures in the rat olfactory bulb. *J Neurophysiol* **88,** 829–838.

Gire DH, Franks KM, Zak JD, Tanaka KF, Whitesell JD, Mulligan AA, Hen R and Schoppa NE (2012). Mitral cells in the olfactory bulb are mainly excited through a multistep signaling path. *J Neurosci* **32,** 2964–2975.

Gire DH and Schoppa NE (2009). Control of on/off glomerular signaling by a local GABAergic microcircuit in the olfactory bulb. *J Neurosci* **29,** 13454–13464.

Graziadei PP and Graziadei GA (1979). Neurogenesis and neuron regeneration in the olfactory system of mammals. I. Morphological aspects of differentiation and structural organization of the olfactory sensory neurons. *J Neurocytol* **8,** 1–18.

Griff ER, Mafhouz M and Chaput MA (2008). Comparison of identified mitral and tufted cells in freely breathing rats: II. Odor-evoked responses. *Chem Senses* **33,** 793–802.

Hálasz N and Greer CA (1993). Terminal arborizations of olfactory nerve fibers in the glomeruli of the olfactory bulb. *J Comp Neurol* **337,** 307–316.

Hayar A, Karnup S, Ennis M and Shipley MT (2004*a*). External tufted cells: a major excitatory element that coordinates glomerular activity. *J Neurosci* **24,** 6676–6685.

Hayar A, Karnup S, Shipley MT and Ennis M (2004*b*). Olfactory bulb glomeruli: external tufted cells intrinsically burst at theta frequency and are entrained by patterned olfactory input. *J Neurosci* **24,** 1190–1199.

Hayar A, Shipley MT and Ennis M (2005). Olfactory bulb external tufted cells are synchronized by multiple intraglomerular mechanisms. *J Neurosci* **25,** 8197–8208.

Hsia AY, Vincent JD and Lledo PM (1999). Dopamine depresses synaptic inputs into the olfactory bulb. *J Neurophysiol* **82,** 1082–1085.

Hudspeth AJ and Logothetis NK (2000). Sensory Systems. *Curr Opin Neurobiol* **10**, 631—641.

Huisman E, Uylings HBM and Hoogland PV (2004). A 100% increase of dopaminergic cells in the olfactory bulb may explain hyposmia in Parkinson's disease. *Mov Disord* **19,** 687–692.

Igarashi KM, Ieki N, An M, Yamaguchi Y, Nagayama S, Kobayakawa K, Kobayakawa R, Tanifuji M, Sakano H, Chen WR and Mori K (2012). Parallel mitral and tufted cell pathways route distinct odor information to different targets in the olfactory cortex. *J Neurosci* **32,** 7970–7985.

Isaacson JS (1999). Glutamate spillover mediates excitatory transmission in the rat olfactory bulb. *Neuron* **23,** 377–384.

Isaacson JS and Strowbridge BW (1998). Olfactory reciprocal synapses: dendritic signaling in the CNS. *Neuron* **20,** 749–761.

Jahr CE and Nicoll RA (1980). Dendrodendritic inhibition: demonstration with intracellular recording. *Science* **207,** 1473–1475.

Jahr CE and Nicoll RA (1982). An intracellular analysis of dendrodendritic inhibition in the turtle in vitro olfactory bulb. *J Physiol* **326,** 213–234.

Johnston J and Delaney KR (2010). Synaptic activation of T-type Ca2+ channels via mGluR activation in the primary dendrite of mitral cells. *J Neurophysiol* **103,** 2557–2569.

Jones DT and Reed RR (1989). G (olf): an olfactory neuron specific-G protein involved in odorant signal transduction. *Science* **244,** 790–796.

Julius D and Katz LC (2004). A Nobel for smell. *Cell* **119,** 747–752.

Kaas, JH (1989). The evolution of complex sensory systems in mammals. *J. Exp. Biol* **146,** 165-176.

Kaneko H, Putzier I, Frings S, Kaupp UB and Gensch T (2004). Chloride accumulation in mammalian olfactory sensory neurons. *J Neurosci* **24,** 7931–7938.

Kasowski HJ, Kim H and Greer CA (1999). Compartmental organization of the olfactory bulb glomerulus. *J Comp Neurol* **407,** 261–274.

Katada S, Hirokawa T, Oka Y, Suwa M and Touhara K (2005). Structural basis for a broad but selective ligand spectrum of a mouse olfactory receptor: mapping the odorant-binding site. *J Neurosci* **25,** 1806–1815.

Kikuta S, Fletcher ML, Homma R, Yamasoba T and Nagayama S (2013). Odorant response properties of individual neurons in an olfactory glomerular module. *Neuron* **77,** 1122–1135.

Kim H and Greer CA (2000). The emergence of compartmental organization in olfactory bulb glomeruli during postnatal development. *J Comp Neurol* **422,** 297–311.

Kiyokage E, Pan Y-Z, Shao Z, Kobayashi K, Szabo G, Yanagawa Y, Obata K, Okano H, Toida K, Puche AC and Shipley MT (2010). Molecular identity of periglomerular and short axon cells. *J Neurosci* **30,** 1185–1196.

Kleene SJ (2008). The electrochemical basis of odor transduction in vertebrate olfactory cilia. *Chem Senses* **33,** 839–859.

Klenoff JR and Greer CA (1998). Postnatal development of olfactory receptor cell axonal arbors. *J Comp Neurol* **390,** 256–267.

Kosaka K, Aika Y and Toida K (2001). Structure of intraglomerular dendritic tufts of mitral cells and their contacts with olfactory nerve terminals and calbindin-immunoreactive type 2 periglomerular neurons. *Journal of Comparative*. Available at: http://onlinelibrary.wiley.com/doi/10.1002/cne.1381/full.

Kosaka T and Kosaka K (2005). Structural organization of the glomerulus in the main olfactory bulb. *Chem Senses* **30 Suppl 1,** i107–i108.

Kurahashi T and Menini A (1997). Mechanism of odorant adaptation in the olfactory receptor cell. *Nature* **385,** 725–729.

Kurahashi T and Shibuya T (1990). Ca2(+)-dependent adaptive properties in the solitary olfactory receptor cell of the newt. *Brain Res* **515,** 261–268.

Kurahashi T and Yau KW (1993). Co-existence of cationic and chloride components in odorant-induced current of vertebrate olfactory receptor cells. *Nature* **363,** 71–74.

Leng G, Hashimoto H, Tsuji C, Sabatier N and Ludwig M (2014). Discharge patterning in rat olfactory bulb mitral cells in vivo. *Physiol Rep*; DOI: 10.14814/phy2.12021.

Liley AW and North KA (1953). An electrical investigation of effects of repetitive stimulation on mammalian neuromuscular junction. *J Neurophysiol* **16,** 509–527.

Liu S, Plachez C, Shao Z, Puche A and Shipley MT (2013). Olfactory bulb short axon cell release of GABA and dopamine produces a temporally biphasic inhibition-excitation response in external tufted cells. *J Neurosci* **33,** 2916–2926.

Liu S, Puche AC and Shipley MT (2016). The Interglomerular Circuit Potently Inhibits Olfactory Bulb Output Neurons by Both Direct and Indirect Pathways. *J Neurosci* **36,** 9604–9617.

Lowe G and Gold GH (1993). Nonlinear amplification by calcium-dependent chloride channels in olfactory receptor cells. *Nature* **366,** 283–286.

Lu H-W and Trussell LO (2016). Spontaneous Activity Defines Effective Convergence Ratios in an Inhibitory Circuit. *J Neurosci* **36,** 3268–3280.

Lynch JW and Barry PH (1989). Action potentials initiated by single channels opening in a small neuron (rat olfactory receptor). *Biophys J* **55,** 755–768.

Maher BJ, McGinley MJ and Westbrook GL (2009). Experience-dependent maturation of the glomerular microcircuit. *Proc Natl Acad Sci U S A* **106,** 16865–16870.

Maher BJ and Westbrook GL (2008). Co-transmission of dopamine and GABA in periglomerular cells. *J Neurophysiol* **99,** 1559–1564.

Malnic B, Godfrey PA and Buck LB (2004). The human olfactory receptor gene family. *Proc Natl Acad Sci U S A* **101,** 2584–2589.

Malnic B, Hirono J, Sato T and Buck LB (1999). Combinatorial receptor codes for odors. *Cell* **96,** 713–723.

Martelli C, Carlson JR and Emonet T (2013). Intensity invariant dynamics and odor-specific latencies in olfactory receptor neuron response. *J Neurosci* **33,** 6285–6297.

McCormick DA and Shepherd GM (2004). The synaptic organization of the brain.

McGann JP, Pírez N, Gainey MA, Muratore C, Elias AS and Wachowiak M (2005). Odorant representations are modulated by intra- but not interglomerular presynaptic inhibition of olfactory sensory neurons. *Neuron* **48,** 1039–1053.

Meister M (2014). Can Humans Really Discriminate 1 Trillion Odors? *arXiv [q-bioNC]*. Available at: http://arxiv.org/abs/1411.0165.

Mennerick S and Matthews G (1996). Ultrafast exocytosis elicited by calcium current in synaptic terminals of retinal bipolar neurons. *Neuron* **17,** 1241–1249.

Molday RS and Moritz OL (2015). Photoreceptors at a glance. *J Cell Sci* **128,** 4039–4045.

Mombaerts P (1999). Molecular biology of odorant receptors in vertebrates. *Annu Rev Neurosci* **22,** 487–509.

Mombaerts P, Wang F, Dulac C, Chao SK, Nemes A, Mendelsohn M, Edmondson J and Axel R (1996). Visualizing an olfactory sensory map. *Cell* **87,** 675–686.

Mori K, Nagao H and Yoshihara Y (1999). The olfactory bulb: coding and processing of odor molecule information. *Science* **286,** 711–715.

Mundiñano I-C, Caballero M-C, Ordóñez C, Hernandez M, DiCaudo C, Marcilla I, Erro M-E, Tuñon M-T and Luquin M-R (2011). Increased dopaminergic cells and protein aggregates in the olfactory bulb of patients with neurodegenerative disorders. *Acta Neuropathol* **122,** 61–74.

Murphy GJ, Darcy DP and Isaacson JS (2005). Intraglomerular inhibition: signaling mechanisms of an olfactory microcircuit. *Nat Neurosci* **8,** 354–364.

Murphy GJ, Glickfeld LL, Balsen Z and Isaacson JS (2004). Sensory neuron signaling to the brain: properties of transmitter release from olfactory nerve terminals. *J Neurosci* **24,** 3023–3030.

Mutoh H, Yuan Q and Knöpfel T (2005). Long-term depression at olfactory nerve synapses. *J Neurosci* **25,** 4252–4259.

Nagai MH, Armelin-Correa LM and Malnic B (2016). Monogenic and Monoallelic Expression of Odorant Receptors. *Mol Pharmacol* **90,** 633–639.

Nagayama S, Enerva A, Fletcher ML, Masurkar AV, Igarashi KM, Mori K and Chen WR (2010). Differential axonal projection of mitral and tufted cells in the mouse main olfactory system. *Front Neural Circuits*; DOI: 10.3389/fncir.2010.00120.

Nagayama S, Homma R and Imamura F (2014). Neuronal organization of olfactory bulb circuits. *Front Neural Circuits* **8,** 98.

Nagayama S, Takahashi YK, Yoshihara Y and Mori K (2004). Mitral and tufted cells differ in the decoding manner of odor maps in the rat olfactory bulb. *J Neurophysiol* **91,** 2532–2540.

Nagel G, Szellas T, Huhn W, Kateriya S, Adeishvili N, Berthold P, Ollig D, Hegemann P and Bamberg E (2003). Channelrhodopsin-2, a directly light-gated cation-selective membrane channel. *Proc Natl Acad Sci U S A* **100,** 13940–13945.

Najac M, De Saint Jan D, Reguero L, Grandes P and Charpak S (2011). Monosynaptic and polysynaptic feed-forward inputs to mitral cells from olfactory sensory neurons. *J Neurosci* **31,** 8722–8729.

Nakamura T and Gold GH (1987). A cyclic nucleotide-gated conductance in olfactory receptor cilia. *Nature* **325,** 442–444.

Neher E (2015). Merits and Limitations of Vesicle Pool Models in View of Heterogeneous Populations of Synaptic Vesicles. *Neuron* **87,** 1131–1142.

Nickell WT, Behbehani MM and Shipley MT (1994). Evidence for GABAB-mediated inhibition of transmission from the olfactory nerve to mitral cells in the rat olfactory bulb. *Brain Res Bull* **35,** 119–123.

Nicoll RA and Jahr CE (1982). Self-excitation of olfactory bulb neurones. *Nature* **296,** 441–444.

Nowycky MC, Mori K and Shepherd GM (1981). GABAergic mechanisms of dendrodendritic synapses in isolated turtle olfactory bulb. *J Neurophysiol* **46,** 639–648.

Oleskevich S, Clements J and Walmsley B (2000). Release probability modulates short-term plasticity at a rat giant terminal. *J Physiol* **524 Pt 2,** 513–523.

Ottoson D (1971). The Electro-Olfactogram. In *Olfaction*, ed. Beidler LM, Handbook of Sensory Physiology, pp. 95–131. Springer Berlin Heidelberg.

Picco C, Gavazzo P, Firestein S and Menini A (1998). Responses of Isolated Olfactory Sensory Neurons to Odorants. In *Neural Circuits and Networks*, ed. Torre V and Nicholls J, NATO ASI Series, pp. 85–93. Springer Berlin Heidelberg.

Pilpel Y and Lancet D (1999). The variable and conserved interfaces of modeled olfactory receptor proteins. *Protein Sci* **8,** 969–977.

Pimentel DO and Margrie TW (2008). Glutamatergic transmission and plasticity between olfactory bulb mitral cells. *J Physiol* **586,** 2107–2119.

Pinching AJ and Powell T (1971). The neuropil of the glomeruli of the olfactory bulb. *J Cell Sci* **9,** 347–377.

Pirez N and Wachowiak M (2008). In Vivo Modulation of Sensory Input to the Olfactory Bulb by Tonic and Activity-Dependent Presynaptic Inhibition of Receptor Neurons. *Journal of Neuroscience* **28,** 6360–6371.

van den Pol AN (1995). Presynaptic metabotropic glutamate receptors in adult and developing neurons: autoexcitation in the olfactory bulb. *J Comp Neurol* **359,** 253–271.

Reese TS and Brightman MW (1970). Olfactory Surface and Central Olfactory Connexions in Some Vertebrates. In *Ciba Foundation Symposium - Internal Secretions of the Pancreas (Colloquia on Endocrinology)*, pp. 115–149. John Wiley and Sons, Ltd.

Regehr WG (2012). Short-term presynaptic plasticity. *Cold Spring Harb Perspect Biol* **4,** a005702.

Ressler KJ, Sullivan SL and Buck LB (1994). Information coding in the olfactory system: evidence for a stereotyped and highly organized epitope map in the olfactory bulb. *Cell* **79,** 1245–1255.

Rice ME and Patel JC (2015). Somatodendritic dopamine release: recent mechanistic insights. *Philos Trans R Soc Lond B Biol Sci*; DOI: 10.1098/rstb.2014.0185.

Rieke F (1999). *Spikes: exploring the neural code*. MIT press.

Rospars J-P, Lánský P, Duchamp A and Duchamp-Viret P (2003). Relation between stimulus and response in frog olfactory receptor neurons in vivo. *Eur J Neurosci* **18,** 1135–1154.

Royet JP, Souchier C, Jourdan F and Ploye H (1988). Morphometric study of the glomerular population in the mouse olfactory bulb: numerical density and size distribution along the rostrocaudal axis. *J Comp Neurol* **270,** 559–568.

Rubin BD and Katz LC (1999). Optical imaging of odorant representations in the mammalian olfactory bulb. *Neuron* **23,** 499–511.

Sakaba T and Neher E (2001). Calmodulin mediates rapid recruitment of fast-releasing synaptic vesicles at a calyx-type synapse. *Neuron* **32,** 1119–1131.

Sanes JR and Masland RH (2015). The types of retinal ganglion cells: current status and implications for neuronal classification. *Annu Rev Neurosci* **38,** 221–246.

Saviane C and Silver RA (2006). Fast vesicle reloading and a large pool sustain high bandwidth transmission at a central synapse. *Nature* **439,** 983–987.

Savigner A, Duchamp-Viret P, Grosmaitre X, Chaput M, Garcia S, Ma M and Palouzier-Paulignan B (2009). Modulation of spontaneous and odorant-evoked activity of rat olfactory sensory neurons by two anorectic peptides, insulin and leptin. *J Neurophysiol* **101,** 2898–2906.

Schneggenburger R, Meyer AC and Neher E (1999). Released fraction and total size of a pool of immediately available transmitter quanta at a calyx synapse. *Neuron* **23,** 399–409.

Schneggenburger R, Sakaba T and Neher E (2002). Vesicle pools and short-term synaptic depression: lessons from a large synapse. *Trends Neurosci* **25,** 206–212.

Schoppa NE, Kinzie JM, Sahara Y, Segerson TP and Westbrook GL (1998). Dendrodendritic inhibition in the olfactory bulb is driven by NMDA receptors. *J Neurosci* **18,** 6790–6802.

Schoppa NE and Urban NN (2003). Dendritic processing within olfactory bulb circuits. *Trends Neurosci* **26,** 501–506.

Schoppa NE and Westbrook GL (2001). Glomerulus-specific synchronization of mitral cells in the olfactory bulb. *Neuron* **31,** 639–651.

Schoppa NE and Westbrook GL (2002). AMPA autoreceptors drive correlated spiking in olfactory bulb glomeruli. *Nat Neurosci* **5,** 1194–1202.

Serizawa S, Ishii T, Nakatani H, Tsuboi A, Nagawa F, Asano M, Sudo K, Sakagami J, Sakano H, Ijiri T, Matsuda Y, Suzuki M, Yamamori T, Iwakura Y and Sakano H (2000). Mutually exclusive expression of odorant receptor transgenes. *Nat Neurosci* **3,** 687–693.

Serizawa S, Miyamichi K and Sakano H (2004). One neuron–one receptor rule in the mouse olfactory system. *Trends Genet* **20,** 648–653.

Shao Z, Puche AC, Kiyokage E, Szabo G and Shipley MT (2009). Two GABAergic intraglomerular circuits differentially regulate tonic and phasic presynaptic inhibition of olfactory nerve terminals. *J Neurophysiol* **101,** 1988–2001.

Shao Z, Puche AC, Liu S and Shipley MT (2012). Intraglomerular inhibition shapes the strength and temporal structure of glomerular output. *J Neurophysiol* **108,** 782–793.

Shao Z, Puche AC and Shipley MT (2013). Intraglomerular inhibition maintains mitral cell response contrast across input frequencies. *J Neurophysiol* **110,** 2185–2191.

Sicard G (1986). Electrophysiological recordings from olfactory receptor cells in adult mice. *Brain Res* **397,** 405–408.

Silver RA, Lubke J, Sakmann B and Feldmeyer D (2003). High-probability uniquantal transmission at excitatory synapses in barrel cortex. *Science* **302,** 1981–1984.

Simmons PA and Getchell TV (1981). Neurogenesis in olfactory epithelium: loss and recovery of transepithelial voltage transients following olfactory nerve section. *J Neurophysiol* **45,** 516–528.

Sineshchekov OA, Jung K-H and Spudich JL (2002). Two rhodopsins mediate phototaxis to low- and high-intensity light in Chlamydomonas reinhardtii. *Proc Natl Acad Sci U S A* **99,** 8689–8694.

Soucy ER, Albeanu DF, Fantana AL, Murthy VN and Meister M (2009). Precision and diversity in an odor map on the olfactory bulb. *Nat Neurosci* **12,** 210–220.

Sui Y, Horne MK and Stanić D (2012). Reduced proliferation in the adult mouse subventricular zone increases survival of olfactory bulb interneurons. *PLoS One* **7,** e31549.

Takeuchi H and Kurahashi T (2005). Mechanism of signal amplification in the olfactory sensory cilia. *J Neurosci* **25,** 11084–11091.

Tan J, Savigner A, Ma M and Luo M (2010). Odor information processing by the olfactory bulb analyzed in gene-targeted mice. *Neuron* **65,** 912–926.

Taschenberger H, Woehler A and Neher E (2016). Superpriming of synaptic vesicles as a common basis for intersynapse variability and modulation of synaptic strength. *Proc Natl Acad Sci U S A* **113,** E4548–E4557.

Thanawala MS and Regehr WG (2016). Determining synaptic parameters using high-frequency activation. *J Neurosci Methods* **264,** 136–152.

Treloar HB, Feinstein P, Mombaerts P and Greer CA (2002). Specificity of glomerular targeting by olfactory sensory axons. *J Neurosci* **22,** 2469–2477.

Trombley PQ and Westbrook GL (1991). Voltage-gated currents in identified rat olfactory receptor neurons. *J Neurosci* **11,** 435–444.

Trussell LO, Zhang S and Raman IM (1993). Desensitization of AMPA receptors upon multiquantal neurotransmitter release. *Neuron* **10,** 1185–1196.

Turecek J, Jackman SL and Regehr WG (2016). Synaptic Specializations Support Frequency-Independent Purkinje Cell Output from the Cerebellar Cortex. *Cell Rep* **17,** 3256–3268.

Urban NN and Sakmann B (2002). Reciprocal intraglomerular excitation and intra- and interglomerular lateral inhibition between mouse olfactory bulb mitral cells. *J Physiol* **542,** 355–367.

Vaaga CE, Borisovska M, Westbrook GL (2014) Dual-transmitter neurons: functional implications of co-release and co-transmission. *Curr Opin Neurobiol* **29**, 25-32.

Vaaga CE and Westbrook GL (2016). Parallel processing of afferent olfactory sensory information. *J Physiol* **594,** 6715–6732.

Vaaga CE, Yorgason JT, Williams JT and Westbrook GL (2017). Presynaptic gain control by endogenous cotransmission of dopamine and GABA in the olfactory bulb. *J Neurophysiol* **117,** 1163–1170.

Vassar R, Chao SK, Sitcheran R, Nuñez JM, Vosshall LB and Axel R (1994). Topographic organization of sensory projections to the olfactory bulb. *Cell* **79,** 981–991.

Wachowiak M and Cohen LB (2001). Representation of odorants by receptor neuron input to the mouse olfactory bulb. *Neuron* **32,** 723–735.

Wachowiak M, Economo MN, Díaz-Quesada M, Brunert D, Wesson DW, White JA and Rothermel M (2013). Optical dissection of odor information processing in vivo using GCaMPs expressed in specified cell types of the olfactory bulb. *J Neurosci* **33,** 5285–5300.

Wachowiak M, McGann JP, Heyward PM, Shao Z, Puche AC and Shipley MT (2005). Inhibition of Olfactory Receptor Neuron Input to Olfactory Bulb Glomeruli Mediated by Suppression of Presynaptic Calcium Influx. *J Neurophysiol* **94,** 2700–2712.

Wadiche JI and Jahr CE (2001). Multivesicular release at climbing fiber-Purkinje cell synapses. *Neuron* **32,** 301–313.

Wang LY and Kaczmarek LK (1998). High-frequency firing helps replenish the readily releasable pool of synaptic vesicles. *Nature* **394,** 384–388.

Wang Z-J, Sun L and Heinbockel T (2012). Cannabinoid receptor-mediated regulation of neuronal activity and signaling in glomeruli of the main olfactory bulb. *J Neurosci* **32,** 8475–8479.

White EL (1973). Synaptic organization of the mammalian olfactory glomerulus: new findings including an intraspecific variation. *Brain Res* **60,** 299–313.

Whitesell JD, Sorensen KA, Jarvie BC, Hentges ST and Schoppa NE (2013). Interglomerular lateral inhibition targeted on external tufted cells in the olfactory bulb. *J Neurosci* **33,** 1552–1563.

Williams MR, DeSpenza T Jr, Li M, Gulledge AT and Luikart BW (2015). Hyperactivity of newborn Pten knock-out neurons results from increased excitatory synaptic drive. *J Neurosci* **35,** 943–959.

Winner B, Geyer M, Couillard-Despres S, Aigner R, Bogdahn U, Aigner L, Kuhn G and Winkler J (2006). Striatal deafferentation increases dopaminergic neurogenesis in the adult olfactory bulb. *Exp Neurol* **197,** 113–121.

Wong AYC, Graham BP, Billups B and Forsythe ID (2003). Distinguishing between presynaptic and postsynaptic mechanisms of short-term depression during action potential trains. *J Neurosci* **23,** 4868–4877.

Xu F, Greer CA and Shepherd GM (2000). Odor maps in the olfactory bulb. *J Comp Neurol* **422,** 489–495.

Xu-Friedman MA and Regehr WG (1999). Presynaptic strontium dynamics and synaptic transmission. *Biophys J* **76,** 2029–2042.

Xu-Friedman MA and Regehr WG (2000). Probing fundamental aspects of synaptic transmission with strontium. *J Neurosci* **20,** 4414–4422.

Yorgason JT, España RA and Jones SR (2011). Demon voltammetry and analysis software: analysis of cocaine-induced alterations in dopamine signaling using multiple kinetic measures. *J Neurosci Methods* **202,** 158–164.

Yuan Q and Knöpfel T (2006). Olfactory nerve stimulation-induced calcium signaling in the mitral cell distal dendritic tuft. *J Neurophysiol* **95,** 2417–2426.

Zhang S and Trussell LO (1994). Voltage clamp analysis of excitatory synaptic transmission in the avian nucleus magnocellularis. *J Physiol* **480 (Pt 1),** 123–136.

Zhang X and Firestein S (2002). The olfactory receptor gene superfamily of the mouse. *Nat Neurosci* **5,** 124–133.

Zozulya S, Echeverri F and Nguyen T (2001). The human olfactory receptor repertoire. *Genome Biol* **2,** RESEARCH0018.